Rea, D.K., Basov, I.A., Janecek, T.R., Palmer-Julson, A., et al., 1993
Proceedings of the Ocean Drilling Program, Initial Reports, Vol. 145

4. SITE 882[1]

Shipboard Scientific Party[2]

HOLE 882A

Date occupied: 5 August 1992

Date departed: 7 August 1992

Time on hole: 1 day, 19 hr, 30 min

Position: 50°21.797′N, 167°35.999′E

Bottom felt (rig floor; m, drill-pipe measurement): 3254.7

Distance between rig floor and sea level (m): 10.93

Water depth (drill-pipe measurement from sea level, m): 3243.8

Total depth (rig floor; m): 3653.0

Penetration (m): 398.3

Number of cores (including cores with no recovery): 42

Total length of cored section (m): 398.3

Total core recovered (m): 411.2

Core recovery (%): 103.2

Oldest sediment cored:
Depth (mbsf): 398.3
Nature: diatom ooze
Age: late Miocene
Measured velocity (km/s): 1.530

HOLE 882B

Date occupied: 7 August 1992

Date departed: 9 August 1992

Time on hole: 2 days, 7 hr

Position: 50°21.798′N, 167°35.976′E

Bottom felt (rig floor; m, drill-pipe measurement): 3255.1

Distance between rig floor and sea level (m): 10.93

Water depth (drill-pipe measurement from sea level, m): 3244.2

Total depth (rig floor; m): 3525.5

Penetration (m): 270.4

Number of cores (including cores with no recovery): 29

Total length of cored section (m): 270.4

Total core recovered (m): 280.9

Core recovery (%): 103.9

Oldest sediment cored:
Depth (mbsf): 270.4
Nature: diatom ooze
Age: late Miocene
Measured velocity(km/s): 1.535

Principal results: The *JOIDES Resolution* arrived at the start of the site survey at proposed location DSM-3 (Site 882; Figs. 1 and 2) at 1345 hr (local time) on 5 August 1992. The survey, following the track of the 1988 Roundabout cruise of the *Thomas Washington*, was routine, and a beacon was dropped for Site 882 during the first pass. APC-coring began early on 6 August. Because of the difficulties experienced at Site 881 trying to recover diatom ooze with the XCB bit, we decided to continue with the APC bit as long as it could stroke out completely. The combination of lithology, siliceous ooze, and surprisingly few dropstones, and weather—calm with no swells —made it possible to complete an APC hole of record length; 42 cores, 398.3 m recovered with more than 100% recovery. Hole 882A exceeds the previous record APC length, at Hole 806B, by eight cores and about 78 m. Coring at Hole 882A was terminated because of time considerations, rather than the inability to conduct piston-coring farther down the section. Hole 882B was spudded on 7 August. Twenty-nine APC cores were recovered that spanned the depth range of 0 to 270.4 mbsf, with more than 100% recovery. On Core 145-882B-30H, the APC rod sheared at the top, and this rod and the core barrel were lost in the hole. The *JOIDES Resolution* departed Site 882 for the location of proposed Site DSM-1 late in the afternoon on 8 August.

All sediments recovered at Site 882 are of a single lithologic unit that can be divided into two lithologic subunits. Subunit IA (0–105 mbsf) is a diatom ooze with ash, clay, and dropstones. Subunit IB is a diatom ooze with accessory nannofossils and sponge spicules; minor amounts of ash recur in the lower part of Subunit IB. Subunit IA is Quaternary to late Pliocene in age (0–2.6 Ma), and Subunit IB is late Pliocene to late Miocene in age (2.6–7.2 Ma). Very good biostratigraphic zonation is possible with diatoms, with some help provided by radiolarians and nannofossils. The upper Pliocene and Pleistocene portion of the section (Subunit IA) is characterized by a much greater influx of both volcanic ash and terrigenous material in the form of clay and dropstones than is Subunit IB. However, dropstones are far less abundant than they were at Site 881, about 300 nmi to the south. A portion of the lower Pliocene section, between about 4.2 and 4.7 Ma, is characterized by an extremely rapid influx of diatoms having sedimentation rates of 135 to 300 m/m.y. This "diatom dump" event occurred at high latitudes during the warm period of early Pliocene time and has been seen in Antarctic Ocean drill sites. Magnetic reversal stratigraphy at Site 882 is good in the more clay- and ash-rich Subunit IA. Reversals associated with the Brunhes/Matuyama boundary; the Jaramillo, Olduvai, and Reunion events; and the Matuyama/Gauss boundary are clear. The nearly pure siliceous oozes of Subunit IB are too weakly magnetized to retain a magnetostratigraphy that could be determined readily on board the ship. Sedimentation rates at Site 882 average 46 m/m.y. between 0 and 4.2 Ma; are 135 to 300 m/m.y. between 4.2 and 4.7 Ma, and 32 m/m.y. in the uppermost Miocene sediments.

BACKGROUND AND SCIENTIFIC OBJECTIVES

Site 882 (proposed Site DSM-3) is the middle of a three-site depth transect down the slopes of Detroit Seamount (Figs. 1 and 2) and was the first site to be drilled. A primary objective was to obtain a high-resolution record of calcium carbonate, and eventually oxygen and carbon isotopic information, to help to define the nature and variability of Northwest Pacific Ocean deep waters. The carbonate record from Site 882 was to be combined with similar records from the shallow and deep Detroit Seamount sites (Sites 883 and 884) to provide a record of

[1] Rea, D.K., Basov, I.A., Janecek, T.R., Palmer-Julson, A., et al., 1993. *Proc. ODP, Init. Repts.*, 145: College Station, TX (Ocean Drilling Program).
[2] Shipboard Scientific Party is as given in list of participants preceding the contents.

carbonate deposition between 2400 and 3800 m for the northwestern Pacific Ocean, at the end of the global deep-water circulation path. These records then could be compared with records from depth transects conducted by ODP in the Atlantic, Indian, and Equatorial Pacific oceans to construct a global picture of deep-water paleoceanography.

Seismic records from the site survey conducted in 1988 by the *Thomas Washington* show about 1.2 s of sediment at Site DSM-3. This sediment is about three times the thickness found at Site 881 and probably lies on a basement of Emperor Seamounts (age perhaps 65 Ma) rather than the regional seafloor (age of 100 Ma). Thus, very high sedimentation rates were expected, especially in the portion of the section to be drilled.

In addition to the carbonate-related objectives, all the high-resolution studies of late Pliocene and Pleistocene phenomena pertained at Site 882: biostratigraphy and evolution of subpolar siliceous and calcareous organisms; magnetostratigraphy of the rapidly accumulating clay-rich sediments; processes of sedimentation pertaining to these very rapidly accumulating deposits; tephrochronology and ash-layer geochemistry; and highly detailed studies of the influx of ice-rafted debris to the Northwest Pacific Ocean.

To accomplish these objectives, one APC hole and one APC/XCB hole were planned. We intended to use the APC in Hole 882A to the sub-bottom depth where APC-coring was halted by the nature of the sediments, then to offset to Hole 882B to repeat the process. Hole 882B was to be continued downward by XCB-coring until time to leave the site. No logging was planned for Site 882.

OPERATIONS

Transit to Proposed Site DSM-3

The transit from Site 881 to proposed Site DSM-3 covered 307.5 nmi at an average speed of 11.0 kt. At 1330 hr (local time) on 5 August, the vessel slowed to stream seismic gear out for a short survey of the proposed site area. A beacon was dropped at the proposed site location at 1500 hr, and the vessel continued with the survey. At 1730 hr, the survey ended, and the ship returned to the site.

Hole 882A

The first piston core at Hole 882A was retrieved at 0110 hr (local time) on 6 August and from it 8.8 m of sediment was recovered to establish the mud line at 3254.7 mbrf (See Table 1 for a summary of coring operations at this site). APC-coring advanced uneventfully to Core 145-882A-11H (94.3–103.8 mbsf), where the first large overpull was encountered (70,000 lb). Overpull then decreased to less than 10,000 lb by Core 145-882A-15H (132.3–141.8 mbsf). Excessive overpull (100,000 lb) while retrieving Core 145-882A-17H (151.3–160.8 mbsf) required us to wash over the barrel before it could be pulled free. This wash-over coring technique was used to free the core barrel for the remainder of the cores at this hole, with the exception of Core 145-882A-20H (179.8–189.3 mbsf), which came free using only 50,000 lb of overpull. The hole was terminated after Core 145-882A-42H because of time constraints, but not before setting a new record for APC penetration depth. Cores 145-882A-4H (27.8–37.3 mbsf) to -29H (265.3–274.8 mbsf) were oriented successfully. APC-coring in Hole 882A recovered 411.2 m of sediment (103.2% recovery). After Core 145-882A-42H was brought on deck, the bit was pulled out of the hole and cleared the mud line at 1030 hr on 7 August, thereby ending Hole 882A.

Hole 882B

After the vessel was offset 20 m west, the first core from this hole was brought on deck at 1130 hr on 7 August with 4.38 m of sediment, establishing the mud line at 3255.1 mbrf. APC-coring advanced to Core 145-882B-19H (165.9–175.4 mbsf) before the first overpull of 100,000 lb was required. By Core 145-882B-20H (175.4–184.9 mbsf), it was necessary to wash over each of the APC core barrels to extract them from the formation. After the barrel for Core 145-882B-30H was run down the pipe and just before it was seated, the assistant driller noticed a decrease in weight of about 5 m higher than the expected landing depth of the core barrel. The pressure in the pipe would not hold to shoot the next piston core; so, the core barrel was retrieved and inspected. When the drill-pipe connection was broken at the rig floor, all that was found of the core barrel assembly was the inner shear pin/landing shoulder and the inside fishing neck. The piston rod and core barrel were gone. Because of this "junking" of the hole, coring was terminated at Hole 882B. At this point, the pipe was pulled out of the hole. By 1730 hr on 8 August, the bit was on deck and the vessel was under way to proposed Site DSM-1. APC-coring at Hole 882B recovered 280.9 m of sediment (103.9% recovery). Cores 145-882B-4H through -29H were oriented.

LITHOSTRATIGRAPHY

Introduction

Drilling at Site 882 (Figs. 1 and 2) recovered one major sedimentary unit (Fig. 3), which is late Miocene to Quaternary in age. This unit is composed predominantly of diatom ooze and clayey diatom ooze with minor beds of volcanic ash, carbonate- or spicule-enriched intervals, and dropstone layers. The diatom concentration (as derived from smear-slide counts) varies between 40% and 100% (Fig. 1). The unit can be divided into two subunits, based on variations in the clay content and the frequency of ash layers (Figs. 3 and 4). Subunit IA (0–105 mbsf) predominantly comprises diatom ooze and clayey diatom ooze with frequent layers of volcanic ash and frequent occurrence of dropstones. Subunit IB (105–398.3 mbsf) is composed of diatom ooze with minor amounts of clay, ash layers, and dropstones. The boundary between Subunits IA and IB is gradational and occurs at about 105 mbsf, within Core 145-882A-12H in Hole 882A and within Core 145-882B-12H in Hole 882B. This transition, dated at 2.6 Ma, also coincides with changes in the physical property data (see "Physical Properties" section, this chapter) and the magnetic susceptibility record (see "Paleomagnetism" section, this chapter). Both subunits are described in the following sections.

Because about 10% of the section was always missing between successive complete APC cores, we attempted to determine the size of the gaps by correlating the GRAPE data of Hole 882A with those of Hole 882B. At Site 882, the coring gaps average just more than 1 m (Table 2; Fig. 5).

Lithologic Units

Subunit IA

Intervals: Cores 145-882A-1H to -12H
Cores 145-882B-1H to -12H
Depth: 0–105.0 mbsf
Age: Quaternary–late Pliocene

Subunit IA is characterized by high diatom concentrations, which fluctuate between 50% and 100%, and clay contents that average greater than 10% (Fig. 3). Diatom ooze and clayey diatom ooze to diatom ooze with clay, the most common sediment types, are predominantly dark green gray in color. Diatom ooze with calcite or spicules is common in the upper 47 m of Subunit IA and is also green gray. Light gray to gray calcareous diatom ooze is the least common sediment type in Subunit IA and is found in Cores 145-882A-4H and 145-882B-3H. The ooze is generally slightly bioturbated, as indicated by centimeter-scale burrow fills. Stiff green and purple, thin (0.5–10 cm) layers are scattered throughout the major lithology, but reveal no significant compositional difference when compared to the surrounding sediment.

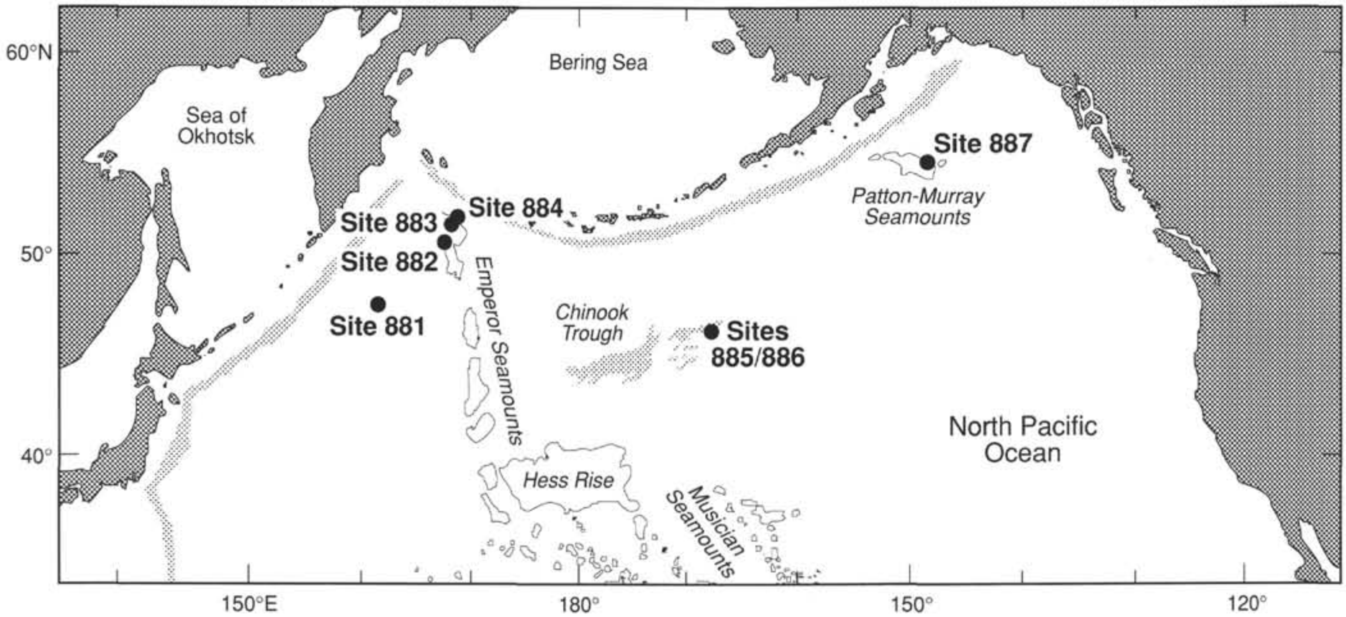

Figure 1. Index map of the North Pacific Ocean showing Leg 145 drill sites.

Subordinate lithotypes include vitric ash beds and dropstones. The abundances of ash layers and dropstone intervals are distinctly higher in Subunit IA than in Subunit IB (Fig. 4). In general, ash layers are light gray, red gray, or black and range in thickness from 1 cm up to several decimeters. Ash layers thicker than 5 cm usually have sharp basal contacts, are normally graded from sand-sized upward to silt-and clay-sized grains, and have gradational upper contacts, often overlain by ash-filled burrows. Ashes are dominated by volcanic lithic detritus and glass shards. Subunit IA contains 52 ash layers in Hole 882A and 55 ash layers in Hole 882B. This difference is most likely because of a less complete core recovery at Hole 882A and/or differential sediment loss at breaks between succeeding cores (Table 2; Fig. 5). Bioturbation also may have obscured the record of ash layers by destroying some ash layers that were initially present. The correlation of ash layers between Holes 882A and 882B (Table 3), based on magnetic susceptibility curves, visual core descriptions, and core photos, indicates 64 ash layers for the upper 101 mbsf. Only five of these ash layers cannot be correlated between holes. Dropstones range in size from coarse sand to pebbles. Most dropstones are dark, fine-grained basaltic rocks. A thin-section study of one dropstone found in Section 145-882A-11H-1, 90–94 cm, identified a sheared metamorphosed basic plutonic rock (gabbro?) that contains veined quartz and sulfides.

Subunit IB

Intervals: Cores 145-882A-12H to -42H
Cores 145-882B-12H to -29H
Depth: 105.0–398.3 mbsf
Age: late Pliocene–late Miocene

This unit is dominated by diatom ooze, which is predominantly reddish-brown and green gray in color. The diatom content, based on smear slide estimates, ranges from 60% to 100% between 105 and 210 mbsf, but exhibits a wider range of 40% to 100% in the lower part of Subunit IB (210–400 mbsf; Fig. 3). Subunit IB is characterized by significantly lower abundances of clay and vitric ash beds compared to the overlying strata (Figs. 3 and 4). Diatom-rich sediments typically are slightly bioturbated and homogeneous in appearance. The measured carbonate content ranges from 0% to 40% (see "Organic Geochemistry" section, this chapter). Interbeds of calcareous diatom ooze or diatom ooze with calcite are common throughout Subunit IB. Interbedded spicule-rich intervals are less common and appear at 113 to 151 mbsf (Cores 145-882A-13H to -16H), and between 270 and 303 mbsf (Cores 145-882A-30H and -32H; Fig. 3). Stiff green and purple layers are less common in Subunit IB than they are in Subunit IA, although their locations throughout the sedimentary section were not recorded in the same detail as were the locations of the ash layers.

Ash layers are less abundant in Subunit IB than in Subunit IA (Fig. 4). Subunit IB contains 17 ash layers in Hole 882A. Only the upper 165.4 m of Subunit IB was recovered from Hole 882B and contained six ash layers, which is consistent with the number of ash layers in Hole 882A, although these do not occur at the same depth intervals.

Dropstone intervals are rare throughout Subunit IB (Fig. 4) and occur in Section 145-882B-21H-2, 115 cm; in Section 145-882B-26H-2, 146 cm; and in Section 145-882A-38H-6, 119 cm. These dropstones are 1 to 2 cm in diameter.

Discussion

The depositional history at Site 882 is dominated by accumulation of biogenic silica. Higher diatom abundances occurred during the last 3.7 m.y. than during the late Miocene and earliest Pliocene (Fig. 3). However, the diatom abundance minima that occur before 3.7 Ma correlate with high abundances of sponge spicules and relatively high carbonate contents (see "Organic Geochemistry" section, this chapter) and probably were produced by dilution effects. The slight long-term decrease in the diatom content (from about 2.6 Ma to the Holocene) was paralleled by an increase in terrigenous sediment supply (Figs. 3 and 4). Thus, in the absence of accurate accumulation rates, one can only speculate whether these long-term fluctuations are due to changes in paleoproductivity and, hence, variations in nutrient supply, or to dilution effects caused by phases of increased ice-rafted material, or to fluctuations in carbonate preservation. However, high sedimentation rates of about 120 m/m.y. between 4.3 and 2.6 Ma, which are higher by a factor of three than the sedimentation rate for the last 2.6 m.y. and higher by a factor of two than the sedimentation rates prior to 4.3 Ma (see "Biostratigraphy" section, this chapter), suggest a long-term maximum in biogenic opal production for the Pliocene time interval of from 2.6 to 4.3 Ma.

The frequency of ash layers (Fig. 4) recorded in the upper Miocene to Holocene sediments provides a record of explosive volcanic activ-

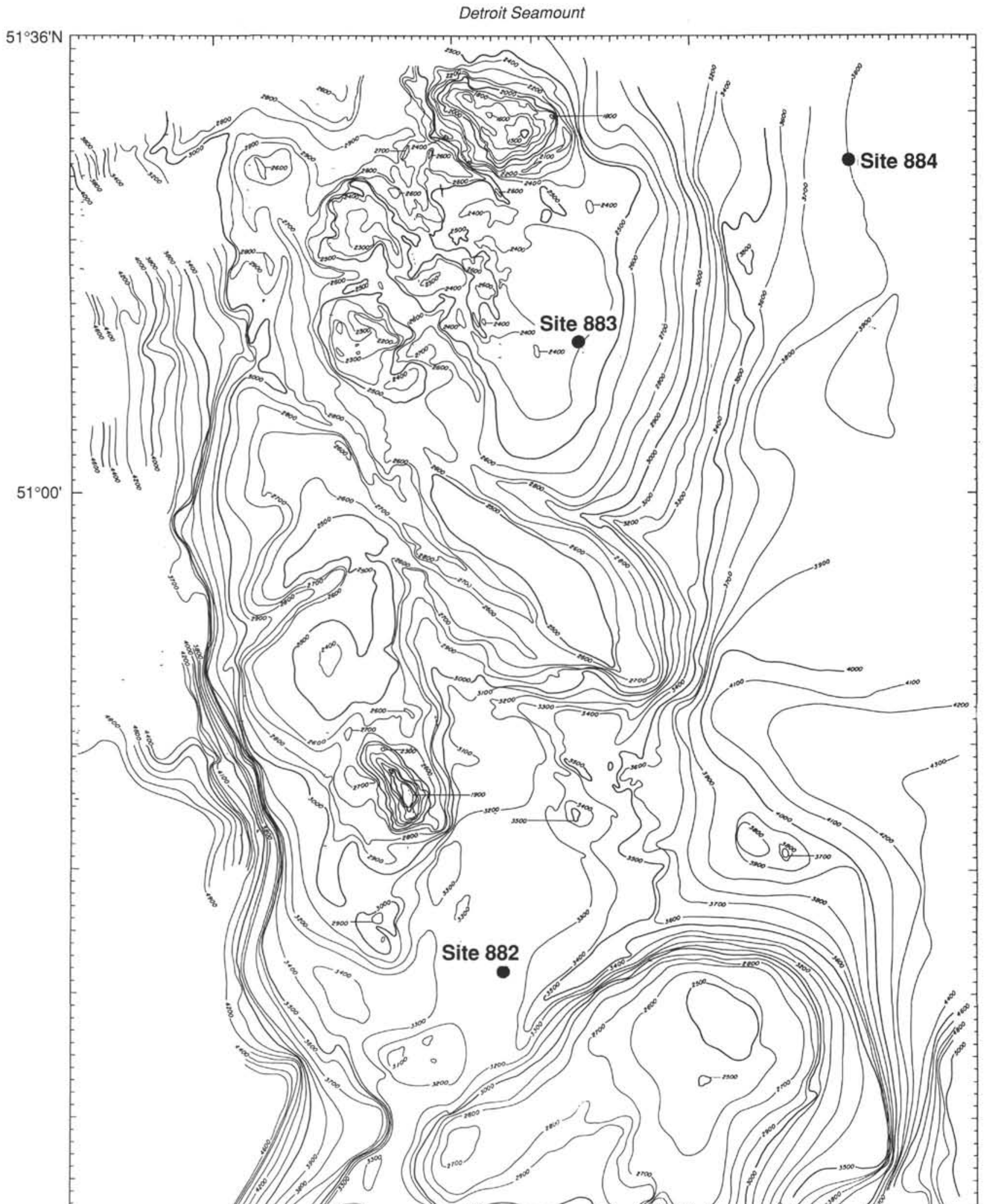

Figure 2. Bathymetry of Detroit Seamount and locations of Leg 145 drill Sites 882, 883, and 884. Contours in meters; map by C. Brenner of Lamont-Doherty Earth Observatory.

Table 1. Summary of coring operations, Site 882.

Core no.	Date (Aug. 1992)	Time (UTC)	Depth (mbsf)	Length cored (m)	Length recovered (m)	Recovery (%)
145-882A-						
1H	5	1410	0.0–8.8	8.8	8.86	100.0
2H	5	1500	8.8–18.3	9.5	9.78	103.0
3H	5	1545	18.3–27.8	9.5	9.75	102.0
4H	5	1620	27.8–37.3	9.5	9.68	102.0
5H	5	1700	37.3–46.8	9.5	9.36	98.5
6H	5	1745	46.8–56.3	9.5	9.88	104.0
7H	5	1820	56.3–65.8	9.5	9.78	103.0
8H	5	1920	65.8–75.3	9.5	9.98	105.0
9H	5	2000	75.3–84.8	9.5	9.82	103.0
10H	5	2045	84.8–94.3	9.5	9.91	104.0
11H	5	2125	94.3–103.8	9.5	9.85	103.0
12H	5	2230	103.8–113.3	9.5	10.02	105.5
13H	5	2305	113.3–122.8	9.5	9.78	103.0
14H	5	2335	122.8–132.3	9.5	9.60	101.0
15H	6	0010	132.3–141.8	9.5	9.34	98.3
16H	6	0040	141.8–151.3	9.5	9.75	102.0
17H	6	0130	151.3–160.8	9.5	9.80	103.0
18H	6	0220	160.8–170.3	9.5	10.10	106.3
19H	6	0300	170.3–179.8	9.5	9.91	104.0
20H	6	0345	179.8–189.3	9.5	9.55	100.0
21H	6	0420	189.3–198.8	9.5	10.04	105.7
22H	6	0500	198.8–208.3	9.5	10.02	105.5
23H	6	0545	208.3–217.8	9.5	10.04	105.7
24H	6	0620	217.8–227.3	9.5	10.01	105.3
25H	6	0650	227.3–236.8	9.5	9.94	104.0
26H	6	0730	236.8–246.3	9.5	10.00	105.2
27H	6	0900	246.3–255.8	9.5	9.87	104.0
28H	6	0955	255.8–265.3	9.5	9.90	104.0
29H	6	1035	265.3–274.8	9.5	10.09	106.2
30H	6	1125	274.8–284.3	9.5	9.44	99.3
31H	6	1220	284.3–293.8	9.5	9.95	105.0
32H	6	1320	293.8–303.3	9.5	10.07	106.0
33H	6	1430	303.3–312.8	9.5	9.38	98.7
34H	6	1515	312.8–322.3	9.5	9.91	104.0
35H	6	1600	322.3–331.8	9.5	9.66	101.0
36H	6	1700	331.8–341.3	9.5	9.91	104.0
37H	6	1740	341.3–350.8	9.5	9.57	101.0
38H	6	1830	350.8–360.3	9.5	9.74	102.0
39H	6	1930	360.3–369.8	9.5	9.05	95.2
40H	6	2020	369.8–379.3	9.5	9.99	105.0
41H	6	2130	379.3–388.8	9.5	10.08	106.1
42H	6	2230	388.8–398.3	9.5	10.04	105.7
Coring totals				398.3	411.20	103.2
145-882B-						
1H	7	0045	0.0–4.4	4.4	4.38	99.5
2H	7	0135	4.4–13.9	9.5	9.65	101.0
3H	7	0215	13.9–23.4	9.5	9.71	102.0
4H	7	0255	23.4–32.9	9.5	9.78	103.0
5H	7	0330	32.9–42.4	9.5	9.60	101.0
6H	7	0410	42.4–51.9	9.5	9.82	103.0
7H	7	0450	51.9–61.4	9.5	9.79	103.0
8H	7	0530	61.4–70.9	9.5	9.95	105.0
9H	7	0600	70.9–80.4	9.5	10.06	105.9
10H	7	0630	80.4–89.9	9.5	9.49	99.9
11H	7	0710	89.9–99.4	9.5	9.97	105.0
12H	7	0750	99.4–108.9	9.5	9.74	102.0
13H	7	0820	108.9–118.4	9.5	9.97	105.0
14H	7	0900	118.4–127.9	9.5	9.86	104.0
15H	7	0930	127.9–137.4	9.5	9.97	105.0
16H	7	1010	137.4–146.9	9.5	10.06	105.9
17H	7	1055	146.9–156.4	9.5	9.90	104.0
18H	7	1130	156.4–165.9	9.5	9.97	105.0
19H	7	1220	165.9–175.4	9.5	9.95	105.0
20H	7	1340	175.4–184.9	9.5	10.11	106.4
21H	7	1435	184.9–194.4	9.5	10.05	105.8
22H	7	1540	194.4–203.9	9.5	9.95	105.0
23H	7	1640	203.9–213.4	9.5	9.96	105.0
24H	7	1810	213.4–222.9	9.5	10.02	105.5
25H	7	1930	222.9–232.4	9.5	9.95	105.0
26H	7	2030	232.4–241.9	9.5	10.05	105.8
27H	7	2120	241.9–251.4	9.5	9.59	101.0
28H	7	2225	251.4–260.9	9.5	9.78	103.0
29H	7	2330	260.9–270.4	9.5	9.82	103.0
Coring totals				270.4	280.90	103.9

ity in the adjacent arcs through time. Three peaks in frequency of ash layers and their cumulative thickness occur in the upper Miocene sediments at about 6.0 Ma and in the lower Pliocene sequence at 5.0 and 3.7 Ma (based on the preliminary magnetostratigraphic and biostratigraphic time scales). A minimum in frequency of ash layers at about 3.5 to 2.6 Ma suggests a low level of explosive volcanic activity during this time. The maximum level in volcanic activity was

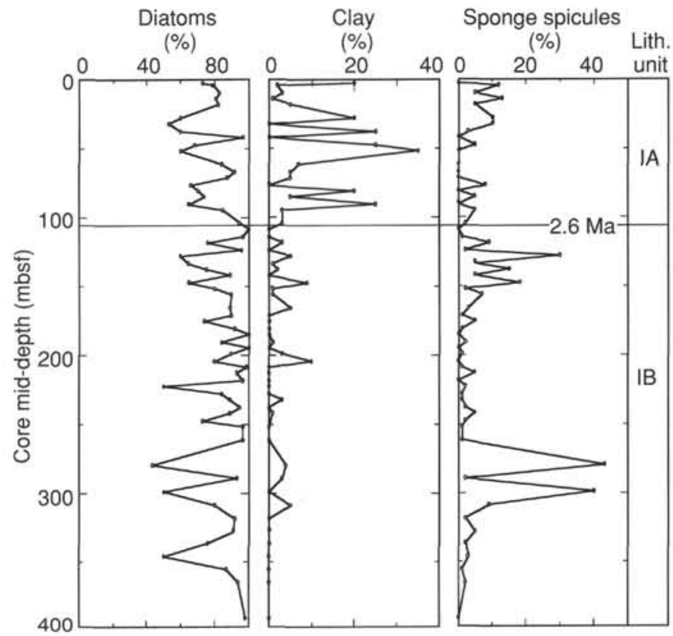

Figure 3. Abundances of diatoms, sponge spicules, and clay at Site 882, as derived from smear slide analyses of dominant lithologies. Ages are based on magnetostratigraphy and biostratigraphy (see "Sedimentation Rates and Fluxes" section, this chapter) using the revised time scale of Cande and Kent (1992).

reached during late Pliocene and Pleistocene time (Kennett and Thunell, 1975). At Site 882, a total of 64 ash layers was recognized for the last 2.6 Ma. Frequencies of ash layers also increase in the sediments of this age at nearby Sites 881, 883, and 884 ("Lithostratigraphy" section, Sites 881, 883, and 884 chapters, this volume) and DSDP Sites 578 and 579 (Heath, Burckle, et al., 1985).

Dropstones are indicative of ice-rafting during the time of deposition. A single dropstone at Site 882 in the lower Pliocene at about 5.0 Ma and two intervals at about 3.8 and 3.4 Ma (Fig. 4) suggest ice-rafting during those times. The frequency of dropstone intervals increased significantly during the last 2.6 Ma, as also was recorded at nearby Sites 881, 883, and 884 (see "Lithostratigraphy" section, Sites 881, 883, and 884 chapters, this volume); at the more southern DSDP Sites 579 and 580 (Krissek et al., 1985), and at Site 887 in the northeastern Pacific (see "Lithostratigraphy" section, "Site 887" chapter, this volume). These intervals parallel the major onset in Northern Hemisphere glaciation at approximately 2.6 Ma (Shackleton et al., 1984; Rea and Schrader, 1985). The variations in clay content at Site 882 also correlate well with the number of dropstone intervals and may have resulted from ice-rafted debris.

Composite Depth Sections

At Site 882, two holes were drilled to obtain a complete sediment record. Correlation between the magnetic susceptibility records generated for Holes 882A and 882B allows us to splice the two records together. Splicing the two records together yields a composite depth section in Table 4 that can be used to eliminate coring gaps between successive cores—elucidated above by the GRAPE data (Table 2; Fig. 5)—and disturbed sediment sections caused by coring. The composite depth sections developed for the upper 135 mbsf (0–3 Ma) at Site 882 are based on continuous high-resolution magnetic susceptibility curves (data point distance = 5 cm), which allow for an accurate correlation of marked short-term fluctuations between one hole and another. Below 135 mbsf, the composite depth sections were based on GRAPE data because the signal from the magnetic susceptibility was too weak for accurate correlations between holes. The upper 25

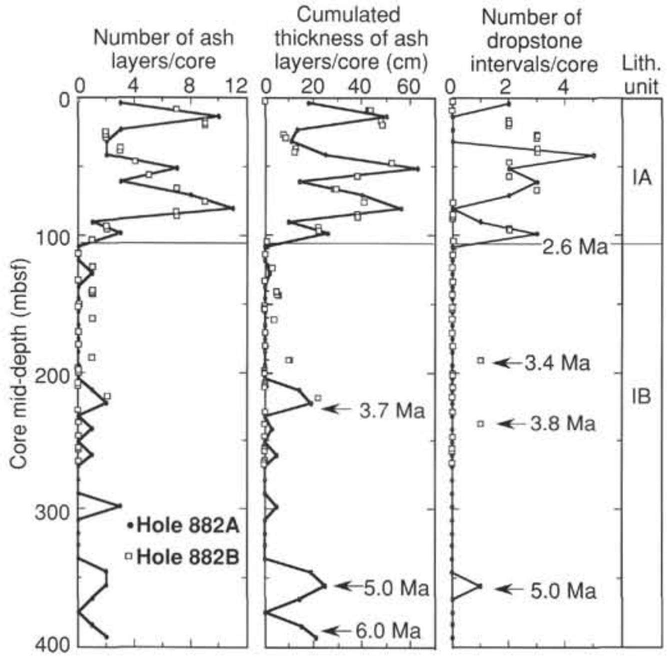

Figure 4. Frequency of ash layers and cumulative thickness of ash layers at Holes 882A and 882B. Ages are based on magnetostratigraphy and biostratigraphy (see "Sedimentation Rates and Fluxes" section, this chapter) using the revised time scale of Cande and Kent (1992). Number of dropstone intervals per core also is shown.

Table 2. Gaps between piston Cores 1H to 24H in Holes 882A and 882B (from correlation of GRAPE records).

Hole 882A coring gaps (cm)			Hole 882B coring gaps (cm)		
Between core and core		is a gap of	Between core and core		is a gap of
145-882A-			145-882B-		
-1H	-2H	194	-1H	-2H	193
-2H	-3H	152	-2H	-3H	90
-3H	-4H	328	-3H	-4H	150
-4H	-5H	80	-4H	-5H	72
-5H	-6H	211	-5H	-6H	52
-6H	-7H	70	-6H	-7H	63
-7H	-8H	137	-7H	-8H	32
-8H	-9H	180	-8H	-9H	(??)
-9H	-10H	140	-9H	-10H	115
-10H	-11H	150	-10H	-11H	160
-11H	-12H	90	-11H	-12H	135
-12H	-13H	75	-12H	-13H	60
-13H	-14H	59	-13H	-14H	162
-14H	-15H	139	-14H	-15H	55
-15H	-16H	44	-15H	-16H	14
-16H	-17H	190	-16H	-17H	154
-17H	-18H	93	-17H	-18H	58
-18H	-19H	135	-18H	-19H	261
-19H	-20H	110	-19H	-20H	223
-20H	-21H	30	-20H	-21H	21
-21H	-22H	61	-21H	-22H	76
-22H	-23H	339(?)	-22H	-23H	147(?)
-23H	-24H	250	-23H	-24H	24
-24H	-25H	54	-24H	-25H	77

core breaks in Hole 882A were covered with overlapping sections from Hole 882B. Below 246 mbsf, the composite depth sections remain uncertain because of only short overlapping sections between holes (core breaks at 145-882A-26H/-27H, -27H/-28H, and -28H/-29H). The upper 2.14 m of the composite section was taken from Hole 882B, because a comparison of the magnetic susceptibility curves from both holes suggests a more complete and undisturbed section for Hole 882B (Fig. 6).

The composite record for Site 882 is summarized in Table 4 and can be identified by reading across the table to see composite sections and depths. The composite depth record is about 15% longer than the measurement of sediment depth below seafloor at Holes 882A and 882B and spans the last 4 m.y. Figure 6 shows the between-hole correlation for the upper 25 m (based on the magnetic susceptibility curves).

BIOSTRATIGRAPHY

An apparently continuous sequence of upper Miocene through Pleistocene sediments was recovered at Site 882. The two holes that were drilled showed an excellent correspondence and penetrated a 398-m-thick section consisting of diatom oozes with intervals of clayey diatom oozes down to approximately 70 mbsf. Below 70 mbsf, scattered intervals of diatom oozes with calcite overlay the diatom ooze. The uppermost 100 m of the sequence contained numerous ash layers, whereas scattered ash layers occurred in the intervals between 200–250 mbsf and 340–365 mbsf, respectively. In Hole 882A, we recovered uppermost Miocene (~5.9 Ma) through Pleistocene sediments, whereas Hole 882B did not extend to the Miocene (<5 Ma, based on diatom datums).

Moderately well-preserved calcareous nannofossils occur in abundances ranging from rare to abundant, but with low species diversities down to approximately 227 mbsf, below which they become rare. An interval of abundant, well-preserved calcareous nannofossils can be observed between Cores 145-882A-13H and -23H (Fig. 7). Moderately well-preserved calcareous foraminifers occur in low abundances at several intervals throughout the sediments drilled at this site, while diatoms are common to abundant and well-preserved throughout the entire sequence. Radiolarians, present throughout the section, are common to abundant in most Pleistocene sediments, rare in Miocene and Pliocene sequences. Only a few samples contain minor (>3 specimens) quantities of reworked fauna.

Figure 7 shows core recovery and siliceous zonation for this site. Table 5 gives the estimated ages of diatom, radiolarian, and calcarous nannofossil datum levels recorded in sediments recovered from Holes 882A and 882B, the interval over which they occur, and the depth of this interval in meters below seafloor (mbsf).

Foraminifers

All core-catcher samples from Holes 882A and 882B were processed and examined for both benthic and planktonic foraminifers. Planktonic foraminifers are never abundant at Site 882. Common or few planktonic foraminifers occur only in the following 10 samples: 145-882A-1H-CC; 145-882A-6H-CC through -7H-CC; 145-882A-14H-CC; 145-882A-16H-CC; 145-882A-37H-CC; 145-882B-10H-CC; 145-882B-12H-CC; and 145-882B-23H-CC through -24H-CC. Assemblages are dominated by the cold and temperate water species *Globigerina bulloides* and *Neogloboquadrina pachyderma* (sinistral). However, five samples (145-882A-16H-CC; 145-882A-21H-CC; and 145-882B-12H-CC; 145-882B-23H-CC to 24H-CC) contain more diverse assemblages of subtropical-temperate species (*N. pachyderma* (dextral), *N. dutertrei, Globorotalia scitula, Globigerinita glutinata* and *Orbulina* spp.) indicative of relatively warm surface-water conditions in the Pliocene.

The samples contain generally rare occurrences of agglutinated and/or robust calcareous benthic foraminifers. Many samples are barren of all calcareous taxa. Benthic foraminifers are never abundant at Site 882; however, 12 samples do contain sparse assemblages of calcareous and agglutinated species (Samples 145-882A-1H-CC; 145-882A-6H-CC through -7H-CC; 145-882A-14H-CC; 145-882A-16H-CC; 145-882A-35H-CC; 145-882A-37H-CC; 145-882B-18H-CC; 145-882B-20H-CC; 145-882B-21H-CC, and 145-882B-23H- CC through -24H-CC).

The species composition remains fairly similar throughout the section recovered. Notable variations occur only in relative abundance. Dominant species include *Gyroidinoides* spp., *Martinottiella commu-*

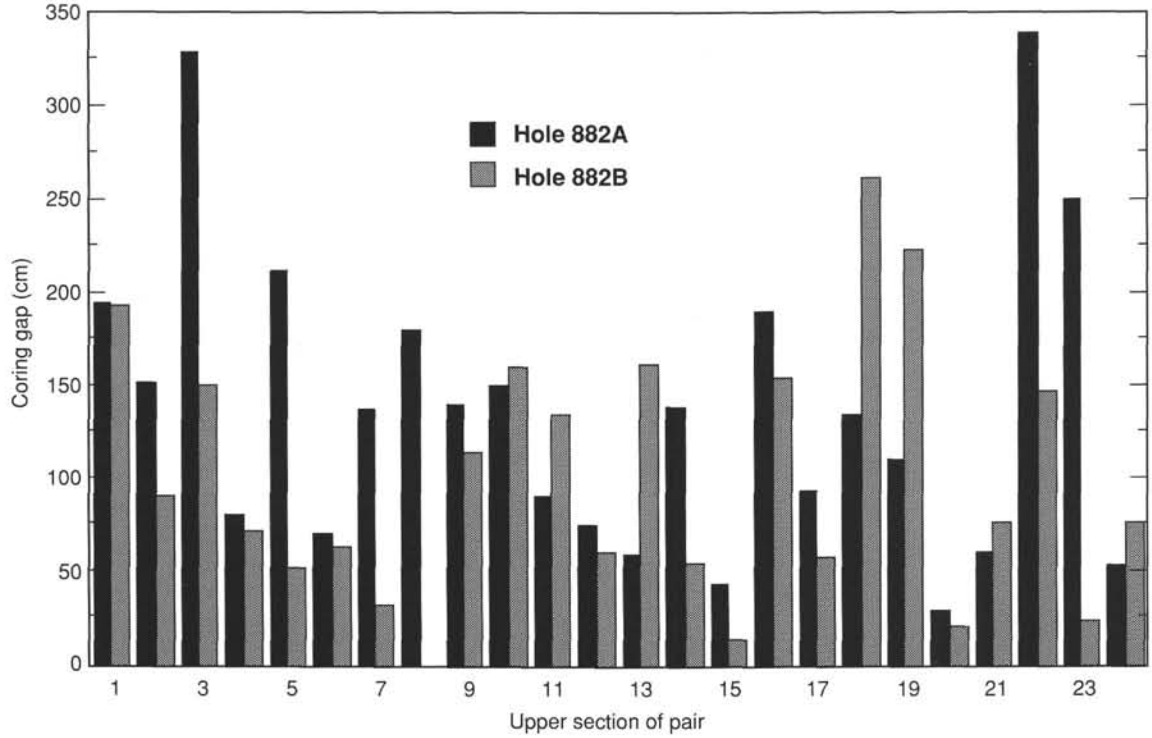

Figure 5. Gaps between APC cores at Site 882, based on Table 2.

nis, *Melonis barleanum*, *Melonis pompilioides*, *Oridorsalis umbonatus*, *Pullenia bulloides*, *Pyrgo murrhina*, *Sphaeroidina bulloides*, and *Uvigerina senticosa*. Other common species are *Cibicidoides robertsonianus*, *Cyclammina cancellata*, *Eggerella bradyi*, *Epistominella exigua*, *Globocassidulina subglobosa*, *Karreriella* spp., *Laticarinina pauperata*, *Lenticulina* spp., and *Planulina wuellerstorfi*.

The benthic foraminiferal fauna of Site 882 indicate a lower-bathyal to abyssal paleodepth (>1000 m), based on van Morkhoven et al. (1986). Deposition appears to have been near the foraminiferal lysocline throughout most of the interval recovered. Where planktonic foraminifers do occur, preservation is moderate, with some evidence of dissolution. Benthic foraminiferal assemblages tend to be dominated by robust, dissolution-resistant taxa.

Calcareous Nannofossils

Calcareous nannofossil assemblages have been examined from all the core-catcher samples obtained from Site 882. The abundance of calcareous nannofossils fluctuates significantly in the sediments. The abundance is generally low in the upper part (Samples 145-882A-1H-CC to -882A-12H-CC and 145-882B-1H-CC to -882B-11H-CC) and in the lower part of the sections (Samples 145-882A-25H-CC to -882A-42H-CC and 145-882B-25H-CC to -882B-28H-CC). Several samples are barren in these intervals. The abundance is much higher between these intervals.

The calcareous nannofossils are well preserved, although overgrowth on placoliths is often present in the upper part of the sections.

The diversity is reduced and fewer than 10 species were encountered in these samples. The assemblages are dominated by *Coccolithus pelagicus* and by small placoliths of *Gephyrocapsa* and *Reticulofenestra*.

Scarce specimens of *Pseudoemiliania lacunosa* can be observed in sediments from Samples 145-882A-5H-CC and 145-882B-4H-CC. In the sections above this level, abundances of calcareous nannofossils in the sediments are too low to permit accurate estimates of the last occurrence datum of this species. *Reticulofenestra pseudoumbilica* is common in sediments from Samples 145-882A-17H-CC and 145-882B-17H-CC, which indicates that the lower/upper Pliocene contact lies within these cores.

Radiolarians

Core-catcher samples from the two holes drilled at Site 882 contain moderately well- to well-preserved upper Miocene through Pleistocene radiolarians. The faunal assemblage in samples from the uppermost sediments from Holes 882A and 882B (145-882A-1H-CC through -2H-CC and 145-882B-1H-CC through -2H-CC) is characteristic of the upper Quaternary *Botryostrobus aquilonaris* Zone (Hays, 1970). Radiolarian abundances in these samples vary from rare to abundant. *Lychnocanoma grande* (last occurrence estimated at 0.05 Ma) is present in core-catcher samples taken from the first core in both holes. Samples 145-882A-2H-CC and -882B-3H-CC contain the last occurrence of *Druppatractus acquilonius*.

The top of the upper Quaternary *Stylatractus universus* Zone (Hays, 1970), marked by the last occurrence of *S. universus* with an estimated age of 0.45 Ma (Hays and Shackleton, 1976; Morley and Shackleton, 1978), occurs between Samples 145-882A-2H-CC and -3H-CC, and Samples 145-882B-2H-CC and -3H-CC. This zone extends through Samples 145-882A-5H-CC and 145-882B-6H-CC. Within this zone, radiolarian abundances vary from rare to abundant. The sediment sequence between Samples 145-882A-6H-CC and -8H-CC, and Samples 145-882B-7H-CC and -9H-CC contains fauna characteristic of the *Eucyrtidium matuyamai* Zone (Hays, 1970; Foreman, 1975). Abundances of radiolarians in these samples range from rare to abundant.

Radiolarian abundances are rare in samples throughout the remaining interval in both holes. Not all the species that define specific zones below the *E. matuyamai* Zone are present in every sample. Specific first and last occurrences that define the characteristic North Pacific Ocean radiolarian zones for the Pliocene and upper Miocene are also inconsistent between the two holes. For example, although the last occurrence of *Stichocorys peregrina*, marking the boundary

Table 3. Correlation of ash layers between Holes 882A and 882B (from correlation of GRAPE records).

Occurrence of ash layers at Site 882 during the last 2.6 Ma			
Hole 882A		Hole 882B	
Core, section, interval (cm)	Depth (mbsf)	Core, section, interval (cm)	Depth (mbsf)
145-882A-		145-882B-	
1H-2, 46–47	1.96–1.97	1H-2, 97–106	2.46–2.57
1H-3, 130–142	4.31–4.43·		(ash-filled burrows)
1H-4, 142–149	5.92–5.99		
1H-6, 82–90	8.32–8.40	?2H-1, 7–12	4.47–4.52
		2H-1, 18–27	4.58–4.67
2H-2, 76–89	9.67–9.80	2H-2, 109–122	6.99–7.12
2H-2, 111–116	10.04–10.09	2H-4, 98–104	9.87–9.93
2H-3, 139–145	11.82–11.87	2H-4, 132–142	10.22–10.32*
	(ash-filled burrows)		(ash-filled burrows)
2H-4, 55–60	12.47–12.52	2H-6, 10–13	12.00–12.03
*2H-4, 132–137	13.25–13.30	2H-6, 70–74	12.60–12.64
2H-5, 21–26	13.61–13.66·	2H-7, 19–22	13.58–13.61
2H-5, 102–103	14.43–14.44		
2H-5, 106–108	14.47–14.48	3H-1, 16–20	14.06–14.12
2H-5, 120–127	14.62–14.69	3H-1, 39–45	14.29–14.35
*2H-6, 97–102	15.88–15.93	3H-2, 27–29	15.66–15.68
	(ash-filled burrows)	3H-2, 84–93	16.23–16.32
2H-6, 147– 2H-7, 2	16.39–16.44	3H-3, 19–25	17.08–17.14
2H-7, 65–69	17.07–17.11	3H-3, 76–80	17.66–17.70
2H-7, 109–112	17.51–17.54	·3H-4, 66–70	19.06–19.10
		3H-5, 80–88	20.69–20.77
3H-1, 82–88	19.12–19.18	3H-7, 31–34	23.20–23.23
3H-3, 65–69	21.94–21.88		
	(ash-filled burrows)	4H-1, 124–129	24.65–24.70
3H-4, 17–21	22.96–23.00·	?4H-5, 133–136	30.73–30.76
3H-5, 71–74	25.00–25.03		
		5H-1, 86–91	33.76–33.81
4H-4, 11–17	32.41–32.47·	5H-4, 9–14	37.49–37.54
*4H-5, 16–19	33.95–33.98	5H-4, 103–110	38.43–38.50
4H-CC, 12–17	?		
		6H-1, 24–37	42.64–42.77
5H-1, 72–84	38.01–38.13	6H-4, 97–116	47.87–48.06
5H-4, 136–149	43.17–43.30	6H-5, 30–34	48.69–48.73
		6H-6, 47–63	50.37–50.53
6H-1, 18–36	46.89–47.16		
6H-1, 106–111	47.86–47.91	7H-1, 1–18	51.90–52.08
6H-2, 141–150	49.71–49.80	7H-4, 79–80	57.18–57.19
6H-3, 0–5	49.80–49.85	?7H-5, 136–138	59.26–59.28
6H-4, 28–34	51.58–51.64	7H-7, 14–27	61.04–61.17
		7H-CC, 10–14	?
7H-1, 70–71	56.99–57.00		
7H-4, 41–46	61.20–61.25	8H-3, 61–63	65.01–65.03
7H-4, 96–104	61.75–61.83	·8H-4, 7–11	65.96–65.70
*7H-7, 16–18	65.46–65.48	8H-5, 112–116	68.52–68.56
		8H-6, 17–23	69.06–69.11
8H-2, 69–71	67.99–68.01	8H-6, 38–49	69.28–69.39
8H-2, 130–136	68.60–68.66	8H-6, 69–70	69.59–69.60
8H-3, 5–14	68.85–68.94	8H-7, 48–49	70.88–70.89
8H3, 36–38	69.16–69.18		
	(ash-filled burrows)	9H-1, 0–10	70.90–71.00
8H-4, 33–41	70.63–70.70	9H-2, 59–60	72.99–73.00
8H-4, 90–91	71.20–71.21	9H-2, 67–72	73.07–73.17
8H-6, 42–45	73.71–73.74	9H-3, 30–36	74.19–74.25
8H-6, 51–61	73.81–73.91	9H-4, 145–147	76.86–76.88
8H-7, 11–15	74.91–74.95	9H-5, 53–59	77.43–77.49
		9H-6, 4–5	78.43–78.44
9H-1, 100–102	76.35–76.37	9H-6, 109–118	79.50–79.59
9H-1, 128–129	76.58–76.59?	9H-6, 137–138	79.77–79.78
9H-2, 11–17	76.91–76.97		
9H-2, 120–121	78.00–78.01	10H-1, 122–135	81.62–81.75
9H-3, 82–93	79.12–79.13	10H-2, 7–18	81.97–82.08
9H-3, 116–117	79.46–79.47	10H-2, 53–54	82.43–82.44
9H-5, 67–81	81.97–82.11	10H-2, 110–114	83.00–83.04
9H-5, 104–114	82.35–82.45	10H-3, 38–39	83.78–83.79
9H-6, 0–2	82.80–82.82	·10H-4, 67–69	85.57–85.59
9H-6, 55–60	83.35–83.40	10H-CC, 0–6	?
9H-6, 133–137	84.13–84.17		
		11H-4, 50–69	94.90–95.09
10H-5, 20–25	91.00–91.05	11H-4, 87–90	95.27–95.30
11H-1, 30–46	94.60–94.74	?12H-1, 125–126	100.65–100.66
11H-1, 63–67	94.93–94.97		
11H-4, 130–138	100.10–100.18·		

Note: correlation of ash layers between Holes 882A and 882B; ·ash layer is missed in the parallel hole due to sediment loss between succeeding cores; ?no ash layer was observed in the parallel hole; *depicted from core photos.

between the *Lamprocyrtis heteroporos* Zone (Hays, 1970; Foreman, 1975) and the *Sphaeropyle langii* Zone (Foreman, 1975), was recovered in Sample 145-882A-18H-CC, single specimens can be found in core-catcher samples from Cores 10H and 11H from Hole 882B (near the base of the *E. matuyamai* Zone). Either the specimens in Hole 882B are reworked, in which case the first occurrence of *S. peregrina* in Hole 882B would coincide with the level of this event in Hole 882A, or the specimens in Hole 882B are in place, in which case a nearly 70-m-thick section is missing from Hole 882B. The former case is preferred because the numerous diatom events at this site are offset between holes by no more than 10 m (Table 5). In spite of these inconsistencies between levels of specific faunal events between the two holes at Site 882, the radiolarian zonation for this site (Fig. 7) below the base of the *E. matuyamai* Zone has been tentatively constructed using the faunal data from Hole 882A only. The base of the *L. heteroporos* Zone falls between Samples 145-882A-17H-CC and -18H-CC in Hole 882A. The boundary between the *S. langii* and the *S. peregrina* zones (Riedel and Sanfilippo, 1970; 1978) has been placed between Samples 145-882A-34H-CC and -35H-CC, with the first occurrence of *L. heteroporos* recorded in Sample 145-882A-34H-CC.

Diatoms

A complete sequence of diatom zones from the late Pleistocene *Neodenticula seminae* Zone to Subzone a of the upper Miocene *Neodenticula kamtschatica* Zone was cored at Site 882 (Fig. 7). Diatoms are generally abundant to common and well preserved to moderately well preserved throughout the sequence, and the assemblages are dominated by subarctic, planktonic taxa. Recognition of diatom datum levels was generally straightforward (Table 5), and agreement is present between the stratigraphic position of datum levels between Holes 882A and 882B. Diatom zonal and subzonal assignments were made using the adopted criteria, although a scarcity of *Rouxia californica* in the upper Miocene meant that the first occurrence of *Thalassiosira oestrupii* became the sole means of recognizing the boundary between Subzone a and subzonal interval b-c of the *N. kamtschatica* Zone.

A surprising result of drilling at Site 882 was the recovery of an anomalously thick lower Pliocene section assignable to the subzone b-c interval of the *N. kamtschatica* Zone. More than 190 m of section (Cores 145-882A-20H through -882A-39H) (about 180 to 370 mbsf) was cored through this interval. The diatom assemblages of this interval are dominated by *Neodenticula kamtschatica* and *Coscinodiscus marginatus,* which are typical of lower Pliocene assemblages of the subarctic North Pacific Ocean. *Chaetoceros* spores, which are indicative of high continental marginal productivity (Sancetta and Silvestri, 1986), are not especially abundant in this interval; however, the high numbers of *Thalassiothrix longissima* found throughout the interval may be an indication of high oceanic productivity (J. Baldauf, pers. comm., 1992). Relative consistent and scattered common occurrences of *Thalassiosira* cf. *oestrupii* and *Thalassionema nitzschioides* indicate incursions of transitional waters that are associated with the subarctic polar front. Sparse occurrences of subtropical taxa, such as *Hemidiscus cuneiformis* and *Azpeitia nodulifer,* may suggest relatively warmer conditions.

PALEOMAGNETISM

Procedures

At Site 882, pass-through measurements were performed on all APC cores from Hole 882A and the first six APC cores from Hole 882B. For the first 20 cores (0–189.2 mbsf) of Hole 882A, both the natural remanent magnetization (NRM) and the remanence after alternating field (AF) demagnetization at 15 mT were measured at a sample spacing of 10 cm. Cores 145-882A-21H through -42H in Hole 882A and Cores 145-882A-1H to -6H in Hole 882B were measured only at the 15 mT demagnetization value to speed up the core flow through the laboratory. Measurement of discrete samples was performed using both the Molspin and the Japanese spinner magnetometers. Two or three 7-cm^3 samples from each section of Hole 882A were demagnetized in five steps up to 30 mT. On one of these samples, the Japanese instrument also provided susceptibility and anhysteretic remanent magnetization (ARM) data. The multishot orientation devices were deployed in the upper parts of Holes 882A and 882B. Orientations were obtained for Cores 145-882A-4H to -12H in Hole 882A and for Cores 145-882B-4H to -11H, -17H to -19H, and -22H to -26H in Hole 882B. In Hole 882A, both the multishot and tensor tools were used, and orientations from the two devices agree to within 4°. Automated susceptibility measurements were performed at 5-cm (0–124.3 mbsf), 10-cm (124.3–144.8 mbsf), and 15-cm (144.8–398.3 mbsf) intervals on whole cores in conjunction with other measurements performed using the multisensor track (MST).

Results

Pass-through measurements of NRM, after 15 mT demagnetization, and whole-core susceptibility are shown in Figure 8 for Hole 882A. Remanence intensities are reasonably high in the upper part of Hole 882A and decrease gradually with depth to 105 mbsf, where intensity abruptly falls off. Mean intensities after demagnetization are about 75 mA/m from 0 to 30 m (varying between 30 and 150 mA/m), 40 mA/m from 30 to 105 m (varying between 5 and 130 mA/m), and less than 10 mA/m from 105 to 398 m. The new core barrel used at this site did not appear to carry a significant remanent magnetization, because the consistent drilling overprint observed at Site 881 was not seen at Site 882. Discrete sample demagnetizations (Figs. 9B and 9C) show that overprints were usually small and consistent with being a viscous component. In both the whole core and discrete samples, the remanent intensity drops by almost an order of magnitude below about 105 mbsf (Fig. 8). In fact, samples were too weak to measure on the spinner magnetometers. This NRM transition coincides with changes of values in many of the other physical properties. It also coincides with the decrease in clay content and percentage of ash layers at the boundary between lithologic Subunits IA and IB.

Whole-core susceptibility measurements again show numerous discrete peaks superimposed on a background value (Fig. 8). These peaks often appear to coincide with the many ash layers, especially the black and brown ash layers. In a similar fashion to the NRM signal, the background susceptibility signal shows a considerable and abrupt decrease at approximately 105 mbsf. For many depth intervals, the susceptibility is below the detection limit. Coincident with this decrease is a drop-off in the frequency and amplitude of discrete susceptibility peaks associated with ash layers.

Measurements of (ARM) demagnetization made on the Japanese spinner magnetometer also show an abrupt change in magnetic properties at 105 mbsf (Fig. 10). Above 105 mbsf, the ARM, imparted in 40 mT AF and 0.03 mT DC field, is in the range of 10^{-4} kA/m (an order of magnitude greater than the NRM). In the deeper portions of the hole, the ARM is more than an order of magnitude weaker (10^{-6} kA/m). In fact, the instrument is incapable of imparting an ARM greater than the noise inherent in the demagnetization and measurement processes. The demagnetization of ARM shows the saw-toothed pattern typical of spurious ARM imparted during demagnetization. Therefore, sediments between 105 and about 300 mbsf often exhibit no stable remanence properties.

With the exception of disturbed parts of the cores, the sediments appear to record stable normal and reversed field directions in the first 105 m of Hole 882A (the axial dipole field inclination is about ±68° at a latitude of 51°11′N) and the six measured cores of Hole 882B (Table 6). For the most part, the discrete sample demagnetizations show a straight line to the origin on the Zijderfeld plots after removal of an overprint between 5 and 10 mT (Figs. 9B and 9C). However, within this depth interval, discrete sample demagnetizations revealed

Table 4. Composite depth model for Site 882 generated by splicing sections from the offset Hole 882B across core breaks in the main hole, Hole 882A.

Hole 882A		Hole 882B			
Core, section, interval (cm)	(Depth) (mbsf)	Core, section, interval (cm)	(Depth) (mbsf)	Interval thickness (m)	Cumulative composite depth (mbsf)
		1H-1, 0	(0.00)		
		1H-2, 65	(2.14)	2.14	2.14
1H-1, 150	(1.50)				
1H-6, 115	(8.65)			7.15	9.29
		2H-2, 144	(7.35)		
		2H-5, 20	(10.59)	3.24	12.53
2H-2, 140	(10.32)				
2H-8, 15	(18.07)			7.75	20.28
		3H-3, 149	(18.40)		
		3H-5, 5	(19.94)	1.54	21.82
3H-1, 20	(18.49)				
3H-5, 144	(25.74)			7.25	29.07
		4H-2, 50	(25.40)		
		4H-4, 109	(28.99)	3.59	32.66
4H-1, 45	(28.24)				
4H-7, 40	(37.19)			8.95	41.61
		5H-3, 145	(37.35)		
		5H-5, 80	(39.70)	2.35	43.96
5H-2, 60	(39.40)				
5H-7, 30	(45.51)			6.11	50.07
		6H-2, 109	(45.00)		
		6H-4, 115	(48.05)	3.05	53.12
6H-1, 35	(47.15)				
6H-7, 5	(55.84)			8.69	61.81
		7H-3, 85	(55.75)		
		7H-4, 45	(56.85)	1.10	62.91
7H-1, 40	(56.70)				
7H-7, 20	(65.50)			8.80	71.71
		8H-3, 65	(65.04)		
		8H-4, 137	(67.27)	2.23	73.94
8H-1, 90	(66.69)				
8H-7, 5	(74.85)			8.16	82.10
		9H-3, 25	(74.15)		
		9H-4, 82	(76.21)	2.06	84.16
9H-1, 45	(75.75)				
9H-7, 15	(84.44)			8.69	92.85
		10H-3, 75	(84.15)		
		10H-4, 104	(85.94)	1.79	94.64
10H-1, 25	(85.05)				
10H-7, 20	(94.00)			8.95	103.59
		11H-3, 30	(93.19)		
		11H-4, 55	(94.94)	1.75	105.34
11H-1, 35	(94.65)				
11H-7, 45	(103.75)			9.1	114.44
		12H-3, 20	(102.60)		
		12-H4, 10	(104.00)	1.40	115.84
12H-1, 35	(104.15)				
12H-6, 75	(112.05)			7.9	123.74
		13H-2, 90	(111.29)		
		13H-4, 90	(114.29)	3.0	126.74
13H-1, 100	(114.30)				
13H-7, 35	(122.65)			8.35	135.09
		14H-2, 139	(121.29)		
		14H-5, 5	(124.44)	3.15	138.24
14H-2, 30	(124.60)				
14H-7, 35	(132.15)			7.55	145.79
		15H-3, 25	(131.14)		
		15H-4, 104	(133.44)	2.30	148.09
15H-1, 85	(133.15)				
15H-6, 104	(140.85)			7.70	155.79
		16H-2, 116	(140.06)		
		16H-4, 42	(142.32)	2.26	158.05
16H-1, 70	(142.50)				
16H-6, 56	(149.86)			7.36	165.41
		17H-2, 49	(148.89)		
		17H-5, 23	(153.12)	4.23	169.64
17, 1H-134	(152.64)				
17H-7, 27	(160.57)			7.93	177.57
		18H-3, 102	(160.42)		
		18H-4, 117	(162.07)	1.65	179.22
18H-1, 70	(161.50)				
18H-7, 20	(170.00)			8.50	187.72
		19H-3, 67	(169.56)		
		19H-6, 1	(173.40)	3.84	191.56
19H-2, 20	(172.00)				
19H-7, 23	(179.53)			7.53	199.09
		20H-3, 9	(178.48)		
		20H-4, 51	(180.40)	1.92	201.01
20H-1, 27	(180.07)				
20H-6, 140	(188.71)			8.64	209.65
		21H-3, 10	(188.00)		
		21H-3, 98	(188.88)	0.88	210.53

Table 4 continued.

Hole 882A		Hole 882B			Cumulative
Core, section, interval (cm)	(Depth) (mbsf)	Core, section, interval (cm)	(Depth) (mbsf)	Interval thickness (m)	composite depth (mbsf)
21H-1, 14	(189.44)				
21H-6, 135	(198.16)			8.72	219.25
		22H-2, 65	(196.54)		
		22H-7, 6	(203.45)	6.91	226.16
22H-1, 4	(198.84)				
22H-6, 126	(207.56)		8.72	234.88	
		23H-2, 26	(205.65)		
		23H-3, 99	(207.89)	2.24	237.12
23H-1, 27	(208.57)				
23H-7, 80	(218.10)			9.53	246.65
		23H-7, 50	(213.40?)		
		24H-3, 72	(217.11)	3.71	250.36
24H-1, 61	(218.41)				
24H-7, 37	(227.17)			8.76	259.12
		25H-1, 91	(223.81)		
		25H-3, 117	(227.07)	3.26	262.38
25H-1, 47	(227.76)				
25H-7, 20	(236.50)			8.74	271.12
		26H-3, 110	(236.50)		
		26H-4, 9	(236.98)	0.48	271.60
26H-1, 42	(237.22)				
26H-7, 47	(246.26)			9.04	280.64
		27H-2, 131	(244.71)		
		27H-4, 135	(247.75)	3.04	283.68
27H-1, 99	(247.29)				
27H-7, 45	(255.75)			8.46	292.14
		28H-3, 46	(254.86)		
		28H-6, 117	(260.07)	5.21	297.35

unstable behavior (Figs. 9A and 9D) in some localized regions (notably, 40.0–44.0 mbsf, 46.8–48.5 mbsf, 54.3–56.3 mbsf, 83.0–85.0 mbsf). Samples from these zones proved susceptible to the acquisition of ARM in the demagnetization process. These zones corresponded to the position of short normal events in the measured whole-core magnetization. These events almost certainly represent a remagnetization of the whole core in the small DC field present in the demagnetization coils of the pass-through system. Therefore, the sample results were useful to help distinguish polarity events that are artifacts from those that are more reliable in the whole-core magnetostratigraphy. In this fashion, the whole-core data magnetostratigraphy was interpreted. As is customary, data at core breaks and other disturbed parts of the core were removed before the final interpretations were made. Aside from the above problem depth intervals, the discrete sample directions after demagnetization at 30 mT show almost perfect agreement with the whole core result (Fig. 9).

Hole 882B data (0–51.8 mbsf) show good agreement with Hole 882A (Fig. 11) and the Brunhes/Matuyama reversal occurring at practically the same depth (35.3 mbsf in Hole 882B compared with 35.5 mbsf in Hole 882A). Measurement of Hole 882B was terminated within the Jaramillo normal chron.

Below 105 mbsf in Hole 882A, the NRM drops by about an order of magnitude and the directional results become noisy and inconsistent. However, between about 300 and 400 mbsf, the signal picks up again and stable magnetic polarity stratigraphy is obtained once again. This rise in intensity is associated with an increase in clay content.

Discussion

A magnetostratigraphic interpretation of the whole core inclination records (Fig. 11) was made after editing the data. The magnetic record of Hole 882A showed a simple magnetostratigraphy that easily could be matched to the time scale of Cande and Kent (1992) as far back as the Matuyama/Gauss boundary at approximately 98 mbsf. Magnetostratigraphic interpretation of the magnetization data from between 105 and 300 mbsf is not possible. However, from 300 mbsf to the base of Hole 882A at 398.3 mbsf, a coherent magnetostratigraphy emerges (Fig. 12). The polarity sequence contains just three substantial normal periods separated by reversed polarities. Unfortunately, this simple sequence is not sufficiently diagnostic to place its location uniquely on the polarity timescale. However, the biostratigraphy suggests that the ages must lie in the range 4 to 8 Ma. Considering the mean duration of polarity chrons within this time interval and the small number of reversals recorded, it is clear that the time interval represented in the last 100 m of Hole 882A is short compared to these limits and that the sedimentation rate is still, therefore, substantial. Possible interpretations of this reversal sequence are considered in the "Sedimentation Rate" section (this chapter).

SEDIMENTATION RATES AND FLUXES

Sedimentation Rates

Rates of sedimentation at Site 882 can be calculated with reasonable confidence only for the upper half of the 400-m section. For the upper time-stratigraphic unit (0–98 mbsf), magnetostratigraphy and biostratigraphy agree well, and the average linear rate of sedimentation is 38 m/m.y. (Fig. 13). That interval was selected for calculation purposes because its base, which is coincident with the Matuyama/Gauss paleomagnetic boundary, lies only 7 m shallower than the level chosen to separate lithologic Subunits IA (clayey diatom ooze) and IB (diatom ooze). Variability of sedimentation rate within that interval is likely to be of shorter term because, for example, the section containing the Olduvai Subchron appears to be unusually short. Thus, our estimate of the average sedimentation rate for the upper interval is a minimum. Based only on biostratigraphy, the rate for the upper part of the underlying diatom ooze is 107 m/m.y. (Fig. 13). That result is heavily dependent on the last occurrence of the diatom *Thalassiosira jacksonii* at 175 mbsf (= 3.3 Ma), which we assume to be accurate because it is a middle- to high-latitude species whose last occurrence is closely tied to magnetostratigraphy in the Sea of Japan (Koizumi, 1992). As noted in Figure 13 and Table 5, the diatom ooze between 175 and 303 mbsf lacks magnetostratigraphic datum levels and contains only a few biostratigraphic datum levels, which leaves its age relatively unconstrained.

Significant magnetic reversals again become common below 303 mbsf, which based on biostratigraphy and correlations with Site 884 (Table 5 and Site 884 chapter, Table 6) are assumed to represent the lower three normally magnetized events of Gilbert reversed-polarity-chron (Chron C3n.2n–C3n.4n). Placing the top of normal-polarity Subchron C3n.2n (4.265 Ma) at 303 mbsf results in average sedimentation rates of 125 m/m.y. for the interval between 175 and 303 mbsf (3.3–4.265 Ma) and 66 m/m.y. for the interval cored between 303 and 398 mbsf at Site 882 (4.265–ca. 5.9 Ma) (Fig. 13).

Sediment Fluxes

Sediment fluxes, or mass accumulation rates, were determined in the conventional way, taking the product of the sedimentation rate, the dry-bulk density, and the concentration of the sediment component. Average fluxes were calculated for four time-stratigraphic intervals, which are delimited by dashed lines in Figure 13. At the boundaries of those intervals, evidence can be seen of significant changes in rate of sedimentation, dry-bulk density, and sediment composition, each of which can influence flux. Raw data for each of these intervals were averaged and are presented in Table 7. Dry-bulk density values were taken from pycnometer measurements, and sedimentary component data come from smear slide estimates, with the exception of percentages of carbonate and total organic carbon (TOC), which were measured analytically. Flux results (in $g/[cm^2 \cdot k.y.]^{-1}$) for diatoms, clay, glass, quartz, and carbonate are listed in Table 7 and are shown as histograms along the right axis of Figure 13 (TOC fluxes are too close to zero to be visible in the histograms). Additional errors may stem from the assumption that the abundance estimates are directly proportional to the weight percentage of each sedimentary component. Thus, taking the 0 to 2.6 Ma interval, for example, we assume that an average of 75% diatoms translates directly to 0.75 g diatoms per gram of bulk sediment. The resultant diatom (opal) flux for that interval, ~1.7 $g(cm^2 \cdot k.y.)^{-1}$, is greater than either the glacial or interglacial opal fluxes (0.5 and 1.5 $g[cm^2 \cdot k.y.]^{-1}$, respectively) in a piston core from nearby Meiji Seamount (Keigwin et al., 1992).

Histograms on the right in Figure 13 show average sediment fluxes for the four time-stratigraphic intervals. Evidently, the flux of minor lithological components changed at 2.6 Ma, when the youngest interval received a higher flux of clay and a lower flux of carbonate. However, the most significant result of this analysis is that there must have been an early Pliocene maximum in opal (diatom) flux. Calculated diatom fluxes for the age model are 4.7 $g(cm^2 \cdot k.y.)^{-1}$, almost three times higher than the Pleistocene flux. If the early Pliocene flux was truly as high as 4.7 $g(cm^2 \cdot k.y.)^{-1}$, then it was about twice the modern Southern Ocean flux (as measured by DeMaster, 1981).

INORGANIC CHEMISTRY

Fifteen interstitial water samples were collected from Hole 882B at depths ranging from 1.45 to 257.35 mbsf. Analytical results are listed in Table 8. The pore water samples span all of lithologic Subunit IA (0–100 mbsf), which comprises diatom ooze, clayey diatom ooze, and frequent volcanic ash layers (see "Lithostratigraphy" section, this chapter). Only the upper half of Subunit IB (100–~400 mbsf), largely diatom ooze, was sampled for pore waters as a consequence of failure of the APC and early termination of drilling at this site.

Chloride concentrations in interstitial waters at Site 882 range from near the Pacific deep-water value (554 mM) in the shallowest sample (1.45 mbsf) to a maximum of 569 mM at 19.85 mbsf (Fig. 14A). The profile shows relatively high concentrations in the upper 70 m and a gradual, slight decrease at greater depths. This distribution provides a particularly good illustration of the ongoing adjustment of the Cl^- concentration in pelagic pore waters to variations in the mean salinity of the ocean. The near-surface decline can be attributed to the freshening of the ocean during the last deglaciation, whereas the deeper portion of the profile reflects the downward propagation of the higher mean salinity characteristic of the Quaternary age (McDuff, 1985).

The oxidant demand associated with the moderate Quaternary accumulation rates of organic carbon at Site 882 (see "Sedimentation Rates and Fluxes" section, this chapter) is sufficient to deplete oxygen by about 10 mbsf, as shown by the measurable presence of NO (0.25 µM) at 10.35 mbsf (Table 8). No nitrite was detected in the samples immediately above or below this horizon, suggesting that the base of the nitrate reduction zone lies between 10.35 and 19.85 mbsf. The dissolved manganese profile supports this interpretation. Maximum concentrations occur in the sample collected at 19.85 mbsf (Table 8), indicating that MnO_2 dissolution is most pronounced near (and probably slightly above) this depth. High, uniform concentrations persist to ~40 mbsf, below which the values decline (Fig. 14B). The minimum present in the profile between ~150 and 200 mbsf suggests that Mn is actively being consumed in this interval, presumably via precipitation of an authigenic carbonate phase such as rhodochrosite ($MnCO_3$) or, more likely, kutnahorite $(Mn,Ca)CO_3$. The increase in the dissolved manganese content below 200 mbsf implies that Mn^{2+} is actively diffusing upward from a source at a greater depth.

Titration alkalinity increases from ~3.5 mM in the uppermost sample to ~7 mM at about 50 mbsf (Fig. 14C). Values are essentially constant below this depth. The upward convexity in the profile between 1.5 and 50 mbsf indicates that the highest rate of production of alkalinity (mostly bicarbonate ion at the pH measured in the samples; Table 8) is occurring in this relatively shallow zone. The SO_4^{2-} content at Site 882 decreases to ~20 mM by 80 mbsf (Fig. 14D). This decline is more severe than that seen at Site 881, suggesting that a higher oxidant demand is furnished by the organic matter buried at this shallower location. The approximately linear sulfate profile between 1.5 and 20 mbsf indicates control by diffusion and an apparent lack of significant sulfate reduction in this zone. Downward concavity in the profile between ~30 and 105 mbsf indicates that the rate of reduction is highest in this interval. The reduction of SO_4^{2-} is normally

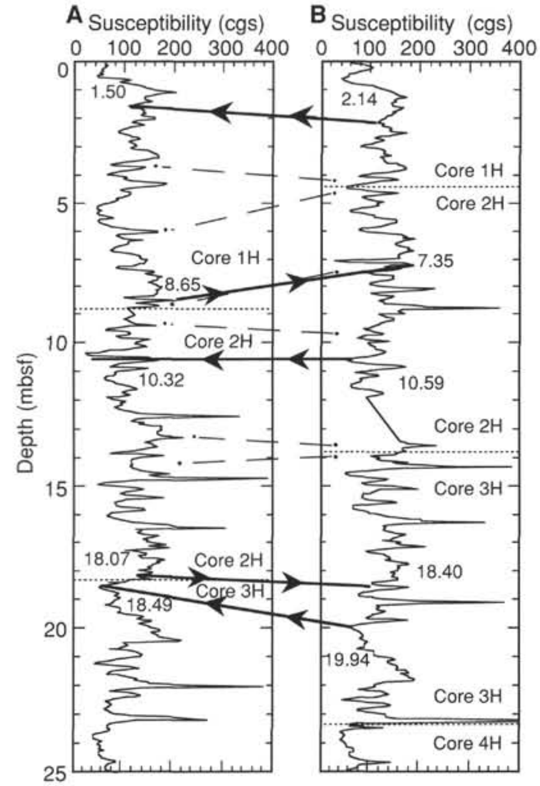

Figure 6. Depth correlation between Holes 882A (**A**) and 882B (**B**) for the upper 25 m, based on magnetic susceptibility curves. Depths of switch-points between holes are indicated. For the between-hole "pathway" of the composite depth (heavy line with arrows), compare with Table 4. Estimated gaps between piston cores from Holes 882A and 882B (Table 2; Fig. 5) are based on GRAPE data correlations (dashed lines). Dotted lines indicate core breaks.

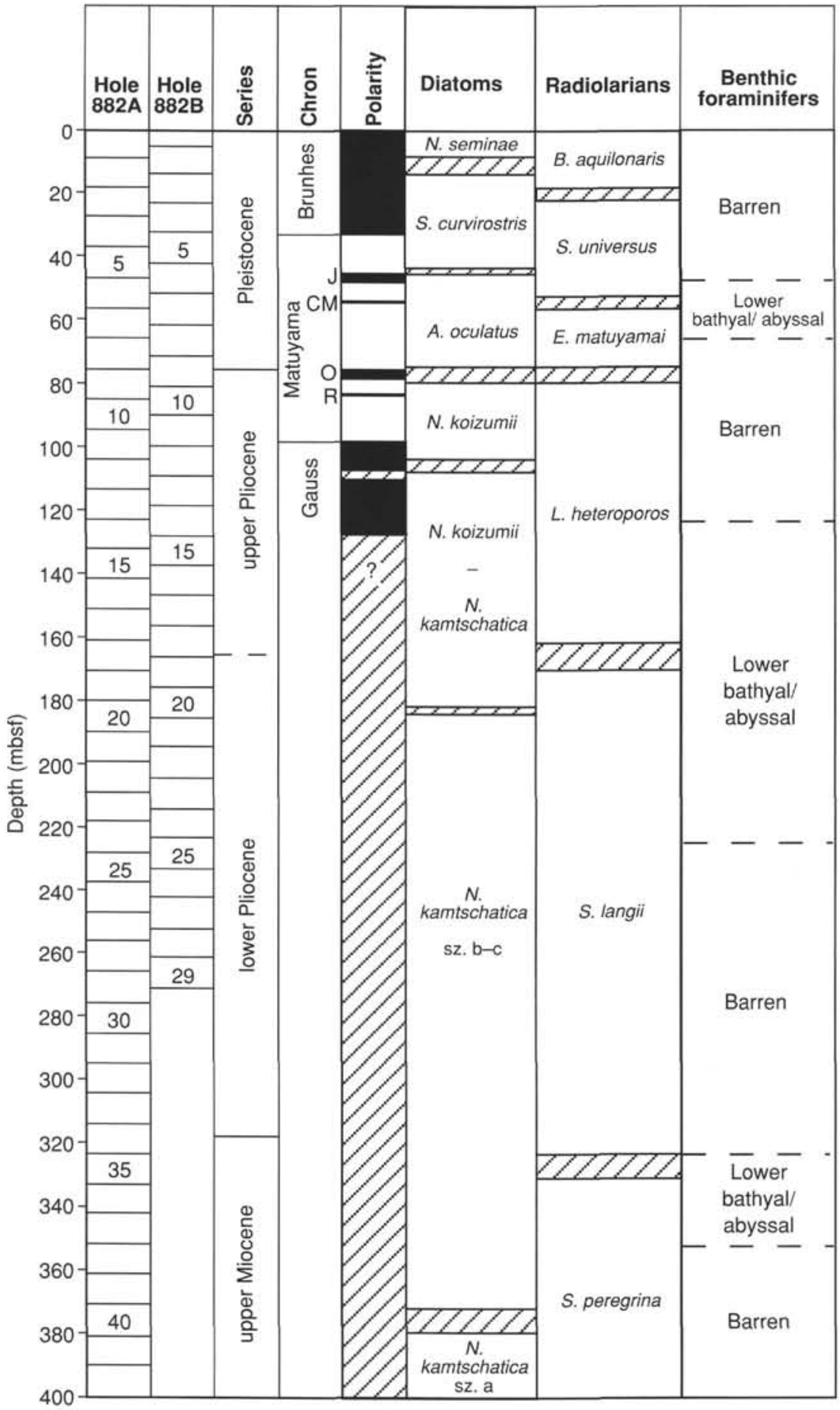

Figure 7. Stratigraphic position of cores, placement of magnetostratigraphic chrons and subchrons, and placement of diatom and radiolarian zones in Holes 882A and 882B. Intervals filled by slanted lines indicate uncertainty in the placement of biostratigraphic boundaries.

matched by a charge-equivalent production of alkalinity. Thus, the reduction of ~8 mM of SO_4^{2-}, as seen in the upper 100 m at Site 882, should be matched by a 16-mmol increase in alkalinity (as HCO_3^-), rather than the ~5 mmol increase actually measured. The sink for the "missing" 11 mmol of alkalinity can be largely attributed to the precipitation of authigenic calcite, which is indicated by the Ca^{2+} profile, as discussed below.

Dissolved ammonium increases progressively with depth at Site 882 (Fig. 15A). Significant upward convexity marks the interval between ~20 and 70 mbsf as being the main zone of release of NH_3 to solution. This is consistent with the sulfate distribution, which indicates that the highest rate of anaerobic decomposition occurs throughout approximately the same depth range. A deep source of upwardly diffusing ammonium is indicated by the linear increase with depth below ~100 mbsf.

Unlike at Site 881, dissolved calcium and magnesium are not oppositely distributed in Site 882 pore waters (Fig. 15B). Dissolved magnesium shows only limited variation with depth. In contrast, the

Table 5. Age and stratigraphic position of radiolarian (R), diatom (D) and calcareous nannofossil (N) datum levels in Holes 882A and 882B.

Sample no.	Datum	CK92 (Ma)	Hole 882A interval	Depth (mbsf)	Hole 882B interval	Depth (mbsf)
R1	LO *Lychnocanoma grande*	0.05	/1H-CC	/8.8	/1H-CC	/4.4
D2	LO *Simonseniella curvirostris*	0.30	1H-CC/2H-CC	8.8/18.3	1H-CC/2H-CC	4.4/13.9
R2	LO *Druppatractus acquilonius*	0.35	1H-CC/2H-CC	8.8/18.3	2H-CC/3H-CC	13.9/23.4
R3	LO *Stylatractus universus*	0.45	2H-CC/3H-CC	18.3/27.8	2H-CC/3H-CC	13.9/23.4
N3	LO *Pseudoemiliania lacunosa*	0.49	3H-CC/5H-CC	27.8/46.8	1H/4H-CC	4.4/32.9
R5	LO *Eucyrtidium matuyamai*	1.05	5H-CC/6H-CC	46.8/56.3	6H-CC/7H-CC	51.9/61.4
D5	LCO *Actinocyclus oculatus*	1.00	4H-CC/5H-CC	37.3/46.8	5H-CC/6H-CC	42.4/51.9
D6	FO *Simonseniella curvirostris*	1.58	7H-CC/8H-CC	65.8/75.3	8H-CC/9H-CC	70.9/80.4
D	LO *Pyxidicula horridus*	1.8	7H-CC/8H-CC	65.8/75.8	9H-CC/10H-CC	80.4/89.9
R7	FO *Eucyrtidium matuyamai*	1.9	8H-CC/9H-CC	75.3/84.8	9H-CC/10H-CC	80.4/89.9
D9	LO *Neodenticula koizumii*	2.0	8H-CC/9H-CC	75.3/84.8	9H-CC/10H-CC	80.4/89.9
D12	LCO *Neodenticula kamtschatica*	2.63–2.7	11H-CC/12H-CC	103.8/113.3	11H-CC/12H-CC	99.4/108.9
D13	FO *Neodenticula seminae*	2.7	11H-CC/12H-CC	103.8/113.3	11H-CC/12H-CC	99.4/108.9
R8	FO *Cycladophora davisiana*	2.8			13H-CC/14H-CC	118.4/127.9
R9	LO *Stichocorys peregrina*	2.9	17H-CC/18H-CC	160.8/170.3	17H-CC/18H-CC	156.4/165.9
D14	LO *Thalassiosira marujamica*	3.2	16H-CC/17H-CC	151.3/160.8	17H-CC/18H-CC	156.4/165.9
D15	LO *Thalassiosira jacksonii*	3.3	18H-CC/19H-CC	170.3/179.3	17H-CC/18H-CC	156.4/165.9
R10	LO *Stichocorys delmontensis*	3.55			17H-CC/18H-CC	156.4/165.9
N15	LO *Reticulofenestra pseudumbilica*	3.71	15H-CC/16H-CC	141.8/151.3	16H-CC/17H-CC	146.9/156.4
D17	FO *Neodenticula koizumii*	3.75	19H-CC/20H-CC	179.8/189.3	19H-CC/20H-CC	175.4/184.9
D18	FO *Actinocyclus oculatus*	3.8	20H-CC/21H-CC	189.3/198.9	20H-CC/21H-CC	184.9/194.4
R11	LO *Theocorys redondoensis*				20H-CC/21H-CC	184.9/194.4
R12	FO *Lamprocyrtis heteroporos*	4.6	34H-CC/35H-CC	322.3/331.8		
D18A	LO *Thalassiosira plicata*	4.6	34H-CC/35H-CC	322.3/331.8		
D19	FO *Thalassiosira latimarginata*	5.05	36H-CC/37H-CC	341.3/350.8		
D21	FO *Thalassiosira oestrupii*	5.4	39H-CC/40H-CC	369.9/379.3		
D23	LO *Thalassiosira miocenica*	5.7	40H-CC/41H-CC	379.3/388.8		
D24B	FO *Thalassiosira miocenica*	6.3	>42H-CC	>398.8		

Samples constraining each datum level are separated by a slash (/), as are the sub-bottom depths (mbsf) of these samples. LO = last occurrence; LCO = last common occurrence; FO = first occurrence. CK92 refers to the Cande and Kent (1992) geomagnetic polarity time scale.

calcium content decreases smoothly by about 40% (~4 mM) between 0 and ~120 mbsf. Downward concavity in the profile indicates that Ca^{2+} is being removed most markedly from solution in the depth interval 30–120 mbsf. Precipitation of authigenic calcite is clearly indicated by these data. Assuming similar rates of diffusion of Ca^{2+} and dissolved carbonate species, about 8 mM of the "missing" 11 mM of alkalinity can be accounted for by the removal of 4 mM of calcium from solution to calcite. Three millimoles per liter of alkalinity are left unaccounted for by this calculation, which suggests that the precipitating phase might not be pure calcite. The inclusion of dolomite precipitation in this mass balance can readily account for the residual "missing" alkalinity, and, in fact, dolomite authigenesis is implied by the dissolved Mg^{2+} profile, which indicates slight depletion of magnesium at depth, particularly in the interval between 20 and 80 mbsf.

The dissolved silicate concentration in the topmost pore water sample at Site 882 (~842 µM) is sharply higher than in the overlying North Pacific Ocean bottom water (~160 µM), reflecting pronounced dissolution of opaline skeletons near the sediment/water interface (Fig. 15C). The concentration remains high and varies little with depth, suggesting that the pore waters throughout the sampled section are saturated with respect to biogenic opal.

Sodium (calculated by charge balance at this site) and potassium show little variation in the pore waters downcore, with concentrations being near those in seawater (Fig. 15D). A very slight, approximately linear decline in the K^+ content throughout the sampled section indicates minor diffusion toward greater depths, possibly reflecting exchange with basaltic basement.

The strontium concentration in the uppermost pore water sample is the same as in modern seawater (87 µM; Fig. 16). Unlike most other elements measured at this site, the Sr^{2+} content slowly increases with depth, reaching a maximum concentration of 108 µM at 257 mbsf. The source of this element is unclear. The near linearity of the profile implies that the strontium may be diffusing from a deeper (unsampled) source.

The lithium content in the shallowest sample in Hole 882B is the same as in modern seawater at 27 µM (Fig. 16). A slight depletion in dissolved Li at shallow depths may reflect uptake by clay minerals, which are relatively abundant in the upper 100 m at this location (see "Lithostratigraphy" section, this chapter). The concentration is invariant below 150 mbsf, where diatom oozes are essentially the sole lithology. These data give no indication that dissolution of opal releases lithium to solution (see Gieskes, 1981, p. 156), suggesting that lithium is largely unreactive in rapidly accumulating diatom oozes.

ORGANIC GEOCHEMISTRY

Volatile Hydrocarbons

The shipboard safety and pollution program requires a real-time monitoring of the light hydrocarbon gases C_1 (methane), C_2 (ethane), and C_3 (propane) immediately after retrieval of cores. Seventy-one samples were taken from Hole 882A and 882B sediments using the headspace technique, and gases were measured in a Carle gas chromatograph. The results are presented in Table 9. Methane concentrations were low (between 3 and 28 ppm), indicating no significant methanogenesis in the sediment column. Ethane and propane were not detected. The low amounts of volatile gases in the sediments can be ascribed to the low concentration of organic matter measured in the samples (see below).

Carbonate Carbon

Samples for inorganic carbon (IC) determination were obtained only from Hole 882A. The Coulometrics carbon dioxide coulometer was used to analyze 143 samples. The results are given in Table 10.

The calcium carbonate content is highly variable with depth in the sediments at Site 882, ranging between 0 and 40 wt% (Fig. 17). Based on the carbonate record, the sedimentary sequence can be divided into three intervals. The first corresponds fairly well to lithologic Subunit IA (see "Lithostratigraphy" section, this chapter). Most of the values are near zero and only a few samples show $CaCO_3$ contents of up to 30 wt%. These spikes are caused by foraminifer-rich layers that occur in the upper 100 m of the sediment column. The second interval, between 100 and 230 mbsf, is characterized by high variability in

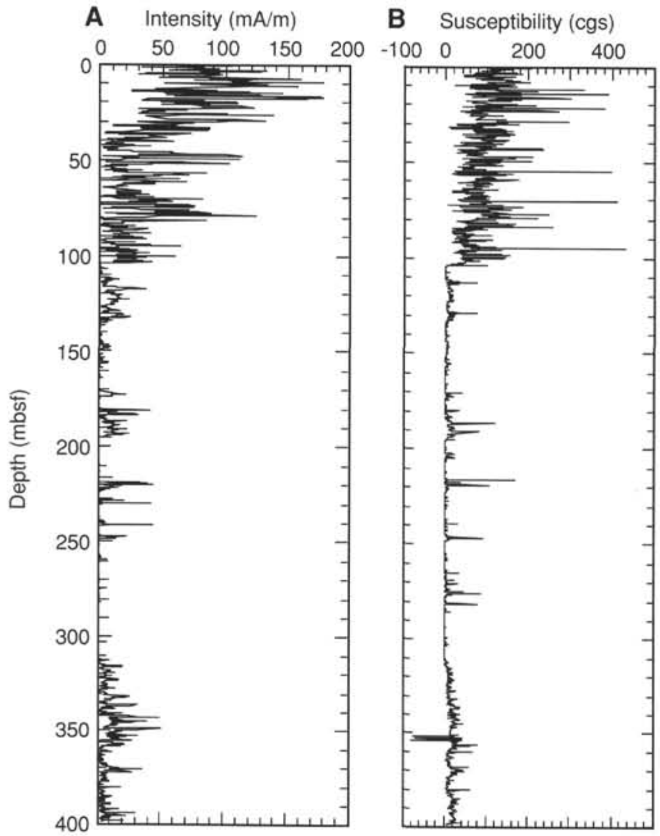

Figure 8. NRM intensities after demagnetization at 15 mT from Hole 882A (**A**) compared with whole-core susceptibility (**B**).

carbonate concentration; only a few samples contain no $CaCO_3$. As shown in Figure 17, this interval corresponds well with the high abundance of calcareous nannofossils recorded between 115 and 205 mbsf (2.9–4.3 Ma; see "Biostratigraphy" section, this chapter). Carbonate contents range from 0 to 10 wt% in the lower third of the sediment section (230–398 mbsf; Fig. 17). Two single spikes containing up to 24 wt% carbonate can probably be correlated to layers with abundant nannofossils as described in the "Biostratigraphy" section (this chapter) for this depth interval.

Organic Carbon

The concentration of total organic carbon was calculated by difference between total carbon (TC) determined by the NCS-Analyzer and inorganic carbon (IC) measured by coulometry. Results for 111 samples collected from Hole 882A are presented in Table 10.

The total organic carbon pattern of this site is comparable to that of the previous Site 881; values are low, ranging between 0.1 and 0.5 wt%, and no depth-related trend is visible (Fig. 18). Total nitrogen contents are commonly near or below the detection limit of the NCS analyzer, precluding discussion of the TOC/TN ratios regarding the composition and provenance of the organic matter.

PHYSICAL PROPERTIES

Continuous measurements on whole-round sections of GRAPE bulk density, magnetic susceptibility, and P-wave velocities were taken in both Holes 882A and 882B. Thermal conductivity was measured at 3-m intervals in Cores 145-882A-1H through -13H and 145-882A-28H through -42H, and also in Cores 145-882B-14H through -29H. Index properties (wet-bulk density, dry-bulk density, wet porosity, dry porosity, wet water content, dry water content, and void ratios) were measured at approximately 75-cm intervals in Cores 145-882A-1H through -16H, at 1.5-m intervals in Cores 145-882A-17H through -42H, and at 1.5-m intervals in cores from Hole 882B. Shear strength was measured at 1.5-m intervals in Hole 882A and at 4.5-m intervals in Hole 882B. Digital sound velocimeter (DSV) measurements were taken at 1.5-m intervals in Cores 145-882A-1H through -9H, and Hamilton Frame velocities in cores 145-882A-9H through -42H. Velocity was measured in Hole 882B once per core. Results of the physical properties and vane shear strength from Site 882 are summarized in Tables 11 and 12.

Profiles of index properties (Figs. 19 through 23) and shear strength (Fig. 24) for Holes 882A and 882B show good correspondence. Wet-bulk density, dry-bulk density, wet porosity, and dry water content in the upper 105 mbsf generally vary between 1.13 and 1.61 g/cm^3, 0.275 and 0.96 g/cm^3, 62% and 88%, 65% and 350%, respectively. At about 105 mbsf in both holes, wet-bulk density and dry-bulk density decrease distinctly corresponding to an increase in wet porosity and dry water content. The decreased clay content at 105 mbsf (see "Lithostratigraphy" section, this chapter) could account for the changes noted. Below 105 mbsf, wet-bulk density and dry-bulk density increase downhole from about 1.1–1.2 to 1.4 g/cm^3 and 0.25–0.4 to 0.6 g/cm^3, respectively, corresponding to a decrease in wet porosity and dry water content. However, high values for the wet-bulk and dry-bulk densities were observed at the depth intervals of 130–140 mbsf, 190 mbsf, 220–230 mbsf, and 340–350 mbsf corresponding to lower values for wet porosity and dry water content, probably the result of the lower diatom content (see "Lithostratigraphy" section, this chapter). The upper 105 mbsf is also characterized by higher grain densities (2.4 and 2.8 g/cm^3), the result of increased clay content. Grain density profiles (Fig. 21) display trends similar to those seen in the wet- and dry-bulk density profiles, except that between 190 and 290 mbsf in Hole 882A values decrease slightly.

GRAPE bulk density data are plotted in Figure 21. GRAPE data have been smoothed using a 29-point moving average (see "Site 881" chapter, "Physical Properties" section, this volume). GRAPE bulk density and wet-bulk density for Holes 882A and 882B show good correspondence. GRAPE bulk density values were higher than those obtained from pycnometer analysis as in Site 881 (see "Physical Properties," Site 881 chapter, this volume).

Figures 22 and 23 show profiles of compressional wave velocity from the P-wave logger, the DSV, and the Hamilton Frame. The DSV and the Hamilton Frame values differ slightly from the P-wave logger data, probably the result of different direction of the measurement. The P-wave logger velocities were measured perpendicular to bedding on the whole cores, whereas the DSV and the Hamilton Frame velocities were measured through to bedding on the split cores and discrete samples. In the upper 105 mbsf, P-wave velocities range between 1440 and 1480 m/s. At 105 mbsf, the measured velocities increase. Below this point, P-wave velocities vary between 1480 and 1520 m/s, increasing downhole. The spiky nature of P-wave logger data may be attributed to the presence of ice-rafted debris, especially in the upper 105 mbsf.

Thermal conductivity data are shown in Figure 24. Thermal conductivities vary between 0.75 and 1.08 W/(m · °C). The profile for thermal conductivity generally mirrors the wet- and dry-bulk density profiles.

Shear strength results are presented in Table 12 and Figure 24. Shear strength values for Holes 882A and 882B correlate well. The increased spiky nature below 250–300 mbsf may be caused by disturbance of the sediment during coring. In the lower parts of the core, the shear strength values are higher, as would be expected.

SEISMIC-LITHOLOGIC CORRELATION

All the Leg 145 drilling locations were surveyed in order to drop the beacon at the proper pre-selected location. In every case, the surveys were run in the figure of the number 4 with the long leg duplicating the site-survey track line used to select the site and with

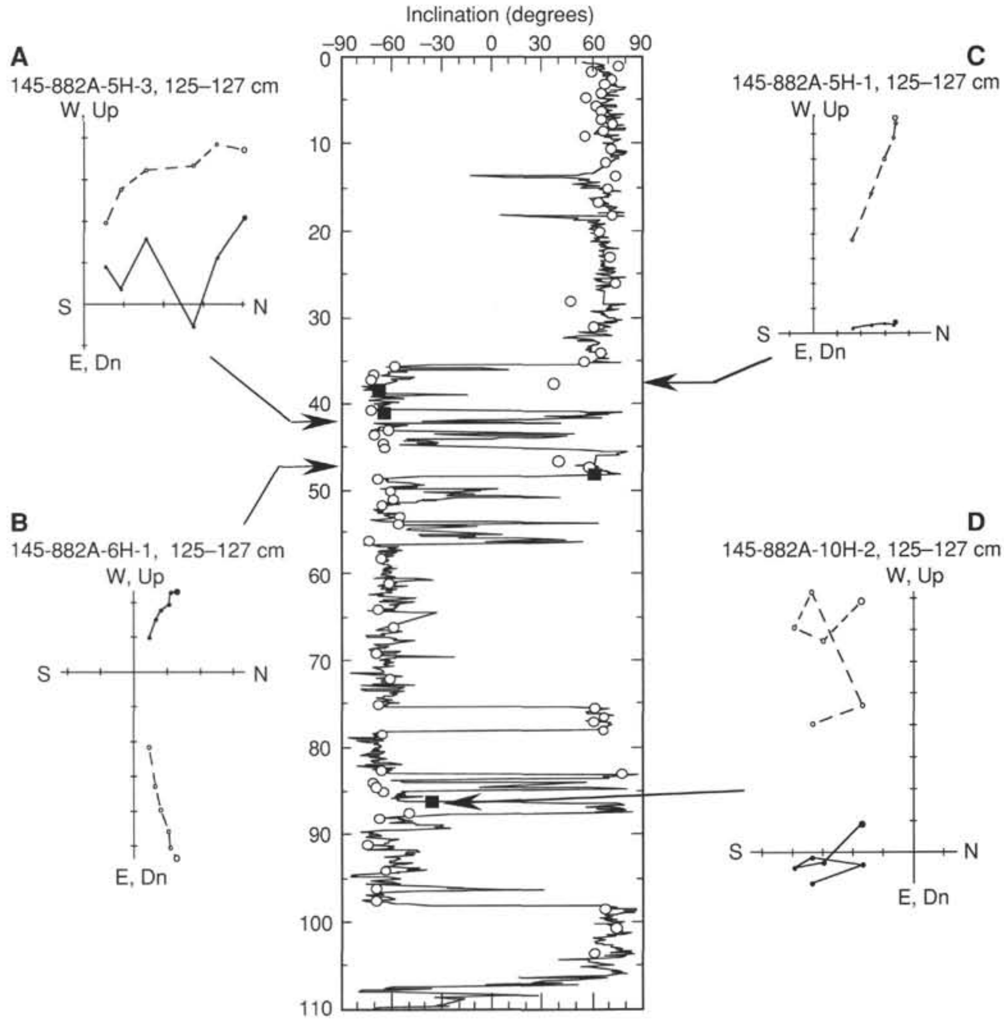

Figure 9. Comparison of results from whole-core measurements of NRM demagnetized at 15 mT (solid line) with results from discrete samples demagnetized to 30 mT (open circles). Examples of Zijderfeld plots are shown for samples presented as filled squares. (**A**) and (**D**) illustrate unstable behavior, thought to be responsible for spurious events in the whole core result. (**B**) and (**C**) illustrate stable behavior, which is predominant for this depth interval.

the cross-leg being as nearly orthogonal as practical. The shipboard air-gun seismic reflection profiling system was used for all the surveys except for Site 883 when it was inoperable; the 3.5-kHz profiling system was used to locate that drill site. Details of the survey and seismic processing techniques are given in the "Site 881" chapter ("Seismic-Lithologic Correlation" section, this volume).

The seismic reflection record crossing Site 882 (Fig. 25) shows approximately 1.1 s (two-way traveltime), about 900 m, of sediment overlying acoustic basement. Figure 25 shows the basement reflector at about 5.5 s. Overlying sediment layering conforms to the regional topography of Detroit Seamount (Fig. 2). Lithologic Subunit IB, the nearly pure diatom ooze, is characterized by a somewhat more acoustically transparent portion of the section than is Subunit IA, the silty diatom ooze with ash layers and dropstones.

SUMMARY AND CONCLUSIONS

Geologic Record

Sediments recovered at Site 882 are 398.3 m of diatom ooze of late Miocene through Quaternary age. The upper 105 m contains higher percentages of clay and relatively more ash layers and dropstones, forming the basis for dividing the section into two lithologic subunits. Subunit IA (0–105 mbsf) is clayey diatom ooze and diatom ooze with clay. The ooze is dark greenish gray and bioturbated. Clay averages roughly 10% of the sediment and occasionally reaches 20% abundance. Ash layers and dropstones are much more abundant in Subunit IA deeper in the section. The ash layers are light gray, reddish gray or black and range in thickness from 1 cm to several tens of centimeters thick. Layers thicker than about 5 cm have sharp lower contacts, burrowed or gradational upper contacts, and normally graded bedding. Dropstones range in size from coarse sand to well-rounded pebbles and are usually dark, fine-grained pieces of basalt. Lithologic Subunit IA is essentially devoid of calcium carbonate. Organic carbon concentrations are low, averaging 0.2% to 0.3% in this unit.

The boundary between the subunits is reasonably abrupt at Site 882; it is well displayed in the physical properties measurements and occurs in just one or two meters. Lithologic Subunit IB (105–398.3 mbsf) is a reddish-brown to greenish-gray bioturbated diatom ooze. Calcium carbonate in the form of nannofossils and micrite particles is an important minor component of much of this subunit, especially between about 105 and 230 mbsf. Below 230 mbsf, calcium carbonate is again in low abundance, although present in many samples. Organic carbon concentrations in Subunit IB are about 0.2%. Sponge spicules make up more than 10% of the sediment at 120–150 and 260–310 mbsf.

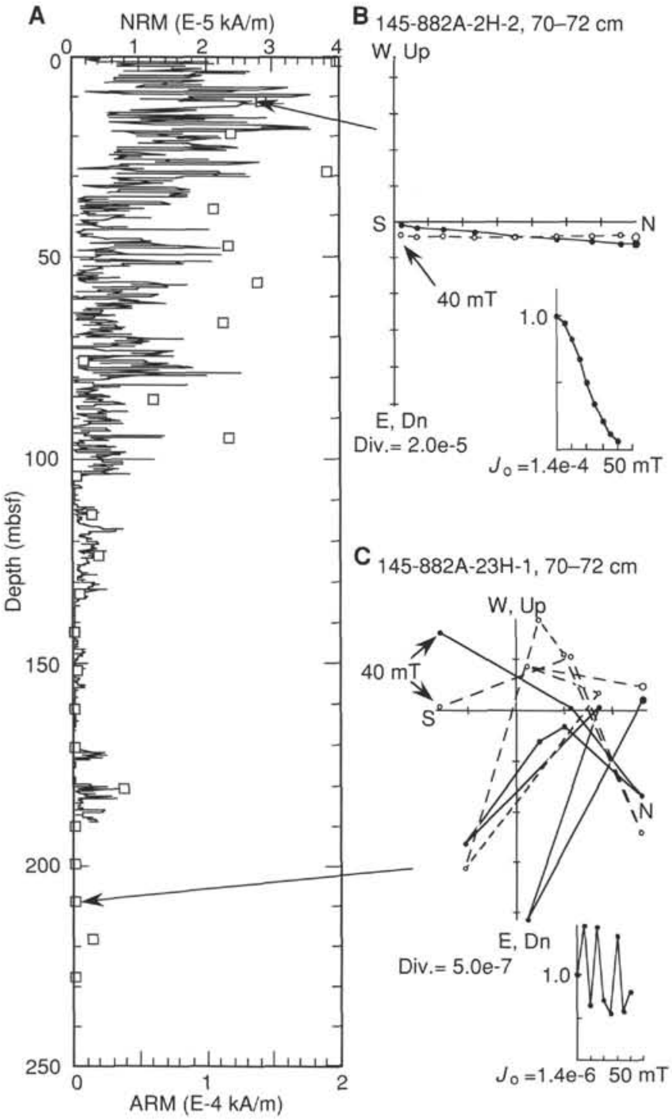

Figure 10. **A.** Comparison of the NRM, demagnetized at 15 mT, with an ARM given in 40 mT AF and 0.03 mT DC fields. **B.** Example Zijderfeld and J/J_0 plot of ARM demagnetization from the region of stable magnetization (0-105 mbsf). **C.** Example Zijderfeld and J/J_0 plot of ARM demagnetization from the region of unstable magnetization (105–300 mbsf).

A few ash layers occur at depths of 210–230 and 340–398 mbsf. Three dropstones occur in this subunit, the deepest at 359 mbsf—approximately 6 m.y. old.

Shipboard analyses of the physical properties of Site 882 sediments reveal a marked change at 105 mbsf. At that level, there is a distinct downward decrease in both wet- and dry-bulk densities and a downward increase in porosity and water content. Throughout the core, these properties can be related directly to diatom content, with the pure oozes having the highest porosities and lowest bulk densities.

Biostratigraphic zonations based on siliceous microfossils provide the basic stratigraphy at Site 882, with nannofossils providing some stratigraphic information in lower Pliocene sediments. Magnetic reversal stratigraphy is clear in the upper, more clayey portion of the core. Reversals related to the Brunhes/Matuyama boundary; Jaramillo, Olduvai, and Reunion events; and the Matuyama/Gauss boundary are clear. The Matuyama/Gauss reversal boundary occurs at the same position in the core as the boundary between lithologic Subunits IA and IB. Sedimentation rates based on biostratigraphic zonations and magnetic reversal stratigraphy are about 40 m/m.y. in sediments younger than 2 to 6 Ma, 107 to 125 m/m.y. in sediments between 2.6 and 4.3 m.y. old, and 66 m/m.y. in lower Pliocene and upper Miocene sediments.

Sediment mass accumulation rates range from 2 to 3 g(cm^2 · k.y.)$^{-1}$ through most of the section to more than 4 g(cm^2 · k.y.)$^{-1}$ during the time of extreme sedimentation rates in the early Pliocene. Fluxes of the individual sedimentary components reflect the influx of terrigenous material in Subunit IA and the extreme diatom flux in the upper portion of Subunit IB. Diatoms accumulated at 1.7 to 4.7 g(cm^2 · k.y.)$^{-1}$ and reached a maximum between about 3.3 and 4.3 Ma. The other biogenic components also reached flux maxima at this time: carbonate reached 0.35 g(cm^2 · k.y.)$^{-1}$, organic carbon fluxes reached about 0.01 g (cm^2 · k.y.)$^{-1}$. Very rapid burial may have acted to preserve these components in this high sedimentation-rate interval. The terrigenous components of the sediment, clay and quartz, accumulated at fairly low rates in the Miocene and Pliocene Subunit IB, but their mass accumulation rates double in the younger Subunit IA. The mass accumulation rate of volcanic ash increased by factor of 4 in sediments younger than the Matuyama/Gauss reversal boundary. At the same time, dropstone numbers increased from one every 10 cores in older sediments to an average of two or three dropstones per core in the upper Pliocene and Quaternary sediments.

Paleoceanography and Paleoclimatology

The late Miocene of the northwestern Pacific Ocean at Site 882 was characterized by ongoing deposition of diatom ooze at rates of 3 g(cm^2 · k.y.)$^{-1}$. The deposition of terrigenous clastics was minor, and there was a small but noticeable amount of volcanic ash accumulating in the sediment. The first/oldest important paleoceanographic event recorded at Site 882 was the increase in diatom flux that occurred during the early Pliocene warm interval, at linear sedimentation rates of up to 125 m/m.y. and corresponding fluxes of about 4.7 g(cm^2 · k.y.)$^{-1}$. These unusual conditions of high silica productivity continued for about 1 m.y. The region of this "diatom dump" is limited to the present subarctic North Pacific Ocean and the Bering Sea; a similar early Pliocene event may have occurred in the Antarctic Ocean region. Calcium carbonate and organic carbon fluxes also reached their maxima during the early and middle Pliocene, probably as a result of the unusual productivity conditions and because rapid burial would have retarded both the dissolution of calcite and the breakdown of organic carbon.

At 2.6 Ma, the fluxes of terrigenous materials, clays, and quartz increased several-fold, although the overall sedimentation rates were reduced. The late Pliocene and Pleistocene flux of these components was in the range of 250 mg(cm^2 · k.y.)$^{-1}$, values typical for late Cenozoic eolian influx to the North Pacific Ocean (Janecek and Rea, 1983; Janecek, 1985; Rea et al., 1985), but at Site 882 only a few hundred kilometers from land, it is not possible to differentiate between eolian and hemipelagic materials without further study.

At least an order of magnitude fewer dropstones were found at Site 882 (at 50.4°N) than at Site 881 (360 km to the south at 47.1°N); examination of the Leg 19 drill sites (Creager, Scholl, et al., 1973) suggests that the northward decline may continue. Sites 579 and 580, drilled during DSDP Leg 86, also encountered ice-rafted debris. Cores recovered at Site 580, at 41.6°N, contained considerably more ice-rafted debris (IRD) than did those from Site 579 at 38.6°N (Krissek et al., 1985). Site 881, with the largest concentration of IRD of any of the DSDP and ODP drill sites, lies just south of the southern tip of the Kamchatka Peninsula and about 300 km seaward of the main opening from the Sea of Okhotsk to the Northwest Pacific Ocean. Because the abundance of IRD decreases both north and south from this point, we conclude that the main source of ice-rafted pebbles in the Northwest Pacific Ocean is the Okhotsk-Kamchatka region of Siberia. In a study of the ice-rafting record in Lamont-Doherty Earth Observatory piston cores raised by the *Vema* and *Conrad* in the 1960s, Conolly and Ewing (1970) also noticed that the concentration of IRD declined both north and south from a location offshore of the southern tip of Kamchatka and suggested a Siberian source for the pebbles. Our work confirms their suggestions and shows that the same IRD depositional pattern has continued for the past 2.6 Ma.

The oldest ice rafting at Site 882 occurred during the latest Miocene and is seen as a pebble in sediments of approximately 6 Ma old. This compares with an age of about 4.3 Ma for the oldest pebble at Site 881. A northerly increase in the age of the oldest pebble exists at the two Leg 145 sites and the Leg 86 sites to the south (Krissek et al., 1985), where the oldest material is late Pliocene in age. Unfortunately the Leg 19 sites to the north were spot-cored, so they do not provide a continuous record to see if this interesting trend continues northward.

The deposition of volcanogenic material increased by several-fold at 2.6 Ma. This increase in ash deposition during the latest Pliocene in the North Pacific Ocean has been known for many years (Kennett and Thunell, 1975; Kennett et al., 1977), but Sites 881 and 882 provide a much better dated sequence than has been available previously for determining timing of onset of the northwestern Pacific portion of this ocean-wide volcanic episode. Examination of the individual ash layers will reveal geochemical trends in Kuril-Kamchatka volcanism.

Site 882, now at a depth of 3255 m, has been at or below the calcium carbonate compensation depth (CCCD) for most of the time since the late Miocene. The exception is the time of very high sedimentation rates in the early Pliocene when the combination of extreme productivity and rapid burial resulted in the preservation of calcite. The late Neogene CCCD in the northwestern Pacific Ocean of 3250 m or shallower is nearly 1 km shallower than the nonequatorial Pacific CCCD at lower latitudes, which is deeper than 4000 or 4100 m (van Andel et al., 1975; Rea and Leinen, 1985).

REFERENCES*

Cande, S.C., and Kent, D.V., 1992. A new geomagnetic polarity timescale for the Late Cretaceous and Cenozoic. *J. Geophys. Res.*, 97:13917–13951.

Conolly, J.R., and Ewing, M., 1970. Ice-rafted detritus in Northwest Pacific deep-sea sediments. *In* Hays, J.D. (Ed.), *Geological Investigations of the North Pacific.* Mem.—Geol. Soc. Am., 12:219–231.

Creager, J.S., Scholl, D.W., et al., 1973. *Init. Repts. DSDP*, 19: Washington (U.S. Govt. Printing Office).

DeMaster, D.J., 1981. The supply and accumulation of silica in the marine environment. *Geochim. Cosmochim. Acta,* 45:1715–1732.

Foreman, H.P., 1975. Radiolaria from the North Pacific, Deep Sea Drilling Project, Leg 32. *In* Larson, R.L., Moberly, R., et al., *Init. Repts. DSDP,* 32: Washington (U.S. Govt. Printing Office), 579–676.

Gieskes, J.M., 1981. Deep-sea drilling interstitial water studies: implications for chemical alteration of the oceanic crust, layers I and II. *In* Warme, J.E., Douglas, R.G., and Winterer, E.L. (Eds.), *The Deep Sea Drilling Project: A Decade of Progress.* Spec. Publ.—Soc. Econ. Paleontol. Mineral., 32:149–167.

Hays, J.D., 1970. Stratigraphy and evolutionary trends of radiolaria in North Pacific deep sea sediments. *In* Hays, J.D. (Ed.), *Geological Investigations of the North Pacific.* Mem.—Geol. Soc. Am., 126:185–218.

Hays, J.D., and Shackleton, N.J., 1976. Globally synchronous extinction of radiolarian *Stylatractus universus. Geology,* 4:649–652.

Heath, G.R., Burckle, L.H., et al., 1985. *Init. Repts. DSDP,* 86: Washington (U.S. Govt. Printing Office).

Janecek, T.R., 1985. Eolian sedimentation in the Northwest Pacific Ocean: a preliminary examination of the data from Deep Sea Drilling Project Sites 576 and 578. *In* Heath, G.R., Burckle, L.H., et al., *Init. Repts. DSDP,* 86: Washington (U.S. Govt. Printing Office), 589–603.

Janecek, T.R., and Rea, D.K., 1983. Eolian deposition in the northeast Pacific Ocean: Cenozoic history of atmospheric circulation. *Geol. Soc. Am. Bull.,* 94:730–738.

Keigwin, L.D., Jones, G.A., and Froelich, N.P., 1992. A 15,000-year paleoenvironmental record from Meiji Seamount, far northwestern Pacific. *Earth Planet Sci. Lett.,* 111:425–440.

Kennett, J.P., McBirney, A.R., and Thunell, R.C., 1977. Episodes of Cenozoic volcanism in the circum-Pacific region. *J. Volcanol. Geotherm. Res.,* 2:145–163.

Kennett, J.P., and Thunell, R.C., 1975. Global increase in Quaternary explosive volcanism. *Science,* 187:497–503.

Koizumi, I., 1992. Diatom biostratigraphy of the Japan Sea: Leg 127. *In* Pisciotto, K.A., Ingle, J.C., Jr., von Breymann, M.T., Barron, J., et al., *Proc. ODP, Sci. Results,* 127/128 (Pt. 1): College Station, TX (Ocean Drilling Program), 249–289.

Krissek, L.A., Morley, J.J., and Lofland, D.K., 1985. The occurrence, abundance, and composition of ice-rafted debris in sediments from Deep Sea Drilling Project Sites 579 and 580, northwest Pacific. *In* Heath, G.R., Burckle, L.H., et al., *Init. Repts. DSDP,* 86: Washington (U.S. Govt. Printing Office), 647–655.

McDuff, R.E., 1985. The chemistry of interstitial waters, Deep Sea Drilling Project, Leg 86. *In* Heath, G.R., Burckle, L.H., et al., *Init. Repts. DSDP,* 86: Washington (U.S. Govt. Printing Office), 675–687.

Morley, J.J., and Shackleton, N.J., 1978. Extension of the radiolarian *Stylatractus universus* as a biostratigraphic datum to the Atlantic Ocean. *Geology,* 6:309–311.

Rea, D.K., and Leinen, M., 1985. Neogene history of the calcite compensation depth and lysocline in the South Pacific Ocean. *Nature,* 316:805–807.

Rea, D.K., Leinen, M., and Janecek, T.R., 1985. A geological approach to the long-term history of atmospheric circulation. *Science,* 227:721–725.

Rea, D.K., and Schrader, H., 1985. Late Pliocene onset of glaciation: ice rafting and diatom stratigraphy of North Pacific DSDP cores. *Palaeogeogr., Palaeoclimatol., Palaeoecol.,* 49:313–325.

Riedel, W.R., and Sanfilippo, A., 1970. Radiolaria, Leg 4, Deep Sea Drilling Project. *In* Bader, R.G., Gerard, R.D., et al., *Init. Repts. DSDP,* 4: Washington (U.S. Govt. Printing Office), 503–575.

————, 1978. Stratigraphy and evolution of tropical Cenozoic radiolarians. *Micropaleontology,* 24:61–96.

Sancetta, C., and Silvestri, S., 1986. Pliocene-Pleistocene evolution of the North Pacific ocean-atmosphere system, interpreted from fossil diatoms. *Paleoceanography,* 1:163–180.

Shackleton, N.J., Backman, J., Zimmerman, H., Kent, D.V., Hall, M.A., Roberts, D.G., Schnitker, D., Baldauf, J.G., Desprairies, A., Homrighausen, R., Huddlestun, P., Keene, J.B., Kaltenback, A.J., Krumsiek, K.A.O., Morton, A.C., Murray, J.W., and Westberg-Smith, J., 1984. Oxygen isotope calibration of the onset of ice-rafting and history of glaciation in the North Atlantic region. *Nature,* 307:620–623.

van Andel, T.H., Heath, G.R., and Moore, T.C., Jr., 1975. Cenozoic tectonics, sedimentation, and paleoceanography of the central equatorial Pacific. *Mem.—Geol. Soc. Am.,* 143.

van Morkhoven, F.P.C.M., Berggren, W.A., and Edwards, A.S., 1986. Cenzoic cosmopolitan deep-water benthic foraminifera. *Bull. Cent. Rech. Explor.-Prod. Elf-Aquitaine,* Mem. 11.

* Abbreviations for names of organizations and publication titles in ODP reference lists follow the style given in *Chemical Abstracts Service Source Index* (published by American Chemical Society).

Ms 145IR-106

NOTE: For all sites drilled, core-description forms ("barrel sheets") and core photographs can be found in Section 3, beginning on page 395. Forms containing smear-slide data can be found in Section 4, beginning on page 985.

Table 6. Depths of polarity chron boundaries in Holes 882A and 882B.

	Hole 882A		Hole 882B		
Polarity chron	Section (cm)	Depth (mbsf)	Section (cm)	Depth (mbsf)	Age (CK92)
Brunhes/Matuyama	4H-4, 120	33.50	5H-1, 40	33.30	0.78
Termination Jaramillo	5H-6, 0-52	44.80–45.32	6H-2, 80	44.70	0.98
Onset Jaramillo	6H-2, 10	48.40			1.05
Cobb Mountain	6H-5, 90–130	53.7—54.10			1.201–1.212
Termination Olduvai	9H-1, 10	75.40			1.76
Onset Olduvai	9H-2, 135	78.15			1.98
Réunion	9H-6, 25–85	83.05-83.65			2.197–2.229
Matuyama/Gauss	11H-3, 80	98.10			2.60

CK92 = Cande and Kent, 1992.

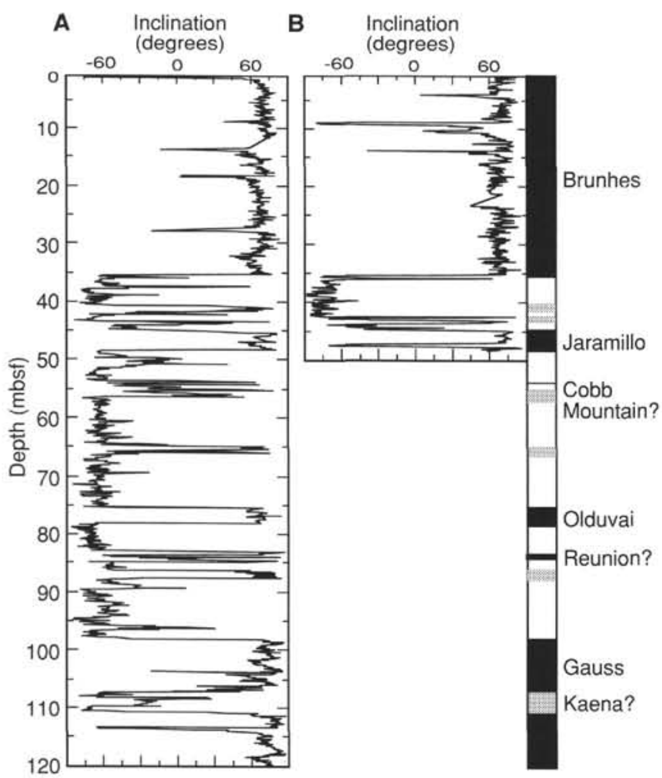

Figure 11. Comparison of whole-core measurements of inclinations after 15 mT demagnetization from Holes 882A (**A**) and 882B (**B**). The magnetostratigraphic interpretation is shown at far right. Events not substantiated by the discrete sample demagnetizations are shown in gray.

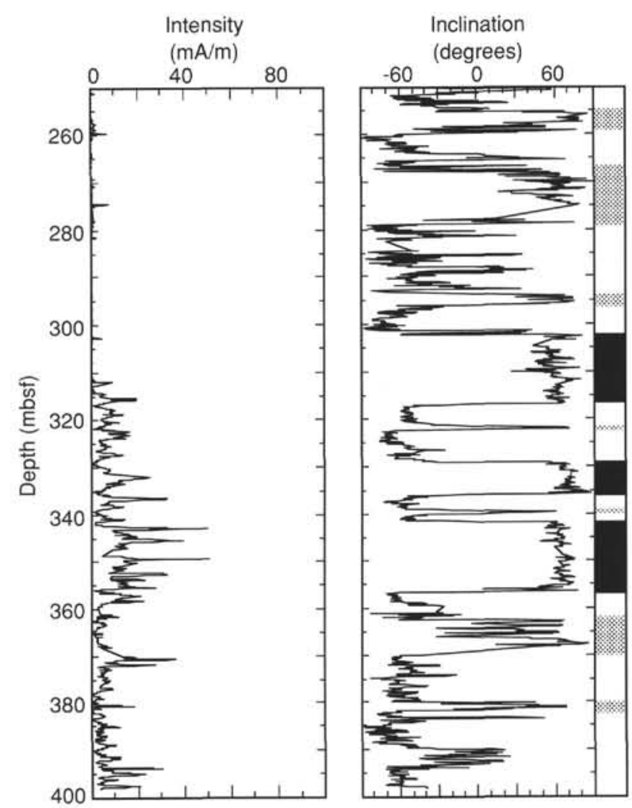

Figure 12. Magnetic inclination and intensity after 15 mT demagnetization from whole-core measurements between 250 and 400 mbsf in Hole 882A. The polarity sequence is shown on the far right, with gray zones representing more poorly defined polarity events occurring at weak intensity.

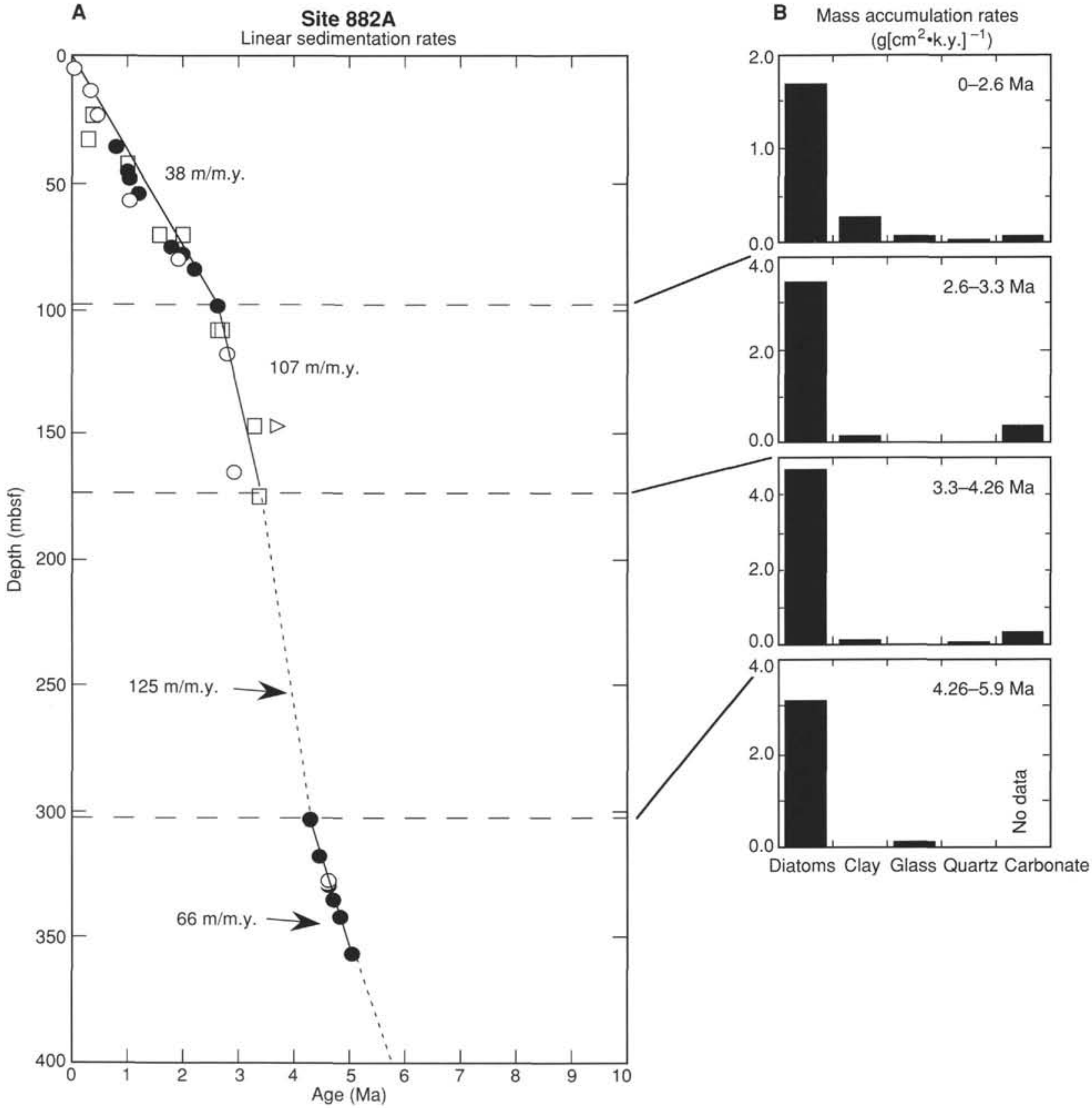

Figure 13. **A.** A plot of sedimentation rate of Site 882 using magnetostratigraphy (solid symbols) and biostratigraphy (open symbols; squares, circles, and triangles = diatoms, radiolarians, and nannofossils, respectively). **B.** Mass accumulation rates in the upper two time-stratigraphic intervals; average diatom fluxes do not appear to vary significantly, whereas significant changes are seen in the average fluxes of clay and carbonate, which account for the boundary between lithologic Subunits IA and IB at 105 mbsf. The most significant change at this site is the dramatically increased diatom flux between 3.3 and 4.26 Ma.

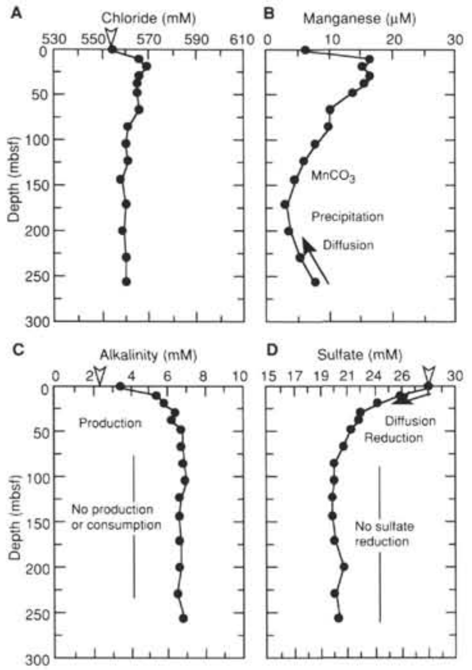

Figure 14. Concentrations in interstitial waters at Site 882 plotted vs. depth. **A**. Chloride. **B**. Manganese. **C**. Alkalinity. **D**. Sulfate. Open arrowhead indicates the concentration in modern seawater.

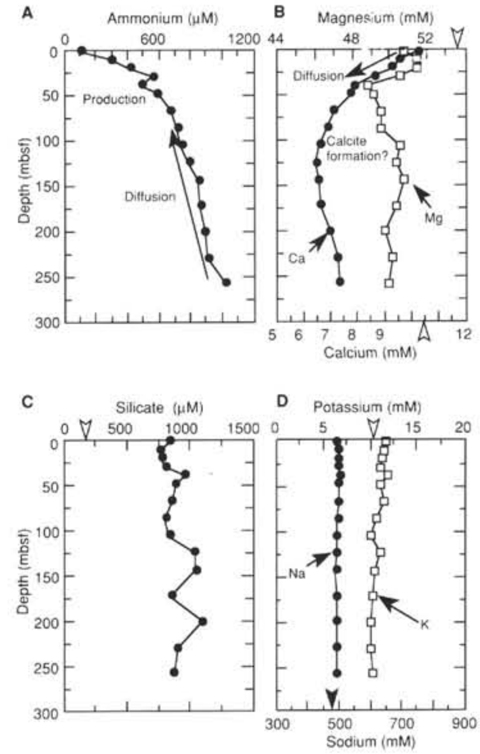

Figure 15. Concentrations in interstitial waters at Site 882 plotted vs. depth. **A**. Ammonium. **B**. Calcium and magnesium. **C**. Silicate. **D**. Potassium and sodium. Open arrowhead indicates the concentration in modern seawater.

Table 7. Listing of average sediment data and flux results for four time-stratigraphic intervals at Site 882.

Depth int. (mbsf)	Age int. (m.y.)	Dry-bulk density (g/cm³)	Linear sed. rate (cm/k.y.)	Diatom		Clay		Glass		Quartz	
				(%)	(g[cm²·k.y.]⁻¹)	(%)	(g[cm²·k.y.]⁻¹)	(%)	(g[cm²·k.y.]⁻¹)	(%)	(g[cm²·k.y.]⁻¹)
0–98	0–2.6	0.59	3.8	75	1.7	10.6	0.24	3.4	0.07	1.3	0.02
98–175	2.6–3.3	0.41	10.7	78	3.4	3.1	0.14	0.4	0.02	0.13	0.004
175–303	3.3–4.26	0.46	12.5	82	4.7	1.8	0.10	0.17	0.01	0.08	0.04
303–398	4.26–5.9	0.55	6.6	84	3.1	0.6	0.02	1.6	0.10	0	0.02

Note: n.d. = no data.

Table 7 (continued).

Carbonate		TOC	
(%)	(g[cm²·k.y.]⁻¹)	(%)	(g[cm²·k.y.]⁻¹)
2.9	0.07	0.2	0.004
7.7	0.36	0.2	0.008
5.5	0.34	0.2	0.01
n.d.		n.d.	

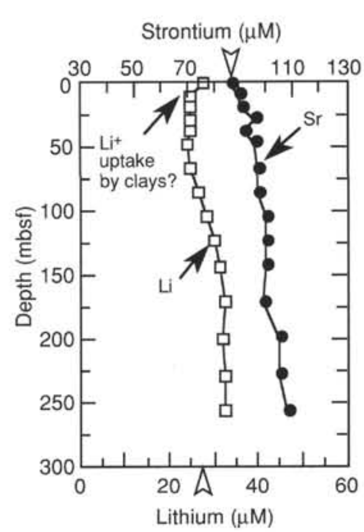

Figure 16. Lithium and strontium concentrations in interstitial waters plotted vs. depth at Site 882. Open arrowhead indicates the concentration in modern seawater.

Table 8. Interstitial water data for Site 882.

Interval (cm)	Depth (mbsf)	pH	Alk. (mM)	Sal. (g/kg)	Cl (mM)	Mg (mM)	Ca (mM)	SO_4 (mM)	NH_4 (µM)	NO_2 (µM)	H_4SiO_4 (µM)	K (mM)	Li (µM)	Na (mM)	Sr (µM)	Mn (µM)	Mg/Ca (mol ratio)
145-882B																	
1H-1, 145–150	1.45	7.71	3.48	35.0	555	50.75	10.25	28.01	108	0	842	11.8	27.8	492	87	6.3	4.95
2H-4, 145–150	10.35	7.88	5.45	35.0	566	51.44	9.56	25.64	294	0.3	770	11.5	24.7	500	90	16.6	5.38
3H-4, 145–150	19.85	7.76	5.80	35.0	569	51.48	9.28	23.79	418	0	780	11.3	24.9	500	91	15.4	5.55
4H-4, 145–150	29.35	7.77	6.43	35.0	566	50.52	8.61	22.51	561	0	810	11.1	24.8	498	96	16.6	5.87
5H-4, 145–150	38.85	7.78	6.22	35.0	565	48.88	7.89	22.34	490	n.m.	963	11.9	24.7	501	92	15.7	6.20
6H-4, 145–150	48.35	7.71	6.76	35.0	565	49.18	7.75	21.70	593	n.m.	889	11.2	24.5	500	96	13.7	6.34
8H-4, 145–150	67.35	7.81	6.73	35.0	566	49.58	7.10	21.12	676	n.m.	864	11.5	25.0	500	97	10.1	6.98
10H-4, 145–150	86.35	7.86	6.86	35.0	561	49.57	6.87	20.38	716	n.m.	805	10.7	26.8	495	97	10.0	7.21
12H-4, 145–150	105.35	7.82	6.94	35.0	560	50.60	6.57	20.32	742	n.m.	835	10.1	28.5	492	100	7.7	7.70
14H-4, 145–150	124.35	7.82	6.65	34.2	561	50.31	6.45	20.24	791	n.m.	1040	11.1	30.2	493	100	5.8	7.79
16H-4, 145–150	143.35	7.76	6.58	34.0	558	50.80	6.54	20.18	852	n.m.	1052	10.4	31.5	489	100	4.5	7.77
19H-4, 145–150	171.85	7.83	6.62	34.0	560	50.40	6.61	20.40	863	n.m.	854	10.3	32.7	492	99	3.0	7.62
22H-4, 145–150	200.35	7.68	6.65	34.0	559	49.78	6.98	21.07	893	n.m.	1102	10.0	31.9	493	105	3.6	7.12
25H-4, 145–150	228.85	7.81	6.52	34.0	560	50.18	7.24	20.41	913	n.m.	902	10.2	32.7	491	105	5.3	6.93
28H-4, 145–150	257.35	7.72	6.86	34.5	560	49.92	7.33	20.74	1027	n.m.	874	10.4	32.6	492	108	7.7	6.80

Note: n.m. = not measured.

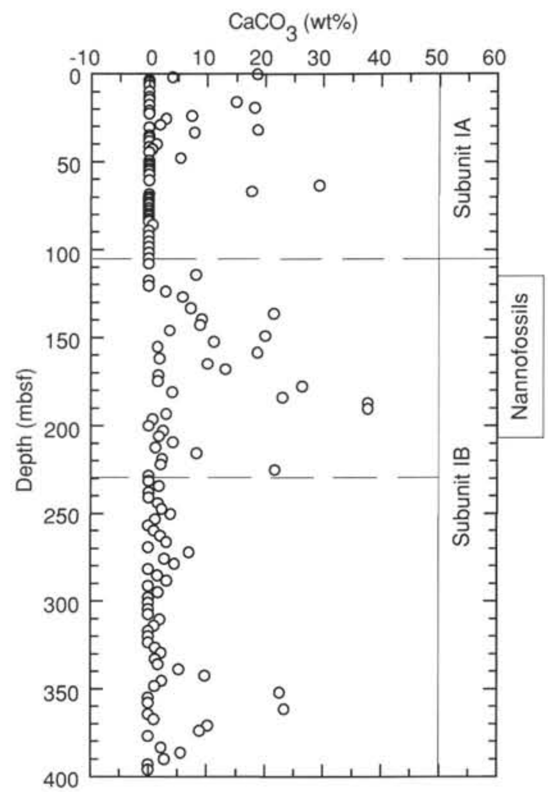

Figure 17. Carbonate contents vs. depth at Site 882. Dashed lines divide the record into three intervals based on calcium carbonate contents.

Table 9. Results of headspace gas analyses from Holes 882A and 882B.

Core, section, interval (cm)	Depth (mbsf)	C_1 (ppm)
145-882A-		
1H-5, 0–3	6.00	3
2H-5, 0–3	13.42	6
3H-5, 0–3	24.30	7
4H-5, 0–3	33.80	9
5H-6, 0–3	44.80	9
6H-4, 0–3	51.30	10
7H-4, 0–3	60.80	5
8H-4, 0–3	70.30	16
9H-4, 0–3	79.80	4
10H-4, 0–3	89.30	14
11H-4, 0–3	98.80	10
12H-4, 0–3	108.30	11
13H-4, 0–3	117.80	11
14H-4, 0–3	127.30	15
15H-4, 0–3	136.80	28
16H-4, 0–3	146.30	18
17H-4, 0–3	155.80	17
18H-4, 0–3	165.30	6
19H-4, 0–3	174.80	14
20H-4, 0–3	184.30	21
21H-4, 0–3	193.80	12
22H-4, 0–3	203.30	13
23H-4, 0–3	212.80	14
24H-4, 0–3	222.30	12
25H-5, 0–3	233.30	17
26H-4, 0–3	241.30	15
27H-4, 0–3	250.[illegible]	16
28H-4, 0–3	[illegible]	14
29H-4, 0–3	269.[illegible]	25
30H-4, 0–3	279.30	21
31H-4, 0–3	2[illegible]3.80	12
32H-4, 0–3	298.30	23
33H-4, 0–3	307.80	14
34H-4, 0–3	317.30	12
35H-4, 0–3	326.80	20
36H-4, 0–3	336.30	18
37H-4, 0–3	345.80	17
38H-4, 0–3	355.30	14
39H-4, 0–3	364.80	21
40H-4, 0–3	374.30	13
41H-4, 0–3	383.80	16
42H-4, 0–3	393.30	17
1H-2, 0–3	1.50	2
2H-5, 0–3	10.40	2
3H-5, 0–3	19.90	7
4H-5, 0–3	29.40	7
5H-5, 0–3	38.90	11
6H-5, 0–3	48.40	11
7H-5, 0–3	57.90	18
8H-5, 0–3	67.40	11
9H-5, 0–3	76.90	16
10H-5, 0–3	86.40	13
11H-4, 0–3	94.40	20
12H-5, 0–3	105.40	7
13H-5, 0–3	114.90	18
14H-5, 0–3	124.40	19
15H-5, 0–3	133.90	13
16H-5, 0–3	143.40	14
17H-5, 0–3	152.90	13
18H-5, 0–3	162.40	17
19H-5, 0–3	171.90	15
20H-5, 0–3	181.40	11
21H-5, 0–3	190.90	12
22H-5, 0–3	200.40	10
23H-4, 0–3	208.40	15
24H-4, 0–3	217.90	10
25H-4, 0–3	227.40	19
26H-4, 0–3	236.90	14
27H-4, 0–3	246.40	15
28H-4, 0–3	255.90	20
29H-5, 0–3	266.90	14

Note: C_1 = methane. All samples are headspace samples.

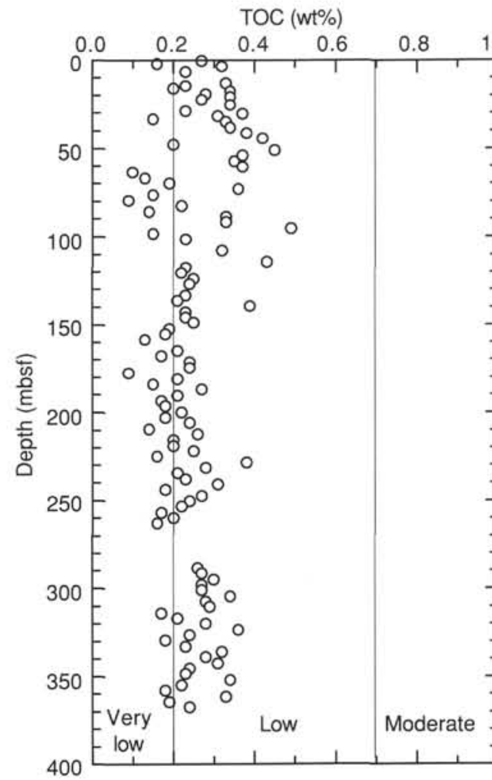

Figure 18. Total organic carbon contents vs. depth at Site 882.

Table 10. Results of geochemical analyses from Hole 882A.

Core, section, interval (cm)	Depth (mbsf)	TC (wt%)	IC (wt%)	TOC (wt%)	$CaCO_3$ (wt%)	TN (wt%)
145-882A-						
1H-1, 40 – 41	0.40	2.50	2.23	0.27	18.60	0.05
1H-2, 41 – 42	1.91	0.64	0.48	0.16	4.00	0.03
1H-3, 41 – 42	3.41	0.32	0.00	0.32	0.00	0.05
1H-4, 41 – 42	4.91		0.00		0.00	
1H-5, 41 – 42	6.41	0.23	0.00	0.23	0.00	0.04
2H-2, 113 – 114	10.05		0.00		0.00	
2H-4, 112 – 113	13.04	0.33	0.00	0.33	0.00	0.05
2H-5, 111 – 112	14.53	0.23	0.00	0.23	0.00	0.04
2H-6, 112 – 113	16.04	2.00	1.80	0.20	15.00	0.00
2H-7, 117 – 118	17.59	0.34	0.00	0.34	0.00	0.05
3H-1, 107 – 108	19.37	2.46	2.18	0.28	18.20	0.04
3H-2, 112 – 113	20.92	0.34	0.00	0.34	0.00	0.05
3H-3, 112 – 113	22.42	0.27	0.00	0.27	0.00	0.05
3H-4, 112 – 113	23.92		0.88		7.30	
3H-5, 112 – 113	25.42	0.69	0.35	0.34	2.90	0.05
4H-1, 112 – 113	28.92	0.46	0.23	0.23	1.90	0.04
4H-2, 112 – 113	30.42	0.37	0.00	0.37	0.00	0.05
4H-3, 112 – 113	31.92	2.57	2.25	0.31	18.70	0.03
4H-4, 112 – 113	33.42	1.09	0.94	0.15	7.80	0.00
4H-5, 112 – 113	34.92	0.33	0.00	0.33	0.00	0.05
4H-6, 113 – 114	36.43		0.00		0.00	
5H-1, 112 – 113	38.42	0.34	0.00	0.34	0.00	0.05
5H-2, 113 – 114	39.93		0.16		1.30	
5H-3, 112 – 113	41.42	0.38	0.00	0.38	0.00	0.05
5H-4, 112 – 113	42.92		0.06		0.50	
5H-5, 112 – 113	44.42	0.42	0.00	0.42	0.00	0.05
6H-1, 115 – 116	47.95	0.85	0.65	0.20	5.40	0.05
6H-2, 115 – 116	49.45		0.00		0.00	
6H-3, 115 – 116	50.95	0.45	0.00	0.45	0.00	0.06
6H-4, 112 – 113	52.42		0.00		0.00	
6H-5, 112 – 113	53.92	0.37	0.00	0.37	0.00	0.05
6H-6, 113 – 114	55.43		0.00		0.00	
7H-1, 111 – 112	57.41	0.35	0.00	0.35	0.00	0.05
7H-3, 113 – 114	60.43	0.37	0.00	0.37	0.00	0.08
7H-5, 113 – 114	63.43	3.62	3.52	0.10	29.30	0.02
8H-1, 112 – 113	66.92	2.26	2.13	0.13	17.70	0.04
8H-2, 113 – 114	68.43		0.00		0.00	
8H-3, 112 – 113	69.92	0.19	0.00	0.19	0.00	0.04
8H-4, 112 – 113	71.42		0.00		0.00	
8H-5, 112 – 113	72.92	0.36	0.00	0.36	0.00	0.05
8H-6, 111 – 112	74.41		0.00		0.00	
9H-1, 112 – 113	76.42	0.15	0.00	0.15	0.00	0.04
9H-2, 112 – 113	77.92		0.00		0.00	
9H-3, 112 – 113	79.42	0.09	0.00	0.09	0.00	0.03
9H-4, 103 – 104	80.83		0.00		0.00	
9H-5, 118 – 119	82.48	0.22	0.00	0.22	0.00	0.04
9H-6, 107 – 108	83.87		0.00		0.00	
10H-1, 111 – 112	85.91	0.23	0.09	0.14	0.70	0.00
10H-3, 111 – 112	88.91	0.33	0.00	0.33	0.00	0.04
10H-5, 105 – 106	91.85	0.33	0.00	0.33	0.00	0.00
11H-1, 112 – 113	95.42	0.49	0.00	0.49	0.00	0.07
11H-3, 110 – 111	98.40	0.15	0.00	0.15	0.00	0.03
11H-5, 110 – 111	101.40	0.23	0.00	0.23	0.00	0.00
12H-1, 112 – 113	104.92		0.00		0.00	
12H-3, 113 – 114	107.93	0.32	0.00	0.32	0.00	0.00
13H-1, 113 – 114	114.43	1.40	0.97	0.43	8.10	0.00
13H-3, 117 – 118	117.47	0.23	0.00	0.23	0.00	0.20
13H-5, 111 – 112	120.41	0.22	0.00	0.22	0.00	0.00
14H-1, 113 – 114	123.93	0.60	0.35	0.25	2.90	0.00
14H-3, 112 – 113	126.92	0.94	0.70	0.24	5.80	0.02
15H-1, 112 – 113	133.42	1.09	0.86	0.23	7.20	0.03
15H-3, 111 – 112	136.41	2.79	2.58	0.21	21.50	0.00
15H-5, 112 – 113	139.42	1.48	1.09	0.39	9.10	0.04
16H-1, 112 – 113	142.92	1.29	1.06	0.23	8.80	0.00
16H-3, 112 – 113	145.92	0.66	0.43	0.23	3.60	0.00
16H-5, 112 – 113	148.92	2.65	2.40	0.25	20.00	0.00
17H-1, 112 – 113	152.42	1.54	1.35	0.19	11.20	0.04
17H-3, 112 – 113	155.42	0.36	0.18	0.18	1.50	0.02
17H-5, 112 – 113	158.42	2.37	2.24	0.13	18.70	0.00
18H-1, 112 – 113	161.92		0.23		1.90	
18H-3, 112 – 113	164.92	1.42	1.21	0.21	10.10	0.04
18H-5, 112 – 113	167.92	1.75	1.58	0.17	13.20	0.03
19H-1, 122 – 123	171.52	0.45	0.21	0.24	1.70	0.05
19H-3, 121 – 122	174.51	0.43	0.19	0.24	1.60	0.05
19H-5, 112 – 113	177.42	3.26	3.17	0.09	26.40	0.03
20H-1, 112 – 113	180.92	0.70	0.49	0.21	4.10	0.03
20H-3, 112 – 113	183.92	2.91	2.76	0.15	23.00	0.04
20H-5, 112 – 113	186.92	4.80	4.53	0.27	37.70	0.00
21H-1, 112 – 113	190.42	4.73	4.52	0.21	37.70	0.03
21H-3, 112 – 113	193.42	0.53	0.36	0.17	3.00	0.05
21H-5, 112 – 113	196.42	0.26	0.08	0.18	0.70	0.00
22H-1, 122 – 123	200.02	0.22	0.00	0.22	0.00	0.04
22H-3, 112 – 113	202.92	0.48	0.30	0.18	2.50	0.00
22H-5, 112 – 113	205.92	0.46	0.22	0.24	1.80	0.04
23H-1, 112 – 113	209.42	0.65	0.51	0.14	4.20	0.03

Table 10 (continued).

Core, section, interval (cm)	Depth (mbsf)	TC (wt%)	IC (wt%)	TOC (wt%)	$CaCO_3$ (wt%)	TN (wt%)
145-882A-						
23H-3, 112 – 113	212.42	0.40	0.14	0.26	1.20	0.05
23H-5, 122 – 123	215.52	1.19	0.99	0.20	8.20	0.03
24H-1, 117 – 118	218.97	0.48	0.28	0.20	2.30	0.04
24H-3, 121 – 122	222.01	0.50	0.25	0.25	2.10	0.04
24H-5, 112 – 113	224.92	2.77	2.61	0.16	21.70	0.04
25H-1, 112 – 113	228.42	0.38	0.00	0.38	0.00	0.05
25H-3, 107 – 108	231.37	0.28	0.00	0.28	0.00	0.05
25H-5, 111 – 112	234.41	0.43	0.22	0.21	1.80	0.00
26H-1, 112 – 113	237.92	0.23	0.00	0.23	0.00	0.04
26H-3, 112 – 113	240.92	0.31	0.00	0.31	0.00	0.06
26H-5, 112 – 113	243.92	0.37	0.19	0.18	1.60	0.03
27H-1, 112 – 113	247.42	0.53	0.26	0.27	2.20	0.05
27H-3, 112 – 113	250.42	0.70	0.46	0.24	3.80	0.05
27H-5, 112 – 113	253.42	0.36	0.14	0.22	1.20	0.03
28H-1, 112 – 113	256.92	0.17	0.00	0.17	0.00	0.03
28H-3, 112 – 113	259.92	0.32	0.12	0.20	1.00	0.04
28H-5, 112 – 113	262.92	0.41	0.25	0.16	2.10	0.02
29H-1, 113 – 114	266.43		0.37		3.10	
29H-3, 113 – 114	269.43		0.00		0.00	
29H-5, 113 – 114	272.43		0.84		7.00	
30H-1, 106 – 107	275.86		0.34		2.80	
30H-3, 115 – 116	278.95		0.54		4.50	
30H-5, 112 – 113	281.92		0.00		0.00	
31H-1, 112 – 113	285.42		0.19		1.60	
31H-3, 112 – 113	288.42	0.64	0.38	0.26	3.20	0.03
31H-5, 112 – 113	291.42	0.27	0.00	0.27	0.00	0.03
32H-1, 112 – 113	294.92	0.51	0.21	0.30	1.70	0.03
32H-3, 111 – 112	297.91	0.27	0.00	0.27	0.00	0.03
32H-5, 112 – 113	300.92	0.27	0.00	0.27	0.00	0.04
33H-1, 111 – 112	304.41	0.34	0.00	0.34	0.00	0.03
33H-3, 111 – 112	307.41	0.28	0.00	0.28	0.00	0.03
33H-5, 111 – 112	310.41	0.53	0.24	0.29	2.00	0.03
34H-1, 112 – 113	313.92	0.29	0.12	0.17	1.00	0.03
34H-3, 112 – 113	316.92	0.21	0.00	0.21	0.00	0.03
34H-5, 112 – 113	319.92	0.28	0.00	0.28	0.00	0.03
35H-1, 111 – 112	323.41	0.36	0.00	0.36	0.00	0.04
35H-3, 111 – 112	326.41	0.38	0.14	0.24	1.20	0.04
35H-5, 111 – 112	329.41	0.44	0.26	0.18	2.20	0.00
36H-1, 112 – 113	332.92	0.37	0.14	0.23	1.20	0.03
36H-3, 112 – 113	335.92	0.52	0.20	0.32	1.70	0.04
36H-5, 112 – 113	338.92	0.91	0.63	0.28	5.20	0.03
37H-1, 112 – 113	342.42	1.47	1.16	0.31	9.70	0.04
37H-3, 112– 113	345.42	0.52	0.28	0.24	2.30	0.04
37H-5, 112 – 113	348.42	0.36	0.13	0.23	1.10	0.00
38H-1, 113 – 114	351.93	3.05	2.71	0.34	22.60	0.02
38H-3, 113 – 114	354.93	0.22	0.00	0.22	0.00	0.04
38H-5, 113 – 114	357.93	0.18	0.00	0.18	0.00	0.03
39H-1, 113 – 114	361.43	3.14	2.81	0.33	23.40	0.03
39H-3, 113 – 114	364.43	0.19	0.00	0.19	0.00	0.03
39H-5, 113 – 114	367.43	0.36	0.12	0.24	1.00	0.04
40H-1, 112 – 113	370.92		1.22		10.20	
40H-3, 112 – 113	373.92		1.06		8.80	
40H-5, 112 – 113	376.92		0.00		0.00	
41H-3, 112 – 113	383.42		0.27		2.20	
41H-5, 112 – 113	386.42		0.67		5.60	
42H-1, 112 – 113	389.92		0.34		2.80	
42H-3, 112 – 113	392.92		0.00		0.00	
42H-5, 112 – 113	395.92		0.00		0.00	

All samples are carbonate samples. TC = total carbon, IC = inorganic carbon, TOC = total organic carbon, and TN = total nitrogen. All results are given in weight percent of bulk dry sediment.

Table 11. Index properties data from Hole 882A and Hole 882B.

Core, section	Interval (cm)	Depth (mbsf)	Wet-bulk density (g/cm³)	Dry-bulk density (g/cm³)	Grain density (g/cm³)	Wet porosity (%)	Dry porosity (%)	Wet water content (%)	Dry water content (%)	Void ratio 1	Void ratio 2
145-882A-											
1H-1	38.0–40.0	0.38	1.33	0.50	2.70	81.20	81.80	62.60	167.20	4.31	4.40
1H-1	109.0–111.0	1.09	1.36	0.54	2.72	79.90	80.40	60.30	151.90	3.97	4.04
1H-2	39.0–41.0	1.89	1.41	0.64	2.66	75.80	76.40	55.00	122.20	3.13	3.18
1H-2	109.0–111.0	2.59	1.31	0.49	2.54	80.40	81.00	62.70	168.00	4.10	4.17
1H-3	39.0–40.0	3.39	1.39	0.58	2.76	78.50	79.10	58.00	138.10	3.66	3.72
1H-3	109.0–111.0	4.09	1.32	0.50	2.63	80.80	81.40	62.50	166.70	4.20	4.28
1H-4	39.0–41.0	4.89	1.28	0.45	2.49	81.70	82.30	65.20	187.40	4.47	4.56
1H-4	109.0–111.0	5.59	1.54	0.84	2.70	68.60	69.10	45.60	83.70	2.18	2.21
1H-5	39.0–41.0	6.39	1.42	0.65	2.68	75.50	76.00	54.40	119.10	3.08	3.12
1H-5	109.0–111.0	7.09	1.37	0.58	2.65	78.00	78.50	58.10	138.90	3.54	3.60
1H-6	40.0–42.0	7.90	1.43	0.67	2.67	74.70	75.20	53.40	114.40	2.94	2.98
1H-6	109.0–111.0	8.59	1.38	0.60	2.56	76.30	76.90	56.70	131.10	3.22	3.27
2H-2	39.0–41.0	9.31	1.36	0.56	2.54	77.60	78.10	58.60	141.60	3.46	3.51
2H-2	110.0–112.0	10.02	1.52	0.82	2.66	68.90	69.40	46.30	86.10	2.21	2.23
2H-3	39.0–41.0	10.81	1.42	0.65	2.62	74.80	75.40	54.10	117.90	2.97	3.01
2H-3	110.0–112.0	11.52	1.36	0.56	2.53	77.30	77.90	58.40	140.40	3.41	3.46
2H-4	39.0–41.0	12.31	1.34	0.51	2.65	80.20	80.80	61.50	159.60	4.06	4.13
2H-4	110.0–112.0	13.02	1.44	0.66	2.73	75.30	75.80	53.70	116.20	3.05	3.09
2H-5	40.0–42.0	13.82	1.30	0.45	2.73	83.30	83.90	65.70	191.50	5.00	5.11
2H-5	109.0–111.0	14.51	1.38	0.62	2.47	74.70	75.30	55.30	123.90	2.95	2.99
2H-6	39.0–41.0	15.31	1.44	0.68	2.65	74.10	74.70	52.80	112.00	2.86	2.90
2H-6	109.0–111.0	16.01	1.28	0.46	2.38	80.20	80.90	64.00	177.60	4.06	4.13
2H-7	39.0–41.0	16.81	1.35	0.55	2.62	78.80	79.40	59.60	147.70	3.72	3.78
2H-7	114.0–116.0	17.56	1.44	0.68	2.72	74.70	75.30	53.10	113.10	2.96	3.00
3H-1	39.0–41.0	18.69	1.41	0.63	2.65	75.80	76.30	55.10	122.70	3.13	3.17
3H-1	104.0–106.0	19.34	1.31	0.48	2.63	81.60	82.20	63.80	175.90	4.43	4.52
3H-2	39.0–41.0	20.19	1.42	0.64	2.71	76.00	76.50	54.80	121.20	3.16	3.21
3H-2	109.0–111.0	20.89	1.51	0.76	2.91	73.60	74.20	49.90	99.70	2.79	2.83
3H-3	39.0–41.0	21.69	1.44	0.67	2.79	75.70	76.20	53.70	115.90	3.11	3.16
3H-3	109.0–111.0	22.39	1.36	0.56	2.61	78.30	78.90	59.10	144.60	3.62	3.68
3H-4	39.0–41.0	23.19	1.39	0.56	2.91	80.30	80.90	59.40	146.20	4.08	4.15
3H-4	109.0–111.0	23.89	1.31	0.51	2.36	78.00	78.70	61.00	156.50	3.55	3.61
3H-5	39.0–41.0	24.69	1.44	0.70	2.55	72.30	72.80	51.50	106.00	2.60	2.63
3H-5	109.0–111.0	25.39	1.30	0.46	2.60	82.00	82.60	64.70	183.00	4.55	4.64
3H-6	39.0–41.0	26.19	1.33	0.49	2.68	81.20	81.80	62.80	168.60	4.33	4.42
4H-1	39.0–41.0	28.19	1.38	0.59	2.64	77.20	77.70	57.10	133.00	3.38	3.43
4H-1	109.0–111.0	28.89	1.41	0.63	2.61	75.40	76.00	54.90	121.70	3.06	3.11
4H-2	39.0–41.0	29.69	1.40	0.62	2.64	76.20	76.80	55.80	126.40	3.21	3.25
4H-2	109.0–111.0	30.39	1.47	0.71	2.80	74.20	74.70	51.60	106.40	2.87	2.91
4H-3	39.0–41.0	31.19	1.32	0.51	2.47	79.00	79.70	61.40	158.90	3.77	3.84
4H-3	109.0–111.0	31.89	1.17	0.26	2.37	88.60	89.30	77.70	348.70	7.79	8.07
4H-4	39.0–41.0	32.69	1.44	0.67	2.67	74.50	75.10	53.20	113.50	2.92	2.96
4H-4	109.0–111.0	33.39	1.37	0.59	2.53	76.40	77.00	57.10	133.40	3.24	3.29
4H-5	39.0–41.0	34.19	1.50	0.76	2.78	72.40	72.90	49.40	97.60	2.62	2.65
4H-5	109.0–111.0	34.89	1.47	0.72	2.75	73.60	74.20	51.30	105.30	2.79	2.83
4H-6	39.0–41.0	35.69	1.39	0.61	2.65	76.70	77.30	56.40	129.10	3.29	3.34
4H-6	109.0–111.0	36.39	1.42	0.64	2.73	76.30	76.90	55.20	123.00	3.22	3.27
4H-7	39.0–41.0	37.19	1.27	0.44	2.43	81.70	82.30	65.70	191.80	4.45	4.54
5H-1	39.0–41.0	37.69	1.40	0.62	2.60	75.70	76.30	55.50	124.50	3.11	3.16
5H-1	109.0–111.0	38.39	1.46	0.70	2.74	74.20	74.80	52.20	109.00	2.88	2.92
5H-2	38.0–40.0	39.18	1.51	0.79	2.66	70.00	70.50	47.60	90.80	2.33	2.36
5H-2	110.0–112.0	39.90	1.41	0.62	2.78	77.30	77.90	56.10	127.80	3.41	3.47
5H-3	39.0–41.0	40.69	1.31	0.49	2.54	80.30	80.90	62.70	167.90	4.08	4.16
5H-3	110.0–112.0	41.40	1.50	0.76	2.71	71.50	72.10	49.00	96.10	2.51	2.54
5H-4	39.0–41.0	42.19	1.36	0.56	2.61	78.30	78.90	59.00	144.00	3.61	3.67
5H-4	110.0–112.0	42.90	1.48	0.73	2.82	73.90	74.40	51.00	104.20	2.83	2.87
5H-5	39.0–41.0	43.69	1.23	0.37	2.29	83.40	84.00	69.60	229.30	5.01	5.12
5H-5	110.0–112.0	44.40	1.41	0.64	2.57	74.70	75.20	54.40	119.20	2.95	2.99
5H-6	39.0–41.0	45.19	1.28	0.44	2.47	81.80	82.40	65.50	189.90	4.48	4.57
6H-1	44.0–46.0	47.24	1.47	0.71	2.78	74.20	74.70	51.80	107.40	2.87	2.91
6H-1	112.0–114.0	47.92	1.35	0.56	2.49	77.20	77.80	58.60	141.70	3.39	3.44
6H-2	44.0–46.0	48.74	1.46	0.72	2.68	72.90	73.50	51.00	104.20	2.69	2.73
6H-2	112.0–114.0	49.42	1.49	0.75	2.68	71.60	72.10	49.30	97.30	2.52	2.55
6H-3	44.0–46.0	50.24	1.33	0.50	2.61	80.30	80.90	62.00	162.90	4.08	4.15
6H-3	112.0–114.0	50.92	1.33	0.51	2.62	80.00	80.60	61.40	159.20	3.99	4.07
6H-4	39.0–41.0	51.69	1.24	0.36	2.66	85.90	86.50	70.70	241.90	6.10	6.27
6H-4	109.0–111.0	52.39	1.32	0.49	2.63	80.90	81.50	62.60	167.60	4.22	4.30
6H-5	39.0–41.0	53.19	1.20	0.30	2.59	88.10	88.80	75.20	302.60	7.40	7.66
6H-5	109.0–111.0	53.89	1.31	0.49	2.50	80.00	80.60	62.60	167.50	4.01	4.08
6H-6	39.0–41.0	54.69	1.29	0.47	2.40	80.20	80.90	63.80	176.40	4.06	4.14
6H-6	109.0–111.0	55.39	1.40	0.63	2.60	75.40	76.00	55.10	122.60	3.07	3.11
6H-6	114.0–116.0	55.44	1.19	0.31	2.29	86.00	86.70	73.90	283.30	6.15	6.33
6H-7	39.0–41.0	56.19	1.33	0.52	2.52	79.20	79.80	61.10	157.20	3.81	3.87
7H-1	49.0–051.0	56.79	1.24	0.35	2.90	87.60	88.20	72.10	259.00	7.08	7.32
7H-1	109.0–111.0	57.39	1.55	0.85	2.77	69.10	69.60	45.50	83.70	2.24	2.26
7H-2	39.0–41.0	58.19	1.26	0.39	2.69	85.30	85.90	69.40	226.50	5.80	5.95
7H-2	114.0–116.0	58.94	1.56	0.87	2.68	67.40	67.90	44.30	79.60	2.06	2.08
7H-3	39.0–41.0	59.69	1.61	0.96	2.64	63.20	63.70	40.20	67.20	1.72	1.73
7H-3	109.0–111.0	60.39	1.44	0.69	2.58	72.70	73.30	51.80	107.30	2.67	2.70
7H-4	39.0–41.0	61.19	1.60	0.96	2.53	61.70	62.20	39.60	65.70	1.61	1.62
7H-4	109.0–111.0	61.89	1.39	0.61	2.60	76.30	76.80	56.30	128.60	3.21	3.26
7H-5	39.0–41.0	62.69	1.39	0.61	2.56	75.70	76.30	55.80	126.30	3.11	3.16

Table 11 (continued).

Core, section	Interval (cm)	Depth (mbsf)	Wet-bulk density (g/cm^3)	Dry-bulk density (g/cm^3)	Grain density (g/cm^3)	Wet porosity (%)	Dry porosity (%)	Wet water content (%)	Dry water content (%)	Void ratio 1	Void ratio 2
7H-5	109.0–111.0	63.39	1.35	0.56	2.55	77.80	78.40	58.80	142.90	3.50	3.56
7H-6	109.0–111.0	64.89	1.26	0.40	2.50	83.40	84.10	67.90	211.50	5.04	5.16
7H-7	39.0–41.0	65.69	1.19	0.30	2.33	86.80	87.50	74.90	298.00	6.58	6.78
8H-1	39.0–41.0	66.19	1.44	0.69	2.61	73.40	74.00	52.30	109.60	2.76	2.80
8H-1	109.0–111.0	66.89	1.34	0.53	2.63	79.60	80.20	60.70	154.80	3.90	3.97
8H-2	39.0–41.0	67.69	1.30	0.49	2.40	79.10	79.80	62.20	164.70	3.80	3.86
8H-2	109.0–111.0	68.39	1.13	0.18	2.50	92.40	93.20	84.20	531.40	12.24	12.96
8H-3	49.0–051.0	69.29	1.46	0.74	2.55	70.80	71.30	49.60	98.50	2.42	2.45
8H-3	109.0–111.0	69.89	1.39	0.62	2.53	75.20	75.80	55.40	124.30	3.03	3.08
8H-4	49.0–051.0	70.79	1.39	0.62	2.47	74.40	75.00	55.00	122.00	2.90	2.94
8H-4	109.0–111.0	71.39	1.33	0.57	2.19	73.60	74.20	56.80	131.70	2.79	2.82
8H-5	44.0–46.0	72.24	1.42	0.66	2.55	73.60	74.10	53.10	113.40	2.78	2.82
8H-5	109.0–111.0	73.67	1.31	0.51	2.42	78.50	79.20	61.20	157.80	3.66	3.72
8H-6	37.0–39.0	74.39	1.34	0.54	2.57	78.70	79.30	60.00	150.00	3.70	3.76
8H-6	109.0–111.0	75.19	1.39	0.60	2.62	76.80	77.40	56.80	131.50	3.32	3.37
8H-7	39.0–41.0	75.64	1.37	0.57	2.61	77.60	78.20	58.10	138.50	3.47	3.53
9H-1	34.0–36.0	76.39	1.34	0.52	2.59	79.50	80.10	60.90	155.90	3.87	3.94
9H-1	109.0–111.0	77.19	1.41	0.64	2.62	75.30	75.90	54.80	121.00	3.05	3.10
9H-2	39.0–41.0	77.89	1.49	0.78	2.62	70.10	70.70	48.10	92.70	2.35	2.37
9H-2	109.0–111.0	78.69	1.37	0.60	2.46	75.10	75.70	56.10	127.70	3.02	3.06
9H-3	39.0–41.0	79.39	1.36	0.55	2.63	78.60	79.20	59.20	145.40	3.67	3.74
9H-3	109.0–111.0	80.24	1.30	0.46	2.57	81.60	82.20	64.40	180.50	4.43	4.52
9H-4	44.0–46.0	80.89	1.22	0.33	2.58	86.70	87.40	72.80	267.60	6.53	6.73
9H-4	109.0–111.0	81.69	1.60	0.96	2.55	62.10	62.60	39.90	66.40	1.64	1.65
9H-5	39.0–41.0	82.39	1.56	0.89	2.60	65.60	66.10	43.10	75.90	1.91	1.93
9H-5	109.— 11.0	83.21	1.49	0.77	2.58	69.80	70.30	48.10	92.70	2.31	2.34
9H-6	41.0–43.0	83.89	1.32	0.50	2.53	80.00	80.60	62.30	165.10	4.00	4.07
9H-6	109.0–111.0	84.69	1.36	0.58	2.50	76.60	77.20	57.60	136.10	3.28	3.33
9H-7	39.0–41.0	85.19	1.26	0.42	2.37	81.90	82.60	66.60	199.80	4.53	4.63
10H-1	39.0–41.0	85.89	1.26	0.40	2.49	83.40	84.00	67.90	211.20	5.03	5.14
10H-1	109.0–111.0	86.69	1.17	0.26	2.38	88.60	89.30	77.60	346.50	7.76	8.05
10H-2	39.0–41.0	87.39	1.24	0.39	2.36	83.10	83.70	68.50	217.90	4.91	5.02
10H-2	109.0–111.0	88.21	1.33	0.53	2.44	77.70	78.30	59.80	148.90	3.49	3.54
10H-3	41.0–43.0	88.89	1.28	0.45	2.43	80.90	81.60	64.60	182.70	4.25	4.33
10H-3	109.0–111.0	89.71	1.32	0.51	2.51	79.20	79.80	61.30	158.50	3.81	3.88
10H-4	41.0–43.0	90.39	1.25	0.40	2.47	83.50	84.20	68.30	215.70	5.08	5.20
10H-4	109.0–111.0	91.19	1.55	0.88	2.58	65.70	66.20	43.40	76.70	1.91	1.93
10H-5	39.0–41.0	91.82	1.39	0.63	2.50	74.50	75.10	54.90	121.50	2.92	2.96
10H-5	102.0–104.0	92.69	1.38	0.59	2.59	77.00	77.60	57.40	134.70	3.36	3.41
10H-6	39.0–41.0	93.39	1.33	0.50	2.66	80.70	81.30	62.20	164.80	4.19	4.28
10H-6	109.0–111.0	94.19	1.43	0.66	2.66	74.70	75.20	53.60	115.30	2.95	2.99
10H-7	39.0–41.0	94.71	1.50	0.82	2.46	66.20	66.80	45.20	82.50	1.96	1.98
11H-1	41.0–43.0	95.39	1.50	0.78	2.70	70.80	71.40	48.30	93.30	2.43	2.46
11H-1	109.0–111.0	96.89	1.32	0.51	2.48	79.00	79.60	61.20	158.00	3.75	3.82
11H-2	109.0–111.0	97.71	1.21	0.33	2.34	85.50	86.20	72.50	264.10	5.88	6.04
11H-3	41.0–43.0	98.39	1.35	0.53	2.64	79.40	80.00	60.40	152.50	3.87	3.93
11H-3	109.0–111.0	99.19	1.37	0.61	2.47	75.10	75.70	56.00	127.20	3.02	3.06
11H-4	39.0–41.0	99.89	1.24	0.37	2.53	84.90	85.60	70.00	233.80	5.63	5.78
11H-4	109.0–111.0	100.69	1.29	0.47	2.48	80.80	81.40	63.90	177.30	4.21	4.29
11H-5	39.0–41.0	101.39	1.25	0.39	2.50	84.10	84.70	68.90	221.50	5.28	5.41
11H-5	109.0–111.0	102.19	1.28	0.43	2.55	82.80	83.50	66.40	198.00	4.83	4.94
11H-6	39.0–41.0	102.89	1.35	0.55	2.54	77.90	78.50	59.20	144.90	3.53	3.59
11H-6	109.0–111.0	103.69	1.19	0.33	2.14	84.10	84.80	72.10	258.40	5.28	5.41
11H-7	39.0–41.0	104.19	1.28	0.48	2.27	78.60	79.20	62.70	168.40	3.67	3.73
12H-1	39.0–41.0	105.67	1.13	0.21	2.27	90.50	91.20	81.80	449.50	9.51	9.94
12H-2	37.0–39.0	106.39	1.17	0.26	2.33	88.30	89.00	77.50	344.60	7.57	7.84
12H-2	109.0–111.0	107.19	1.19	0.31	2.29	86.10	86.80	74.10	286.40	6.21	6.39
12H-3	39.0–41.0	107.89	1.21	0.35	2.16	83.20	84.00	70.70	241.60	4.97	5.08
12H-3	109.0–111.0	108.69	1.26	0.43	2.34	81.20	81.80	65.80	192.80	4.32	4.40
12H-4	39.0–41.0	109.39	1.18	0.30	2.20	85.80	86.60	74.40	290.10	6.06	6.23
12H-4	109.0–111.0	110.19	1.27	0.46	2.29	79.70	80.40	64.10	178.90	3.93	4.00
12H-5	39.0–41.0	110.89	1.23	0.36	2.38	84.40	85.10	70.50	238.90	5.42	5.56
12H-5	109.0–111.0	111.69	1.19	0.32	2.19	85.20	85.90	73.50	276.80	5.75	5.91
12H-6	39.0–41.0	112.39	1.12	0.18	2.35	91.90	92.60	83.90	520.10	11.33	11.94
12H-6	109.0–111.0	113.19	1.15	0.24	2.14	88.30	89.00	78.90	373.30	7.52	7.79
12H-7	39.0–41.0	113.69	1.25	0.41	2.27	81.50	82.20	67.00	202.80	4.41	4.50
13H-1	39.0–41.0	114.39	1.29	0.46	2.48	81.30	81.90	64.60	182.70	4.34	4.42
13H-1	109.0–111.0	115.19	1.27	0.45	2.27	79.70	80.40	64.40	180.50	3.93	4.00
13H-2	39.0–41.0	115.89	1.22	0.35	2.36	84.90	85.60	71.50	250.40	5.61	5.76
13H-2	109.0–111.0	116.69	1.25	0.41	2.29	81.70	82.40	67.10	203.60	4.46	4.55
13H-3	39.0–41.0	117.39	1.18	0.31	2.18	85.50	86.20	74.00	284.30	5.90	6.06
13H-3	109.0–111.0	118.19	1.17	0.29	2.17	86.20	86.90	75.10	302.40	6.23	6.41
13H-4	39.0–41.0	118.89	1.21	0.36	2.23	83.60	84.30	70.60	239.70	5.10	5.22
13H-4	109.0–111.0	119.69	1.24	0.41	2.25	81.50	82.20	67.30	205.60	4.42	4.51
13H-5	39.0–41.0	120.39	1.19	0.30	2.28	86.20	86.90	74.30	289.60	6.25	6.43
13H-5	109.0–111.0	121.19	1.23	0.39	2.25	82.20	82.90	68.20	214.80	4.61	4.71
13H-6	39.0–41.0	121.89	1.20	0.34	2.17	83.80	84.50	71.50	250.50	5.18	5.30
13H-6	109.0–111.0	122.69	1.27	0.46	2.30	79.80	80.40	64.10	178.70	3.94	4.01
13H-7	39.0–41.0	123.21	1.27	0.43	2.38	81.50	82.20	66.00	194.20	4.42	4.51
14H-1	41.0–43.0	123.89	1.21	0.35	2.30	84.40	85.10	71.20	246.70	5.40	5.54
14H-1	109.0–111.0	124.69	1.24	0.39	2.32	82.60	83.30	68.20	214.90	4.75	4.86
14H-2	39.0–41.0	125.39	1.26	0.41	2.49	83.30	83.90	67.80	210.40	4.99	5.11
14H-2	109.0–111.0	126.21	1.16	0.24	2.35	89.40	90.10	79.20	381.10	8.41	8.74

Table 11 (continued).

Core, section	Interval (cm)	Depth (mbsf)	Wet-bulk density (g/cm^3)	Dry-bulk density (g/cm^3)	Grain density (g/cm^3)	Wet porosity (%)	Dry porosity (%)	Wet water content (%)	Dry water content (%)	Void ratio 1	Void ratio 2
14H-3	41.0–43.0	126.89	1.20	0.32	2.33	86.00	86.70	73.60	279.10	6.16	6.34
14H-3	109.0–111.0	127.69	1.19	0.29	2.32	86.90	87.60	75.10	302.00	6.64	6.84
14H-4	39.0–41.0	128.39	1.30	0.49	2.40	79.30	80.00	62.50	166.80	3.84	3.91
14H-4	109.0–111.0	129.21	1.22	0.36	2.22	83.20	83.90	70.10	234.50	4.96	5.07
14H-5	41.0–43.0	129.89	1.20	0.34	2.18	84.20	85.00	72.00	257.00	5.34	5.47
14H-5	109.0–111.0	130.69	1.19	0.29	2.42	87.60	88.30	75.70	310.70	7.09	7.33
14H-6	39.0–41.0	131.59	1.27	0.44	2.45	81.90	82.50	65.90	192.80	4.52	4.62
14H-6	129.0–131.0	132.19	1.38	0.63	2.42	73.80	74.40	54.70	120.70	2.82	2.86
14H-7	39.0–41.0	132.69	1.56	0.95	2.34	59.20	59.70	39.00	63.80	1.45	1.46
15H-1	39.0–41.0	133.39	1.36	0.59	2.41	75.20	75.80	56.70	130.70	3.03	3.08
15H-1	109.0–111.0	134.19	1.22	0.49	1.73	71.10	71.90	59.60	147.40	2.46	2.49
15H-2	39.0–41.0	134.89	1.35	0.59	2.33	74.50	75.10	56.60	130.20	2.92	2.96
15H-2	109.0–111.0	135.74	1.50	0.82	2.44	65.90	66.40	45.10	82.00	1.93	1.95
15H-3	44.0–46.0	136.39	1.54	0.91	2.34	60.60	61.10	40.40	67.80	1.54	1.55
15H-3	109.0–111.0	137.19	1.36	0.62	2.26	72.40	73.00	54.60	120.10	2.62	2.65
15H-4	39.0–41.0	137.89	1.46	0.79	2.33	65.90	66.40	46.10	85.60	1.93	1.95
15H-4	109.0–111.0	138.69	1.28	0.48	2.26	78.50	79.20	62.80	168.90	3.66	3.72
15H-5	39.0–41.0	139.39	1.28	0.47	2.26	78.70	79.40	63.10	171.00	3.70	3.77
15H-5	109.0–111.0	140.19	1.30	0.51	2.27	77.20	77.80	60.80	155.30	3.39	3.44
15H-6	39.0–41.0	140.89	1.22	0.37	2.28	83.40	84.10	69.80	231.20	5.03	5.14
15H-6	109.0–111.0	141.44	1.26	0.44	2.27	80.20	80.80	65.00	186.10	4.04	4.12
15H-7	14.0–16.0	142.24	1.27	0.45	2.29	80.00	80.70	64.60	182.70	4.00	4.08
16H-1	44.0–46.0	142.89	1.23	0.37	2.34	84.00	84.70	70.20	235.60	5.26	5.39
16H-1	109.0–111.0	143.69	1.28	0.47	2.23	78.50	79.10	63.00	170.40	3.65	3.71
16H-2	39.0–41.0	144.39	1.18	0.29	2.22	86.40	87.10	75.10	301.10	6.33	6.51
16H-2	109.0–111.0	145.19	1.21	0.35	2.24	83.80	84.50	70.80	242.70	5.18	5.31
16H-3	39.0–41.0	145.89	1.19	0.30	2.43	87.40	88.10	75.10	302.30	6.95	7.17
16H-3	109.0–111.0	146.69	1.21	0.35	2.24	83.80	84.50	70.80	242.90	5.18	5.30
16H-4	39.0–41.0	147.39	1.24	0.40	2.31	82.50	83.10	68.10	213.60	4.71	4.81
16H-4	109.0–111.0	148.21	1.27	0.46	2.26	79.20	79.80	63.70	175.30	3.80	3.87
16H-5	41.0–43.0	148.89	1.29	0.48	2.38	79.50	80.20	63.00	170.10	3.88	3.95
16H-5	109.0–111.0	149.69	1.35	0.56	2.46	76.70	77.30	58.20	139.40	3.29	3.34
16H-6	39.0–41.0	150.40	1.32	0.53	2.35	77.00	77.60	59.70	148.00	3.34	3.39
16H-6	110.0–112.0	151.19	1.44	0.74	2.38	68.50	69.00	48.60	94.50	2.17	2.19
16H-7	39.0–41.0	151.72	1.31	0.52	2.30	77.00	77.60	60.20	151.10	3.34	3.39
17H-1	42.0–44.0	152.39	1.26	0.42	2.40	82.00	82.60	66.50	198.40	4.55	4.64
17H-1	109.0–111.0	153.19	1.31	0.50	2.39	78.80	79.40	61.80	161.80	3.71	3.77
17H-2	39.0–41.0	153.89	1.26	0.43	2.31	81.10	81.80	66.00	193.80	4.29	4.38
17H-2	109.0–111.0	154.72	1.27	0.45	2.30	80.00	80.60	64.40	180.70	3.99	4.07
17H-3	42.0–44.0	155.39	1.29	0.48	2.30	78.80	79.50	62.80	169.00	3.73	3.79
17H-3	109.0–111.0	156.89	1.35	0.57	2.38	75.70	76.30	57.60	135.70	3.11	3.15
17H-4	109.0–111.0	158.39	1.32	0.53	2.40	77.80	78.40	60.30	151.70	3.50	3.56
17H-5	109.0–111.0	159.89	1.29	0.48	2.36	79.10	79.70	62.60	167.30	3.79	3.85
17H-6	109.0–111.0	160.69	1.34	0.57	2.36	75.70	76.30	57.80	136.90	3.11	3.15
17H-7	39.0–41.0	161.89	1.31	0.49	2.45	79.70	80.30	62.50	166.60	3.92	3.99
18H-1	109.0–111.0	163.39	1.27	0.43	2.40	81.90	82.50	66.30	196.70	4.52	4.61
18H-2	109.0–111.0	164.90	1.26	0.45	2.16	78.70	79.40	64.10	178.30	3.70	3.77
18H-3	110.0–112.0	166.39	1.36	0.58	2.45	76.00	76.60	57.40	134.80	3.17	3.22
18H-4	109.0–111.0	167.89	1.30	0.49	2.34	78.70	79.30	62.10	164.00	3.69	3.75
18H-5	109.0–111.0	169.39	1.36	0.59	2.41	75.40	76.00	56.90	132.00	3.07	3.11
18H-6	109.0–111.0	170.19	1.30	0.50	2.32	78.00	78.60	61.40	159.10	3.55	3.60
18H-7	39.0–41.0	171.49	1.23	0.37	2.28	83.30	84.00	69.60	229.30	4.99	5.11
19H-1	119.0–121.0	172.89	1.25	0.41	2.36	82.40	83.00	67.40	207.10	4.67	4.77
19H-2	109.0–111.0	174.47	1.24	0.40	2.28	82.10	82.70	67.70	209.60	4.57	4.67
19H-3	117.0–119.0	175.89	1.26	0.42	2.34	81.60	82.30	66.50	198.80	4.44	4.53
19H-4	109.0–111.0	177.39	1.37	0.60	2.47	75.30	75.90	56.20	128.30	3.05	3.09
19H-5	109.0–111.0	178.89	1.28	0.46	2.39	80.40	81.00	64.10	178.60	4.09	4.17
19H-6	109.0–111.0	179.69	1.31	0.51	2.43	78.80	79.40	61.40	159.30	3.71	3.77
19H-7	39.0–41.0	180.89	1.25	0.41	2.36	82.00	82.70	67.00	202.90	4.57	4.66
20H-1	109.0–111.0	182.39	1.27	0.46	2.25	79.00	79.60	63.50	174.00	3.75	3.82
20H-2	109.0–111.0	183.89	1.33	0.55	2.36	76.10	76.70	58.40	140.60	3.19	3.23
20H-3	109.0–111.0	185.39	1.36	0.60	2.33	74.00	74.60	55.90	126.90	2.84	2.88
20H-4	109.0–111.0	186.89	1.40	0.63	2.58	75.20	75.80	55.10	122.50	3.04	3.08
20H-5	109.0–111.0	188.39	1.45	0.71	2.57	72.20	72.80	51.20	104.90	2.60	2.63
20H-6	109.0–111.0	190.39	1.43	0.68	2.54	72.80	73.40	52.20	109.20	2.68	2.71
21H-1	109.0–111.0	191.89	1.34	0.55	2.45	77.20	77.90	59.10	144.50	3.40	3.45
21H-2	109.0–111.0	193.39	1.31	0.50	2.42	78.80	79.40	61.60	160.10	3.72	3.78
21H-3	109.0–111.0	194.89	1.30	0.49	2.43	79.60	80.30	62.70	167.90	3.91	3.98
21H-4	109.0–111.0	196.39	1.27	0.46	2.27	79.40	80.10	63.90	177.20	3.86	3.93
21H-5	109.0–111.0	197.89	1.27	0.44	2.30	80.40	81.00	65.00	186.10	4.10	4.18
21H-6	109.0–111.0	198.69	1.32	0.55	2.28	75.70	76.30	58.70	142.00	3.12	3.16
21H-7	39.0–41.0	199.99	1.23	0.38	2.21	82.20	82.90	68.70	219.70	4.63	4.73
22H-1	119.0–121.0	201.39	1.27	0.42	2.48	82.70	83.30	66.80	201.60	4.76	4.87
22H-2	109.0–111.0	202.89	1.24	0.40	2.28	81.90	82.50	67.40	207.20	4.52	4.61
22H-3	109.0–111.0	204.39	1.27	0.45	2.27	79.60	80.30	64.20	179.70	3.91	3.98
22H-4	109.0–111.0	205.89	1.25	0.43	2.15	79.50	80.20	65.30	188.50	3.88	3.95
22H-5	109.0–111.0	207.39	1.27	0.46	2.23	79.00	79.70	63.80	175.90	3.77	3.84
22H-6	109.0–111.0	208.19	1.27	0.47	2.16	77.70	78.40	62.70	167.90	3.49	3.54
22H-7	39.0–41.0	209.39	1.26	0.45	2.18	79.10	79.80	64.50	181.30	3.79	3.86
23H-1	109.0–111.0	210.89	1.27	0.47	2.21	78.60	79.20	63.40	173.10	3.66	3.72
23H-2	109.0–111.0	212.39	1.27	0.46	2.27	79.40	80.10	63.90	177.10	3.86	3.92
23H-3	109.0–111.0	213.89	1.28	0.48	2.21	77.80	78.50	62.30	165.20	3.51	3.56
23H-4	109.0–111.0	215.49	1.27	0.46	2.20	78.90	79.50	63.90	176.80	3.73	3.80

Table 11 (continued).

Core, section	Interval (cm)	Depth (mbsf)	Wet-bulk density (g/cm^3)	Dry-bulk density (g/cm^3)	Grain density (g/cm^3)	Wet porosity (%)	Dry porosity (%)	Wet water content (%)	Dry water content (%)	Void ratio 1	Void ratio 2
23H-5	119.0–121.0	216.99	1.25	0.43	2.19	79.80	80.50	65.30	188.50	3.96	4.03
23H-6	119.0–121.0	217.69	1.26	0.46	2.13	78.20	78.90	63.60	174.70	3.58	3.64
23H-7	39.0–41.0	218.94	1.26	0.43	2.25	80.30	81.00	65.40	189.30	4.08	4.15
24H-1	114.0–116.0	220.39	1.25	0.44	2.19	79.50	80.20	64.90	184.80	3.87	3.94
24H-2	109.0–111.0	221.98	1.38	0.64	2.34	72.50	73.10	53.80	116.50	2.63	2.66
24H-3	118.0–120.0	223.49	1.30	0.50	2.25	77.30	77.90	61.10	157.00	3.40	3.45
24H-4	119.0–121.0	224.89	1.38	0.62	2.47	74.60	75.20	55.30	123.50	2.94	2.98
24H-5	109.0–111.0	226.39	1.29	0.47	2.39	79.80	80.50	63.30	172.80	3.96	4.04
24H-6	109.0–111.0	227.19	1.30	0.51	2.23	76.60	77.20	60.40	152.50	3.27	3.32
24H-7	39.0–41.0	228.39	1.26	0.42	2.38	81.90	82.50	66.40	197.90	4.51	4.61
25H-1	109.0–111.0	229.95	1.28	0.46	2.31	79.80	80.40	64.00	177.70	3.94	4.01
25H-2	115.0–117.0	231.35	1.23	0.38	2.27	82.80	83.50	69.00	222.90	4.83	4.93
25H-3	105.0–107.0	232.87	1.21	0.38	2.08	81.30	82.00	68.50	217.70	4.34	4.42
25H-4	107.0–109.0	234.40	1.23	0.39	2.24	82.20	82.90	68.20	214.90	4.61	4.71
25H-5	110.0–112.0	235.90	1.24	0.40	2.27	81.90	82.60	67.60	209.10	4.54	4.63
25H-6	110.0–112.0	236.69	1.28	0.46	2.31	79.60	80.20	63.80	175.90	3.89	3.96
25H-7	39.0–41.0	237.89	1.18	0.34	1.99	82.70	83.40	71.50	250.70	4.77	4.87
26H-1	109.0–111.0	239.39	1.24	0.41	2.23	81.30	82.00	67.10	203.60	4.35	4.44
26H-2	109.0–111.0	240.89	1.28	0.46	2.31	79.60	80.20	63.80	176.30	3.90	3.97
26H-3	109.0–111.0	242.39	1.28	0.45	2.41	80.80	81.40	64.60	182.20	4.21	4.29
26H-4	109.0–111.0	243.89	1.25	0.42	2.25	80.80	81.40	66.10	195.20	4.20	4.28
26H-5	109.0–111.0	245.39	1.28	0.46	2.33	79.80	80.40	63.90	176.90	3.95	4.02
26H-6	109.0–111.0	246.19	1.31	0.52	2.34	77.50	78.10	60.50	153.00	3.45	3.50
26H-7	39.0–41.0	247.39	1.26	0.42	2.34	81.70	82.30	66.50	198.90	4.45	4.54
27H-1	109.0–111.0	248.89	1.28	0.45	2.41	81.10	81.70	65.00	186.00	4.29	4.38
27H-2	109.0–111.0	250.39	1.28	0.47	2.26	78.80	79.40	63.10	171.10	3.71	3.78
27H-3	109.0–111.0	251.89	1.30	0.51	2.29	77.30	77.90	60.70	154.50	3.40	3.45
27H-4	109.0–111.0	253.39	1.24	0.41	2.18	80.90	81.60	66.90	202.50	4.23	4.31
27H-5	109.0–111.0	254.89	1.26	0.45	2.23	79.40	80.10	64.30	180.50	3.86	3.93
27H-6	109.0–111.0	255.69	1.27	0.45	2.31	80.20	80.80	64.70	183.10	4.05	4.12
27H-7	39.0–41.0	256.89	1.25	0.43	2.25	80.60	81.30	65.80	192.70	4.16	4.24
28H-1	109.0–111.0	258.39	1.24	0.43	2.08	79.10	79.80	65.40	189.30	3.78	3.85
28H-2	109.0–111.0	259.89	1.27	0.46	2.31	79.90	80.60	64.20	179.70	3.98	4.05
28H-3	109.0–111.0	261.39	1.29	0.47	2.39	79.70	80.40	63.20	172.10	3.94	4.01
28H-4	109.0–111.0	262.89	1.30	0.49	2.39	79.00	79.60	62.10	163.70	3.76	3.82
28H-5	109.0–111.0	264.39	1.28	0.48	2.24	78.20	78.80	62.50	166.70	3.58	3.64
28H-6	109.0–111.0	265.19	1.21	0.44	1.75	74.30	75.10	63.10	171.30	2.89	2.93
28H-7	39.0–41.0	266.39	1.30	0.50	2.27	77.50	78.10	61.20	157.80	3.44	3.50
29H-1	109.0–111.0	267.89	1.29	0.48	2.35	79.30	80.00	62.90	169.80	3.83	3.90
29H-2	109.0–111.0	269.39	1.29	0.49	2.25	77.70	78.30	61.70	161.10	3.48	3.54
29H-3	109.0–111.0	270.89	1.31	0.54	2.24	75.70	76.30	59.10	144.50	3.11	3.16
29H-4	109.0–111.0	272.39	1.31	0.53	2.29	76.60	77.20	59.80	148.60	3.28	3.33
29H-5	109.0–111.0	273.89	1.33	0.54	2.37	76.90	77.50	59.40	146.20	3.33	3.38
29H-6	109.0–111.0	274.69	1.26	0.47	2.11	77.20	77.80	62.50	166.80	3.38	3.43
29H-7	39.0–41.0	275.84	1.30	0.50	2.29	77.80	78.50	61.50	159.50	3.51	3.56
30H-1	104.0–106.0	277.32	1.30	0.49	2.35	78.80	79.50	62.30	165.50	3.73	3.79
30H-2	102.0–104.0	278.93	1.26	0.44	2.21	79.80	80.50	65.00	186.10	3.95	4.02
30H-3	113.0–115.0	280.39	1.25	0.43	2.23	80.50	81.20	65.90	193.60	4.14	4.22
30H-4	109.0–111.0	281.89	1.28	0.47	2.26	78.80	79.40	63.10	171.20	3.71	3.77
30H-5	109.0–111.0	282.72	1.40	0.49	4.37	88.30	88.90	64.80	184.00	7.57	7.84
30H-6	42.0–44.0	283.39	1.28	0.49	2.14	76.80	77.50	61.70	161.20	3.32	3.37
30H-7	39.0–41.0	285.39	1.25	0.44	2.14	79.20	79.90	65.00	185.80	3.82	3.89
31H-1	109.0–111.0	286.89	1.24	0.41	2.21	80.90	81.60	66.60	199.70	4.23	4.31
31H-2	109.0–111.0	288.39	1.25	0.43	2.25	80.80	81.40	66.00	194.50	4.20	4.28
31H-3	109.0–111.0	289.89	1.26	0.47	2.06	77.10	77.80	62.90	169.60	3.36	3.41
31H-4	109.0–111.0	291.39	1.27	0.45	2.27	79.70	80.40	64.40	180.70	3.93	4.00
31H-5	109.0–111.0	292.89	1.25	0.41	2.29	81.50	82.20	66.80	201.40	4.41	4.50
31H-6	109.0–111.0	293.69	1.29	0.50	2.16	76.30	77.00	60.80	155.30	3.22	3.27
31H-7	39.0–41.0	294.89	1.24	0.42	2.17	80.30	81.00	66.30	196.50	4.08	4.15
32H-1	109.0–111.0	296.39	1.26	0.45	2.22	79.60	80.30	64.70	183.30	3.91	3.98
32H-2	109.0–111.0	297.89	1.27	0.47	2.23	78.70	79.30	63.20	172.00	3.68	3.75
32H-3	109.0–111.0	299.39	1.27	0.47	2.15	77.70	78.30	62.80	168.60	3.48	3.53
32H-4	109.0–111.0	300.89	1.30	0.51	2.27	77.30	78.00	61.00	156.40	3.41	3.46
32H-5	109.0–111.0	302.39	1.25	0.42	2.17	80.10	80.80	65.90	193.20	4.02	4.10
32H-6	109.0–111.0	303.19	1.27	0.46	2.16	78.20	78.90	63.30	172.60	3.59	3.65
32H-7	39.0–41.0	304.39	1.25	0.41	2.27	81.60	82.20	67.00	203.50	4.43	4.52
33H-1	109.0–111.0	305.89	1.25	0.43	2.13	79.30	80.00	65.20	187.30	3.83	3.90
33H-2	109.0–111.0	307.39	1.25	0.41	2.26	81.40	82.10	66.90	202.30	4.37	4.46
33H-3	109.0–111.0	308.89	1.24	0.42	2.17	80.30	81.00	66.20	196.00	4.08	4.16
33H-4	109.0–111.0	310.39	1.27	0.45	2.24	79.40	80.00	64.20	179.40	3.85	3.92
33H-5	109.0–111.0	311.89	1.26	0.46	2.18	78.70	79.40	63.90	176.90	3.70	3.76
33H-6	109.0–111.0	312.39	1.40	0.67	2.34	71.00	71.60	52.00	108.40	2.45	2.48
33H-7	9.0–11.0	313.89	1.29	0.48	2.30	78.60	79.20	62.50	166.40	3.67	3.73
34H-1	109.0–111.0	315.39	1.29	0.51	2.21	76.70	77.40	60.80	154.90	3.30	3.35
34H-2	109.0–111.0	316.89	1.25	0.48	1.93	74.80	75.50	61.40	159.30	2.97	3.01
34H-3	109.0–111.0	318.39	1.32	0.53	2.36	77.10	77.80	59.80	148.90	3.37	3.43
34H-4	109.0–111.0	319.89	1.29	0.51	2.23	77.00	77.70	61.00	156.20	3.35	3.40
34H-5	109.0–111.0	321.39	1.30	0.51	2.23	76.60	77.30	60.50	153.00	3.28	3.33
34H-6	109.0–111.0	322.19	1.31	0.53	2.27	76.40	77.00	59.80	148.50	3.24	3.29
34H-7	39.0–41.0	323.39	1.28	0.48	2.26	78.60	79.20	62.80	169.10	3.67	3.73
35H-1	109.0–111.0	324.89	1.27	0.46	2.20	78.60	79.20	63.40	173.40	3.67	3.73
35H-2	109.0–111.0	326.39	1.31	0.50	2.38	78.60	79.20	61.60	160.70	3.68	3.74
35H-3	109.0–111.0	327.89	1.32	0.53	2.34	76.80	77.50	59.50	147.20	3.32	3.37

Table 11 (continued).

Core, section	Interval (cm)	Depth (mbsf)	Wet-bulk density (g/cm^3)	Dry-bulk density (g/cm^3)	Grain density (g/cm^3)	Wet porosity (%)	Dry porosity (%)	Wet water content (%)	Dry water content (%)	Void ratio 1	Void ratio 2
35H-4	109.0–111.0	329.39	1.28	0.50	2.15	76.60	77.30	61.30	158.50	3.27	3.32
35H-5	109.0–111.0	330.89	1.32	0.54	2.33	76.50	77.10	59.20	145.30	3.26	3.31
35H-6	109.0–111.0	331.69	1.33	0.56	2.29	75.30	75.90	58.10	138.50	3.05	3.09
35H-7	39.0–41.0	332.89	1.28	0.48	2.20	77.80	78.50	62.40	166.10	3.51	3.56
36H-1	109.0–111.0	334.39	1.29	0.49	2.25	78.10	78.80	62.30	165.00	3.57	3.63
36H-2	109.0–111.0	335.89	1.31	0.53	2.27	76.20	76.90	59.50	146.70	3.21	3.26
36H-3	109.0–111.0	337.39	1.31	0.51	2.33	77.70	78.40	61.00	156.30	3.49	3.55
36H-4	109.0–111.0	338.89	1.29	0.50	2.24	77.30	77.90	61.20	157.70	3.40	3.46
36H-5	109.0–111.0	340.39	1.46	0.70	2.69	73.50	74.00	51.70	107.00	2.77	2.81
36H-6	109.0–111.0	341.19	1.45	0.72	2.55	71.70	72.20	50.70	102.60	2.53	2.56
36H-7	39.0–41.0	342.39	1.34	0.57	2.37	75.70	76.30	57.70	136.70	3.12	3.16
37H-1	109.0–111.0	343.89	1.34	0.57	2.35	75.50	76.10	57.70	136.30	3.09	3.13
37H-2	109.0–111.0	345.39	1.33	0.53	2.45	78.00	78.60	60.10	150.40	3.54	3.60
37H-3	109.0–111.0	346.89	1.45	0.72	2.50	70.80	71.40	50.20	100.70	2.43	2.45
37H-4	109.0–111.0	348.39	1.34	0.55	2.46	77.10	77.70	58.80	142.60	3.37	3.42
37H-5	109.0–111.0	349.89	1.43	0.67	2.57	73.40	73.90	52.70	111.40	2.76	2.79
37H-6	109.0–111.0	351.89	1.37	0.60	2.40	74.70	75.30	56.00	127.30	2.95	2.99
37H-7	39.0–41.0	353.39	1.31	0.53	2.27	76.10	76.80	59.40	146.10	3.19	3.24
38H-1	109.0–111.0	354.89	1.32	0.56	2.24	74.90	75.50	58.00	138.10	2.98	3.02
38H-2	109.0–111.0	356.39	1.32	0.55	2.28	75.70	76.30	58.60	141.80	3.11	3.16
38H-3	109.0–111.0	357.89	1.34	0.56	2.33	75.40	76.10	57.80	137.20	3.07	3.12
38H-4	109.0–111.0	359.39	1.36	0.59	2.37	74.70	75.30	56.40	129.50	2.95	2.99
38H-5	109.0–111.0	360.19	1.34	0.56	2.43	76.70	77.30	58.50	140.90	3.29	3.34
38H-6	109.0–111.0	361.39	1.35	0.57	2.38	75.60	76.20	57.40	135.00	3.09	3.14
38H-7	39.0–41.0	362.89	1.33	0.54	2.39	77.10	77.70	59.50	146.90	3.37	3.42
39H-1	109.0–111.0	364.39	1.29	0.49	2.26	77.80	78.40	61.70	161.00	3.50	3.56
39H-2	109.0–111.0	365.89	1.29	0.52	2.14	75.30	75.90	59.70	148.00	3.04	3.09
39H-3	109.0–111.0	367.39	1.29	0.50	2.18	76.60	77.30	60.90	155.90	3.28	3.32
39H-4	109.0–111.0	367.99	1.35	0.58	2.38	75.20	75.80	57.00	132.50	3.03	3.08
39H-5	109.0–111.0	368.63	1.35	0.56	2.46	76.90	77.50	58.50	140.80	3.33	3.38
39H-6	19.0–21.0	370.89	1.33	0.57	2.21	74.00	74.60	57.20	133.60	2.84	2.88
39H-7	39.0–41.0	372.39	1.35	0.58	2.36	75.20	75.80	57.10	133.40	3.03	3.08
40H-1	109.0–111.0	373.89	1.32	0.52	2.38	77.60	78.30	60.30	151.90	3.47	3.53
40H-2	109.0–111.0	375.39	1.36	0.60	2.34	74.20	74.80	56.00	127.40	2.87	2.91
40H-3	109.0–111.0	376.89	1.34	0.57	2.37	75.80	76.40	57.80	137.20	3.13	3.17
40H-4	109.0–111.0	378.39	1.33	0.55	2.33	76.00	76.60	58.50	141.20	3.16	3.21
40H-5	109.0–111.0	379.19	1.36	0.57	2.49	76.80	77.40	58.10	138.40	3.32	3.37
40H-6	109.0–111.0	379.69	1.34	0.55	2.43	76.90	77.50	58.80	142.60	3.33	3.39
40H-7	39.0–41.0	381.89	1.28	0.48	2.24	78.30	79.00	62.70	167.80	3.61	3.67
41H-1	39.0–41.0	383.39	1.33	0.52	2.53	78.90	79.50	60.70	154.20	3.75	3.81
41H-2	109.0–111.0	384.89	1.36	0.57	2.51	76.80	77.40	57.90	137.40	3.31	3.36
41H-3	109.0–111.0	386.39	1.36	0.58	2.46	76.00	76.60	57.30	134.00	3.17	3.22
41H-4	109.0–111.0	387.89	1.40	0.64	2.52	74.10	74.70	54.10	117.90	2.86	2.90
41H-5	109.0–111.0	388.69	1.33	0.56	2.35	76.10	76.70	58.40	140.40	3.18	3.23
41H-6	109.0–111.0	389.89	1.34	0.56	2.34	75.80	76.50	58.20	139.10	3.14	3.18
41H-7	39.0–41.0	391.39	1.37	0.60	2.41	74.80	75.40	56.10	128.00	2.98	3.02
42H-1	109.0–111.0	392.89	1.36	0.59	2.36	74.50	75.10	56.30	128.60	2.93	2.96
42H-2	109.0–111.0	394.39	1.40	0.64	2.55	74.50	75.10	54.40	119.40	2.93	2.97
42H-3	109.0–111.0	395.89	1.37	0.58	2.54	76.80	77.40	57.60	136.10	3.32	3.37
42H-4	109.0–111.0	397.39	1.39	0.63	2.49	74.30	74.80	54.60	120.10	2.89	2.92
42H-5	109.0–111.0	398.19	1.37	0.59	2.48	75.70	76.30	56.70	130.90	3.12	3.17
42H-6	109.0–111.0										
42H-7	39.0–41.0										
145-882B-											
1H-1	109.0–111.0	1.09	1.37	0.57	2.67	78.40	79.00	58.60	141.80	3.63	3.69
1H-2	109.0–111.0	2.59	1.37	0.55	2.74	79.40	80.00	59.50	147.10	3.87	3.94
1H-3	109.0–111.0	4.09	1.49	0.80	2.52	68.10	68.60	46.70	87.60	2.13	2.15
2H-1	109.0–111.0	5.49	1.36	0.55	2.58	78.10	78.70	59.10	144.30	3.57	3.63
2H-2	104.0–106.0	6.94	1.45	0.69	2.73	74.50	75.10	52.70	111.30	2.92	2.96
2H-3	109.0–111.0	8.49	1.36	0.55	2.66	78.80	79.40	59.40	146.10	3.72	3.79
2H-4	109.0–111.0	9.99	1.32	0.48	2.75	82.10	82.70	63.50	174.20	4.58	4.68
2H-5	109.0–111.0	11.49	1.26	0.41	2.53	83.50	84.20	67.80	210.20	5.08	5.20
3H-1	109.0–111.0	14.99	1.42	0.67	2.57	73.70	74.20	53.00	112.90	2.80	2.83
3H-2	109.0–111.0	16.49	1.38	0.56	2.83	79.80	80.40	59.30	145.90	3.96	4.03
3H-3	114.0–116.0	18.04	1.38	0.57	2.71	78.60	79.20	58.60	141.30	3.67	3.73
3H-4	109.0–111.0	19.49	1.36	0.56	2.60	78.10	78.60	58.70	142.20	3.56	3.62
3H-5	109.0–111.0	20.99	1.39	0.59	2.77	78.30	78.90	57.60	136.10	3.61	3.67
3H-6	109.0–111.0	22.49	1.26	0.42	2.41	82.30	82.90	66.80	201.60	4.64	4.74
3H-7	39.0–41.0	23.29	1.34	0.51	2.82	81.70	82.30	62.30	165.30	4.46	4.56
4H-1	109.0–111.0	24.49	1.36	0.55	2.72	79.40	80.00	59.70	148.00	3.86	3.92
4H-2	109.0–111.0	25.99	1.47	0.70	2.79	74.50	75.00	52.10	108.70	2.92	2.96
4H-3	109.0–111.0	27.49	1.20	0.32	2.31	85.80	86.50	73.40	276.40	6.06	6.23
4H-4	109.0–111.0	28.99	1.42	0.64	2.76	76.60	77.10	55.20	123.00	3.27	3.32
4H-5	109.0–111.0	30.49	1.48	0.72	2.79	73.70	74.20	51.00	104.20	2.80	2.83
4H-6	109.0–111.0	31.99	1.17	0.25	2.50	89.50	90.20	78.40	363.50	8.54	8.88
4H-7	39.0–41.0	32.79	1.23	0.37	2.42	84.30	85.00	70.00	233.10	5.38	5.51
5H-1	109.0–111.0	33.99	1.42	0.65	2.67	75.20	75.70	54.10	117.70	3.03	3.07
5H-2	113.0–115.0	35.53	1.36	0.55	2.74	79.70	80.30	59.90	149.30	3.93	4.00
5H-3	109.0–111.0	36.99	1.42	0.64	2.67	75.70	76.30	54.80	121.10	3.12	3.16
5H-4	113.0–115.0	38.53	1.43	0.66	2.62	74.30	74.90	53.40	114.70	2.89	2.93
5H-5	109.0–110.0	39.99	1.33	0.52	2.53	79.10	79.70	60.90	156.00	3.79	3.86
5H-6	109.0–110.0	41.49	1.42	0.65	2.61	74.80	75.40	54.10	117.80	2.97	3.01
5H-7	29.0–31.0	42.19	1.35	0.54	2.67	79.30	79.90	60.00	149.90	3.84	3.91

Table 11 (continued).

Core, section	Interval (cm)	Depth (mbsf)	Wet-bulk density (g/cm^3)	Dry-bulk density (g/cm^3)	Grain density (g/cm^3)	Wet porosity (%)	Dry porosity (%)	Wet water content (%)	Dry water content (%)	Void ratio 1	Void ratio 2
6H-1	109.0–110.0	43.49	1.25	0.39	2.48	83.90	84.50	68.80	220.60	5.21	5.34
6H-2	109.0–110.0	44.99	1.29	0.44	2.63	82.70	83.30	65.60	190.80	4.79	4.90
6H-3	109.0–110.0	46.49	1.39	0.60	2.67	77.10	77.70	56.70	131.00	3.37	3.42
6H-4	119.0–121.0	48.09	1.50	0.77	2.68	71.00	71.50	48.60	94.50	2.45	2.47
6H-5	109.0–110.0	49.49	1.42	0.67	2.56	73.50	74.10	53.00	112.80	2.78	2.82
6H-6	109.0–110.0	50.99	1.34	0.54	2.52	78.10	78.70	59.60	147.40	3.57	3.63
6H-7	39.0–41.0	51.79	1.37	0.61	2.39	74.10	74.60	55.30	123.90	2.86	2.89
7H-1	111.0–113.0	53.01	1.37	0.58	2.61	77.40	78.00	57.70	136.20	3.42	3.47
7H-2	109.0–110.0	54.49	1.33	0.53	2.46	78.00	78.60	60.10	150.40	3.55	3.60
7H-3	109.0–110.0	55.99	1.30	0.47	2.52	80.80	81.40	63.60	174.50	4.21	4.30
7H-4	109.0–110.0	57.49	1.47	0.73	2.66	72.40	72.90	50.50	102.10	2.62	2.65
7H-5	114.0–116.0	59.04	1.50	0.78	2.67	70.40	70.90	48.00	92.20	2.38	2.40
7H-6	109.0–110.0	60.49	1.42	0.65	2.69	75.60	76.20	54.50	119.80	3.10	3.14
7H-7	39.0–41.0	61.29	1.44	0.67	2.72	74.90	75.50	53.30	114.00	2.99	3.03
8H-1	109.0–110.0	62.49	1.47	0.72	2.68	72.80	73.30	50.80	103.20	2.67	2.70
8H-2	109.0–110.0	63.99	1.44	0.69	2.58	73.10	73.60	52.10	109.00	2.71	2.75
8H-3	114.0–116.0	65.54	1.32	0.51	2.51	79.20	79.80	61.20	158.00	3.81	3.87
8H-4	109.0–110.0	66.99	1.43	0.66	2.65	74.60	75.20	53.60	115.30	2.94	2.98
8H-5	109.0–110.0	68.49	1.45	0.71	2.54	71.60	72.20	50.80	103.10	2.52	2.55
8H-6	109.0–110.0	69.99	1.44	0.70	2.58	72.50	73.10	51.50	106.20	2.64	2.67
8H-7	39.0–41.0	70.79	1.44	0.69	2.64	73.70	74.20	52.40	110.20	2.80	2.84
9H-1	112.0–114.0	72.02	1.43	0.64	2.82	76.80	77.40	55.00	122.40	3.32	3.37
9H-2	109.0–110.0	73.49	1.48	0.75	2.62	71.00	71.60	49.20	96.80	2.45	2.48
9H-3	109.0–110.0	74.99	1.49	0.75	2.79	72.90	73.40	50.00	99.90	2.69	2.72
9H-4	109.0–110.0	76.49	1.40	0.61	2.75	77.40	77.90	56.40	129.50	3.42	3.47
9H-5	109.0–110.0	77.99	1.44	0.68	2.69	74.50	75.10	53.00	112.90	2.93	2.97
9H-6	104.0–106.0	79.44	1.50	0.78	2.67	70.40	70.90	48.00	92.30	2.38	2.41
9H-7	49.0–51.0	80.39	1.42	0.65	2.69	75.60	76.10	54.50	119.80	3.10	3.14
10H-1	109.0–110.0	81.49	1.42	0.66	2.60	74.10	74.60	53.30	114.20	2.86	2.89
10H-2	119.0–121.0	83.09	1.52	0.81	2.64	69.10	69.60	46.70	87.50	2.23	2.26
10H-3	109.0–110.0	84.49	1.44	0.68	2.70	74.40	74.90	52.80	111.70	2.90	2.94
10H-4	109.0–110.0	85.99	1.32	0.52	2.44	78.50	79.10	60.90	155.90	3.66	3.72
10H-5	109.0–110.0	87.49	1.28	0.47	2.30	79.00	79.70	63.10	170.90	3.76	3.83
10H-6	119.0–121.0	89.09	1.34	0.53	2.56	79.00	79.60	60.40	152.70	3.75	3.82
10H-7	14.0–16.0	89.54	1.47	0.73	2.60	71.50	72.00	50.00	99.90	2.51	2.54
11H-1	109.0–110.0	90.99	1.39	0.60	2.64	77.00	77.60	56.90	132.00	3.35	3.40
11H-2	109.0–110.0	92.49	1.44	0.68	2.66	74.20	74.80	52.90	112.30	2.88	2.92
11H-3	109.0–110.0	93.99	1.38	0.58	2.61	77.20	77.80	57.50	135.50	3.40	3.45
11H-4	109.0–110.0	95.49	1.44	0.70	2.58	72.70	73.30	51.70	107.10	2.67	2.70
11H-5	109.0–110.0	96.99	1.38	0.60	2.57	76.40	77.00	56.70	131.10	3.24	3.29
11H-6	109.0–110.0	98.49	1.44	0.69	2.66	73.90	74.40	52.40	110.30	2.83	2.87
11H-7	39.0–41.0	99.29	1.36	0.58	2.47	76.10	76.70	57.30	134.40	3.19	3.24
12H-1	109.0–110.0	100.49	1.39	0.62	2.55	75.20	75.70	55.20	123.40	3.03	3.07
12H-2	109.0–110.0	101.99	1.37	0.59	2.50	76.20	76.80	57.10	133.10	3.20	3.25
12H-3	109.0–110.0	103.49	1.24	0.41	2.23	81.40	82.10	67.20	205.20	4.39	4.48
12H-4	109.0–110.0	104.99	1.22	0.39	2.09	81.10	81.80	68.30	215.00	4.30	4.38
12H-5	109.0–110.0	106.49	1.25	0.38	2.52	84.60	85.30	69.60	229.40	5.51	5.65
12H-6	109.0–110.0	107.99	1.23	0.39	2.28	82.60	83.20	68.50	217.40	4.73	4.84
12H-7	49.0–51.0	108.89	1.24	0.41	2.27	81.60	82.30	67.20	205.00	4.45	4.54
13H-1	109.0–110.0	109.99	1.26	0.43	2.33	81.10	81.70	65.70	191.80	4.29	4.37
13H-2	109.0–110.0	111.49	1.21	0.37	2.15	82.40	83.10	69.50	228.00	4.68	4.78
13H-3	109.0–110.0	112.99	1.29	0.46	2.52	81.50	82.10	64.60	182.60	4.41	4.50
13H-4	109.0–110.0	114.49	1.27	0.45	2.31	80.20	80.90	64.70	183.00	4.06	4.13
13H-5	109.0–110.0	115.99	1.28	0.45	2.33	80.10	80.80	64.40	180.60	4.03	4.10
13H-6	109.0–110.0	117.49	1.25	0.42	2.21	80.70	81.40	66.40	197.40	4.18	4.26
13H-7	49.0–51.0	118.39	1.31	0.52	2.35	77.70	78.30	60.70	154.20	3.48	3.54
14H-1	109.0–110.0	119.49	1.27	0.46	2.26	79.20	79.90	63.80	176.00	3.81	3.88
14H-2	109.0–110.0	120.99	1.30	0.50	2.31	78.00	78.70	61.50	160.00	3.56	3.61
14H-3	109.0–110.0	122.49	1.27	0.46	2.26	79.10	79.70	63.60	174.40	3.78	3.85
14H-4	109.0–110.0	123.99	1.27	0.45	2.26	79.60	80.20	64.30	179.80	3.90	3.97
14H-5	109.0–110.0	125.49	1.30	0.52	2.26	76.90	77.50	60.40	152.80	3.32	3.37
14H-6	109.0–110.0	126.99	1.23	0.39	2.23	82.10	82.80	68.20	214.60	4.58	4.68
14H-7	49.0–51.0	127.89	1.25	0.42	2.27	80.90	81.60	66.10	195.40	4.24	4.33
15H-1	109.0–110.0	128.99	1.26	0.42	2.33	81.70	82.30	66.70	200.00	4.46	4.55
15H-2	109.0–110.0	130.49	1.20	0.40	1.84	77.70	78.50	66.30	197.10	3.48	3.54
15H-3	109.0–110.0	131.99	1.34	0.57	2.33	75.00	75.60	57.30	134.10	3.01	3.05
15H-4	109.0–110.0	133.49	1.27	0.44	2.34	80.90	81.50	65.40	188.90	4.23	4.31
15H-5	109.0–110.0	134.99	1.28	0.47	2.29	79.10	79.70	63.20	172.10	3.78	3.85
15H-6	109.0–110.0	136.49	1.29	0.48	2.36	79.20	79.90	62.70	168.20	3.81	3.88
15H-7	49.0–51.0	137.39	1.28	0.49	2.19	77.20	77.90	61.70	160.90	3.39	3.44
16H-1	109.0–110.0	138.49	1.26	0.43	2.26	80.40	81.00	65.40	189.30	4.09	4.17
16H-2	109.0–110.0	139.99	1.32	0.55	2.24	75.10	75.70	58.30	139.60	3.01	3.05
16H-3	109.0–110.0	141.49	1.24	0.42	2.19	80.60	81.30	66.50	198.20	4.15	4.23
16H-4	109.0–110.0	142.99	1.28	0.46	2.33	79.90	80.60	64.10	178.50	3.99	4.06
16H-5	109.0–110.0	144.49	1.25	0.43	2.20	80.00	80.60	65.40	189.10	3.99	4.07
16H-6	109.0–110.0	145.99	1.25	0.42	2.19	80.30	81.00	66.00	194.40	4.08	4.15
16H-7	39.0–41.0	146.79	1.29	0.47	2.45	80.50	81.20	63.80	176.50	4.14	4.22
17H-1	109.0–110.0	147.99	1.31	0.52	2.32	77.40	78.10	60.60	153.60	3.43	3.48
17H-2	109.0–110.0	149.49	1.31	0.53	2.29	76.70	77.30	59.90	149.50	3.29	3.34
17H-3	109.0–110.0	150.99	1.31	0.52	2.29	77.10	77.70	60.40	152.70	3.36	3.41
17H-4	109.0–110.0	152.49	1.28	0.48	2.23	77.90	78.60	62.30	164.90	3.53	3.59
17H-5	109.0–110.0	153.99	1.26	0.44	2.22	79.70	80.30	64.80	184.30	3.92	3.99
17H-6	109.0–110.0	155.49	1.26	0.44	2.23	79.70	80.40	64.80	184.00	3.93	4.00

Table 11 (continued).

Core, section	Interval (cm)	Depth (mbsf)	Wet-bulk density (g/cm^3)	Dry-bulk density (g/cm^3)	Grain density (g/cm^3)	Wet porosity (%)	Dry porosity (%)	Wet water content (%)	Dry water content (%)	Void ratio 1	Void ratio 2
17H-7	39.0–41.0	156.29	1.25	0.45	2.11	78.20	78.90	63.90	177.30	3.59	3.65
18H-1	109.0–110.0	157.49	1.29	0.48	2.34	79.30	79.90	63.00	170.00	3.82	3.89
18H-2	109.0–110.0	158.99	1.50	0.85	2.30	62.50	63.00	42.80	74.90	1.67	1.68
18H-3	109.0–110.0	160.49	1.31	0.51	2.37	77.90	78.60	60.80	155.20	3.53	3.59
18H-4	109.0–110.0	161.99	1.29	0.48	2.31	78.90	79.60	62.80	169.10	3.75	3.81
18H-5	109.0–110.0	163.49	1.27	0.45	2.23	79.30	79.90	64.10	178.80	3.82	3.89
18H-6	109.0–110.0	164.99	1.28	0.47	2.28	78.80	79.50	63.10	170.60	3.73	3.79
18H-7	49.0–51.0	165.89	1.25	0.45	2.11	78.20	78.90	63.90	176.80	3.58	3.64
19H-1	109.0–110.0	166.99	1.25	0.45	2.13	78.60	79.30	64.30	180.30	3.68	3.74
19H-2	109.0–110.0	168.49	1.39	0.64	2.41	73.00	73.60	53.70	116.20	2.70	2.74
19H-3	109.0–110.0	169.99	1.26	0.44	2.30	80.60	81.30	65.30	188.30	4.15	4.23
19H-4	109.0–110.0	171.49	1.24	0.43	2.12	79.50	80.20	65.70	191.30	3.88	3.95
19H-5	109.0–110.0	172.99	1.21	0.36	2.14	82.70	83.50	70.10	234.30	4.80	4.90
19H-6	109.0–110.0	174.49	1.23	0.39	2.17	81.80	82.50	68.40	216.30	4.50	4.59
19H-7	39.0–41.0	175.29	1.25	0.43	2.20	80.10	80.80	65.70	191.30	4.03	4.11
20H-1	109.0–110.0	176.49	1.38	0.61	2.48	74.90	75.50	55.60	125.30	2.99	3.03
20H-2	109.0–110.0	177.99	1.27	0.45	2.29	80.00	80.60	64.60	182.10	3.99	4.06
20H-3	109.0–110.0	179.49	1.28	0.48	2.25	78.50	79.10	62.80	168.50	3.64	3.70
20H-4	109.0–110.0	180.99	1.28	0.46	2.32	79.90	80.50	64.10	178.50	3.97	4.04
20H-5	109.0–110.0	182.49	1.25	0.44	2.20	79.90	80.50	65.30	187.80	3.97	4.04
20H-6	109.0–110.0	183.99	1.28	0.47	2.28	79.00	79.60	63.20	171.60	3.75	3.82
20H-7	49.0–51.0	184.89	1.28	0.47	2.25	78.60	79.20	63.00	170.10	3.67	3.73
21H-1	109.0–110.0	185.99	1.34	0.57	2.33	75.10	75.70	57.40	134.60	3.02	3.06
21H-2	109.0–110.0	187.49	1.42	0.67	2.53	73.30	73.90	53.00	112.50	2.75	2.78
21H-3	109.0–110.0	188.99	1.34	0.55	2.42	76.80	77.40	58.70	142.30	3.31	3.36
21H-4	109.0–110.0	190.49	1.31	0.51	2.37	78.20	78.90	61.30	158.20	3.60	3.65
21H-5	109.0–110.0	191.99	1.43	0.70	2.44	70.90	71.40	50.80	103.30	2.44	2.46
21H-6	109.0–110.0	193.49	1.27	0.45	2.24	79.40	80.00	64.20	179.30	3.85	3.92
21H-7	49.0–51.0	194.39	1.30	0.51	2.29	77.30	78.00	60.80	155.20	3.41	3.46
22H-1	109.0–110.0	195.49	1.25	0.43	2.16	79.50	80.20	65.20	187.40	3.88	3.95
22H-2	109.0–110.0	196.99	1.28	0.47	2.31	79.20	79.80	63.20	172.00	3.81	3.88
22H-3	109.0–110.0	198.49	1.25	0.42	2.26	81.20	81.80	66.60	199.20	4.31	4.39
22H-4	109.0–110.0	199.99	1.23	0.39	2.19	81.80	82.50	68.20	214.70	4.49	4.59
22H-5	109.0–110.0	201.49	1.25	0.42	2.20	80.40	81.10	66.10	194.90	4.10	4.18
22H-6	109.0–110.0	202.99	1.25	0.44	2.21	79.90	80.60	65.30	187.90	3.98	4.05
22H-7	49.0–51.0	203.89	1.23	0.39	2.21	82.10	82.80	68.50	217.30	4.59	4.69
23H-1	109.0–110.0	204.99	1.25	0.43	2.18	80.00	80.70	65.70	191.30	4.00	4.07
23H-2	109.0–110.0	206.49	1.25	0.43	2.19	80.20	80.90	65.80	192.70	4.05	4.12
23H-3	109.0–110.0	207.99	1.24	0.42	2.13	80.10	80.80	66.30	197.10	4.03	4.10
23H-4	109.0–110.0	209.49	1.27	0.45	2.28	79.80	80.40	64.30	179.90	3.94	4.01
23H-5	109.0–110.0	210.99	1.28	0.48	2.22	77.80	78.50	62.20	164.80	3.51	3.57
23H-6	109.0–110.0	212.49	1.27	0.46	2.19	78.50	79.10	63.40	173.30	3.64	3.70
23H-7	39.0–41.0	213.29	1.29	0.50	2.26	77.60	78.20	61.50	159.60	3.46	3.52
24H-1	109.0–110.0	214.49	1.28	0.48	2.29	78.80	79.40	62.80	169.10	3.71	3.77
24H-2	109.0–110.0	215.99	1.25	0.43	2.18	80.10	80.80	65.80	192.00	4.02	4.10
24H-3	109.0–110.0	217.49	1.51	0.81	2.53	67.50	68.00	45.90	84.80	2.07	2.09
24H-4	109.0–110.0	218.99	1.27	0.46	2.26	79.50	80.20	64.20	179.00	3.88	3.95
24H-5	109.0–110.0	220.49	1.32	0.54	2.28	76.10	76.70	59.20	145.00	3.18	3.23
24H-6	109.0–110.0	221.99	1.27	0.46	2.23	78.90	79.60	63.70	175.30	3.75	3.82
24H-7	39.0–41.0	222.79	1.38	0.61	2.46	74.80	75.40	55.70	125.60	2.97	3.01
25H-1	109.0–110.0	223.99	1.23	0.42	2.06	79.10	79.80	65.70	191.90	3.78	3.85
25H-2	109.0–110.0	225.49	1.26	0.44	2.22	79.70	80.30	64.80	184.30	3.92	3.99
25H-3	109.0–110.0	226.99	1.24	0.41	2.21	80.90	81.60	66.70	199.90	4.23	4.32
25H-4	109.0–110.0	228.49	1.29	0.48	2.32	78.90	79.50	62.60	167.50	3.73	3.80
25H-5	109.0–110.0	229.99	1.27	0.45	2.31	80.10	80.80	64.60	182.70	4.04	4.11
25H-6	109.0–110.0	231.49	1.22	0.38	2.16	82.30	83.00	69.20	224.50	4.64	4.74
25H-7	39.0–41.0	232.29	1.24	0.41	2.15	80.50	81.20	66.60	199.80	4.12	4.20
26H-1	114.0–116.0	233.54	1.20	0.37	2.02	81.20	82.00	69.10	223.20	4.32	4.41
26H-2	109.0–110.0	234.99	1.23	0.39	2.19	81.70	82.40	68.10	213.00	4.47	4.56
26H-3	109.0–110.0	236.49	1.23	0.43	2.05	78.70	79.40	65.30	188.20	3.70	3.76
26H-4	109.0–110.0	237.99	1.23	0.39	2.18	81.90	82.60	68.50	217.10	4.52	4.61
26H-5	109.0–110.0	239.49	1.24	0.39	2.28	82.50	83.20	68.30	215.80	4.71	4.81
26H-6	109.0–110.0	240.99	1.29	0.49	2.29	78.30	78.90	62.20	164.20	3.61	3.67
27H-1	114.0–116.0	243.04	1.27	0.46	2.22	78.90	79.60	63.70	175.70	3.74	3.80
27H-2	109.0–110.0	244.49	1.28	0.46	2.38	80.50	81.10	64.40	181.10	4.12	4.20
27H-3	109.0–110.0	245.99	1.28	0.47	2.32	79.50	80.10	63.50	174.00	3.88	3.94
27H-4	109.0–110.0	247.49	1.27	0.46	2.21	78.80	79.40	63.70	175.20	3.71	3.78
27H-5	109.0–110.0	248.99	1.25	0.43	2.17	80.00	80.60	65.80	192.20	3.99	4.06
27H-6	109.0–110.0	250.49	1.28	0.49	2.22	77.70	78.30	62.00	163.10	3.48	3.54
28H-1	109.0–110.0	252.49	1.23	0.40	2.15	81.00	81.70	67.40	206.80	4.26	4.34
28H-2	109.0–110.0	253.99	1.25	0.42	2.21	80.50	81.20	66.10	194.80	4.13	4.20
28H-3	109.0–110.0	255.49	1.24	0.40	2.30	82.30	83.00	67.90	211.30	4.65	4.75
28H-4	109.0–110.0	256.99	1.28	0.47	2.32	79.50	80.20	63.60	174.90	3.89	3.95
28H-5	109.0–110.0	258.49	1.27	0.45	2.26	79.90	80.60	64.70	183.30	3.98	4.05
28H-6	109.0–110.0	259.99	1.28	0.47	2.29	79.20	79.80	63.40	173.20	3.80	3.87
29H-1	114.0–116.0	262.04	1.27	0.44	2.33	80.70	81.30	65.20	187.40	4.18	4.26
29H-2	109.0–110.0	263.49	1.27	0.45	2.30	79.90	80.60	64.30	180.50	3.98	4.05
29H-3	109.0–110.0	264.99	1.28	0.46	2.31	79.70	80.40	64.00	177.60	3.94	4.01
29H-4	109.0–110.0	266.49	1.31	0.51	2.30	77.30	77.90	60.60	154.00	3.41	3.46
29H-5	109.0–110.0	267.99	1.29	0.47	2.35	79.50	80.20	63.30	172.80	3.89	3.96
29H-6	109.0–110.0	269.49	1.34	0.54	2.46	77.50	78.10	59.40	146.20	3.45	3.50

Table 12. Vane shear strength data from Hole 882A and Hole 882B.

Core, section, interval (cm)	Depth (mbsf)	Shear strength (kPa)
145-882A-		
1H-1, 113	1.13	6.27
1H-2, 110	2.60	11.09
1H-3, 110	4.10	11.92
1H-4, 110	5.60	19.94
1H-5, 110	7.10	11.59
1H-6, 110	8.60	18.09
2H-2, 110	10.02	25.97
2H-3, 110	11.52	19.02
2H-4, 110	13.02	17.16
2H-5, 109	14.51	15.76
2H-6, 110	16.02	23.27
2H-7, 115	17.57	24.02
3H-1, 105	19.35	27.77
3H-2, 110	20.90	16.51
3H-3, 110	22.40	24.02
3H-4, 110	23.90	28.52
3H-5, 110	25.40	17.26
4H-1, 110	28.90	23.27
4H-2, 110	30.40	24.02
4H-3, 110	31.90	38.27
4H-4, 110	33.40	28.52
4H-5, 110	34.90	33.02
4H-6, 111	36.41	42.78
5H-1, 110	38.40	33.02
5H-2, 110	39.90	33.77
5H-3, 110	41.40	36.02
5H-4, 110	42.90	45.78
5H-5, 110	44.40	33.02
6H-1, 112	47.92	31.52
6H-2, 100	49.30	43.53
6H-3, 100	50.80	37.52
6H-4, 110	52.40	51.78
6H-5, 110	53.90	43.53
6H-6, 100	55.30	51.03
6H-6, 115	55.45	41.28
6H-7, 40	56.20	45.03
7H-1, 110	57.40	53.28
7H-2, 115	58.95	42.78
7H-3, 110	60.40	42.03
7H-4, 110	61.90	61.54
7H-5, 110	63.40	44.28
7H-6, 112	64.92	43.53
7H-7, 40	65.70	21.01
8H-1, 110	66.90	47.28
8H-2, 110	68.40	48.03
8H-3, 110	69.90	48.03
8H-4, 110	71.40	63.04
8H-5, 110	72.90	62.29
8H-6, 110	74.40	82.55
8H-7, 40	75.20	58.54
9H-1, 110	76.40	66.04
9H-2, 110	77.90	78.05
9H-3, 110	79.40	68.29
9H-4, 110	80.90	77.30
9H-5, 120	82.50	46.53
9H-6, 110	83.90	64.54
9H-7, 40	84.70	63.79
10H-1, 110	85.90	69.04
10H-2, 110	87.40	33.77
10H-3, 110	88.90	48.78
10H-4, 110	90.40	62.29
10H-5, 103	91.83	74.30
10H-6, 110	93.40	75.05
10H-7, 40	94.20	70.55
11H-1, 110	95.40	60.79
11H-2, 110	96.90	74.30
11H-3, 110	98.40	78.05
11H-4, 110	99.90	78.05
11H-5, 110	101.40	75.80
11H-6, 110	102.90	66.79
11H-7, 40	103.70	25.52
12H-1, 110	104.90	31.52
12H-2, 110	106.40	23.27
12H-6, 110	112.40	47.28
12H-7, 40	113.20	78.05
13H-2, 110	115.90	31.52
13H-3, 110	117.40	39.03
13H-4, 110	118.90	49.53
13H-5, 110	120.40	62.29
13H-6, 110	121.90	50.28
13H-7, 40	122.70	53.28
14H-1, 110	123.90	30.02
14H-2, 110	125.40	33.77
14H-3, 110	126.90	31.52
14H-4, 110	128.40	32.27
14H-5, 110	129.90	67.54
14H-6, 130	131.60	45.78
15H-2, 110	134.90	3.00
15H-3, 110	136.40	6.75
16H-1, 110	142.90	45.03
16H-2, 110	144.40	34.52
16H-3, 110	145.90	33.02
16H-4, 110	147.40	41.28
16H-5, 110	148.90	48.78
16H-6, 111	150.41	48.78
17H-1, 110	152.40	48.03
17H-2, 110	153.90	33.77
17H-3, 110	155.40	60.04
17H-4, 110	156.90	54.79
17H-5, 110	158.40	46.53
17H-6, 110	159.90	48.78
18H-1, 110	161.90	41.28
18H-2, 110	163.40	36.02
18H-3, 111	164.91	36.77
18H-4, 110	166.40	51.78
18H-5, 110	167.90	63.04
18H-6, 110	169.40	62.29
19H-1, 120	171.50	29.27
19H-3, 118	174.48	32.27
19H-4, 110	175.90	42.03
19H-5, 110	177.40	59.29
19H-6, 110	178.90	68.29
20H-1, 110	180.90	35.27
20H-2, 110	182.40	40.53
20H-3, 110	183.90	39.03
20H-4, 110	185.40	50.28
20H-5, 110	186.90	54.03
20H-6, 110	188.40	54.03
21H-1, 110	190.40	86.31
21H-2, 110	191.90	78.80
21H-3, 110	193.40	81.05
21H-4, 110	194.90	63.79
21H-5, 110	196.40	58.54
21H-6, 110	197.90	48.03
22H-1, 120	200.00	24.77
22H-2, 110	201.40	27.02
22H-3, 110	202.90	39.03
22H-4, 110	204.40	37.52
22H-5, 110	205.90	35.27
22H-6, 110	207.40	57.79
23H-1, 110	209.40	39.03
23H-2, 110	210.90	24.02
23H-3, 110	212.40	51.78
23H-5, 120	215.50	35.27
23H-6, 120	217.00	33.77
24H-1, 115	218.95	34.52
24H-2, 110	220.40	38.27
24H-3, 119	221.99	33.77
24H-4, 120	223.50	45.03
24H-5, 110	224.90	72.80
24H-6, 110	226.40	84.80
25H-1, 110	228.40	54.03
25H-2, 115	229.95	56.29
25H-3, 105	231.35	54.03
25H-4, 107	232.87	57.79
25H-5, 110	234.40	71.30
25H-6, 110	235.90	80.30
26H-1, 110	237.90	57.04
26H-2, 110	239.40	54.79
26H-3, 110	240.90	67.54
26H-4, 110	242.40	66.04
26H-5, 110	243.90	69.79
26H-6, 110	245.40	64.54
27H-1, 110	247.40	46.53
27H-2, 110	248.90	54.79
27H-3, 110	250.40	84.05
27H-4, 110	251.90	123.83
27H-5, 110	253.40	62.29
27H-6, 110	254.90	112.57
28H-1, 110	256.90	40.53
28H-2, 115	258.45	41.28
28H-3, 110	259.90	54.03
28H-4, 110	261.40	64.54
28H-5, 110	262.90	93.06
28H-6, 110	264.40	68.29

Table 12 (continued).

Core, section, interval (cm)	Depth (mbsf)	Shear strength (kPa)
29H-1, 110	266.40	61.54
29H-2, 110	267.90	41.28
29H-3, 110	269.40	37.52
29H-4, 115	270.95	75.80
29H-5, 110	272.40	81.80
29H-6, 110	273.90	168.86
30H-3, 113	278.93	68.29
30H-4, 110	280.40	84.80
30H-5, 110	281.90	98.31
30H-6, 43	282.73	90.81
31H-1, 110	285.40	45.03
31H-2, 110	286.90	55.54
31H-3, 110	288.40	58.54
31H-4, 110	289.90	81.05
31H-5, 110	291.40	91.56
31H-6, 110	292.90	79.55
32H-1, 110	294.90	33.02
32H-2, 110	296.40	60.04
32H-3, 110	297.90	57.79
32H-4, 110	299.40	61.54
32H-5, 110	300.90	101.31
32H-6, 110	302.40	127.58
33H-2, 110	305.90	49.53
33H-3, 110	307.40	45.03
33H-4, 110	308.90	57.04
33H-5, 110	310.40	70.55
33H-6, 110	311.90	74.30
34H-1, 110	313.90	66.04
34H-2, 110	315.40	70.55
34H-3, 110	316.90	66.04
34H-4, 110	318.40	81.05
34H-5, 110	319.90	72.05
34H-6, 110	321.40	120.08
35H-1, 110	323.40	47.28
35H-2, 110	324.90	42.03
35H-3, 110	326.40	63.04
35H-4, 110	327.90	78.05
35H-5, 110	329.40	81.80
35H-6, 110	330.90	124.58
36H-1, 110	332.90	36.02
36H-2, 110	334.40	45.78
36H-3, 110	335.90	57.04
36H-4, 110	337.40	45.78
36H-5, 110	338.90	57.79
36H-6, 110	340.40	87.81
37H-1, 110	342.40	60.04
37H-2, 110	343.90	100.56
37H-3, 110	345.40	122.33
37H-4, 110	346.90	93.81
37H-5, 110	348.40	161.35
37H-6, 110	349.90	85.55
38H-1, 110	351.90	62.29
38H-2, 110	353.40	93.81
38H-3, 110	354.90	74.30
38H-4, 124	356.54	67.54
38H-5, 110	357.90	108.07
38H-6, 110	359.40	81.80
39H-1, 110	361.40	42.03
39H-2, 110	362.90	60.79
39H-3, 110	364.40	59.29
39H-4, 110	365.90	72.05
39H-5, 110	367.40	85.55
40H-1, 110	370.90	105.82
40H-2, 110	372.40	84.05
40H-3, 110	373.90	91.56
40H-4, 110	375.40	109.57
40H-5, 110	376.90	144.09
40H-6, 110	378.40	141.09
41H-2, 110	381.90	75.80
41H-3, 110	383.40	64.54
41H-4, 110	384.90	115.57
41H-5, 110	386.40	134.34
41H-6, 110	387.90	138.84
42H-1, 110	389.90	69.79
42H-2, 110	391.40	85.55
42H-3, 110	392.90	69.79
42H-4, 110	394.40	133.58
42H-5, 110	395.90	125.33
42H-6, 110	397.40	173.36
145-882B-		
1H-1, 110	1.10	12.97
1H-3, 110	4.10	16.11
2H-1, 110	5.50	10.67
2H-3, 110	8.50	9.74
2H-5, 110	11.50	19.48
3H-1, 110	15.00	18.09
3H-3, 115	18.05	20.87
3H-5, 110	21.00	23.65
4H-1, 110	24.50	38.96
4H-3, 110	27.50	33.02
4H-5, 110	30.50	46.53
5H-1, 110	34.00	35.27
5H-3, 110	37.00	32.27
5H-5, 110	40.00	54.79
6H-3, 110	46.50	48.03
6H-5, 110	49.50	25.52
7H-1, 112	53.02	48.78
7H-3, 110	56.00	47.28
7H-5, 115	59.05	53.28
8H-1, 110	62.50	62.29
8H-3, 115	65.55	44.28
8H-5, 110	68.50	59.29
9H-1, 110	72.00	51.03
9H-3, 110	75.00	69.79
9H-5, 110	78.00	78.05
10H-1, 110	81.50	66.04
10H-3, 110	84.50	62.29
10H-5, 110	87.50	90.81
11H-1, 110	91.00	60.79
11H-3, 110	94.00	58.54
11H-5, 110	97.00	85.55
12H-1, 110	100.50	63.79
12H-3, 110	103.50	40.53
12H-5, 110	106.50	33.77
13H-1, 110	110.00	37.52
13H-3, 110	113.00	41.28
13H-5, 110	116.00	50.28
14H-1, 110	119.50	48.78
14H-3, 110	122.50	48.78
14H-5, 110	125.50	54.03
15H-1, 110	129.00	32.27
15H-3, 110	132.00	45.78
15H-5, 110	135.00	37.52
16H-1, 110	138.50	42.03
16H-3, 110	141.50	5.25
16H-5, 110	144.50	3.75
17H-1, 110	148.00	33.77
17H-3, 110	151.00	30.77
17H-5, 110	154.00	39.78
18H-1, 110	157.50	33.77
18H-3, 110	160.50	27.77
18H-5, 110	163.50	38.27
19H-1, 110	167.00	33.02
19H-3, 110	170.00	26.27
19H-5, 110	173.00	31.52
20H-1, 110	176.50	55.54
20H-3, 110	179.50	40.53
20H-5, 110	182.50	39.03
21H-1, 110	186.00	43.53
21H-3, 110	189.00	57.04
21H-5, 110	192.00	66.79
22H-1, 110	195.50	48.78
22H-3, 110	198.50	22.51
22H-5, 110	201.50	44.28
23H-1, 110	205.00	38.27
23H-3, 110	208.00	35.27
23H-5, 120	211.10	63.79
24H-1, 110	214.50	18.01
24H-3, 110	217.50	20.26
24H-5, 110	220.50	41.28
25H-1, 110	224.00	57.04
25H-3, 110	227.00	36.77
25H-5, 110	230.00	40.53
26H-1, 115	233.55	48.78
26H-3, 110	236.50	76.55
26H-5, 110	239.50	63.04
27H-1, 115	243.05	50.28
27H-3, 110	246.00	70.55
27H-5, 110	249.00	78.80
28H-3, 110	255.50	53.28
28H-5, 110	258.50	54.79
29H-1, 115	262.05	57.79
29H-3, 110	265.00	62.29
29H-5, 110	268.00	110.32

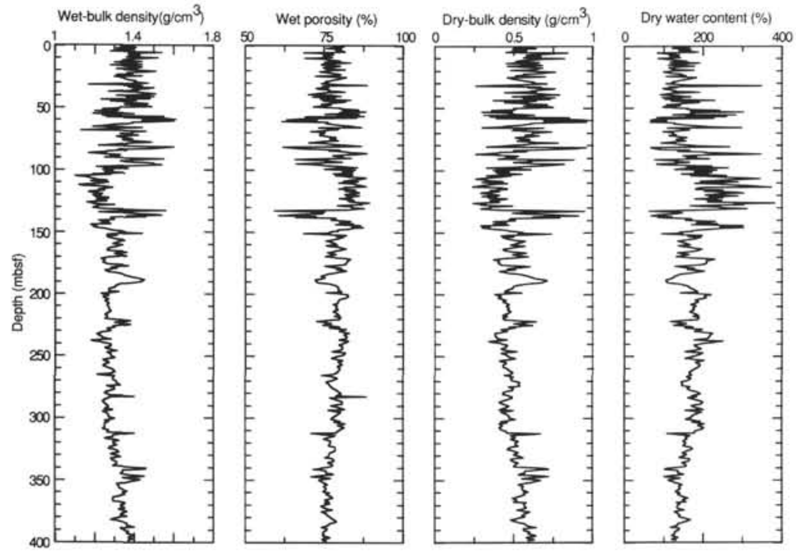

Figure 19. Index property data for Hole 882A.

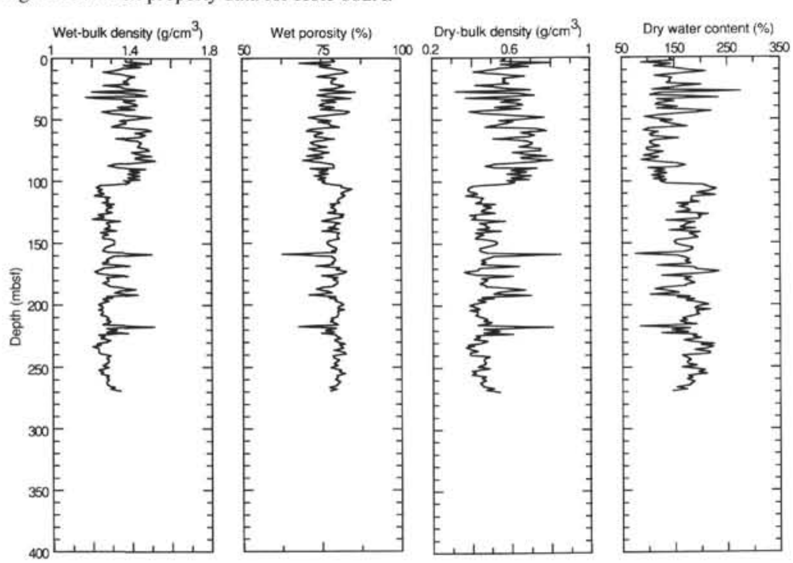

Figure 20. Index property data for Hole 882B.

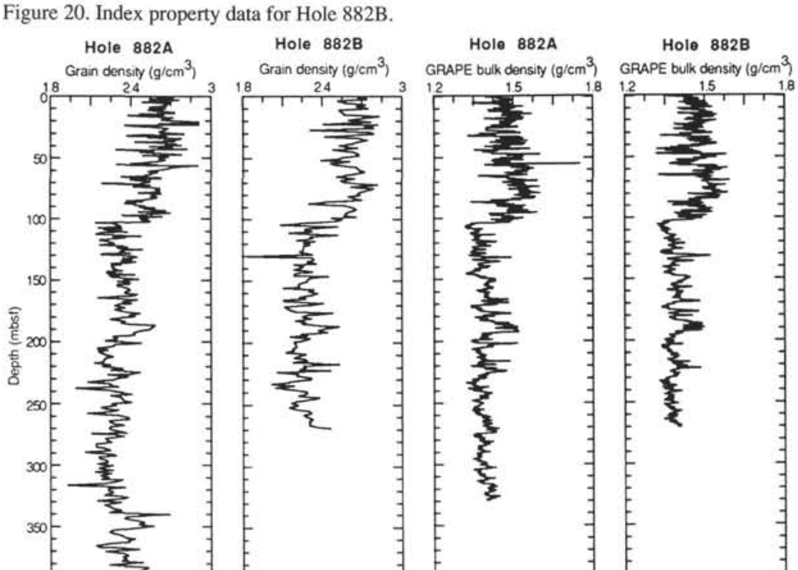

Figure 21. Grain density and GRAPE bulk density data for Holes 882A and 882B.

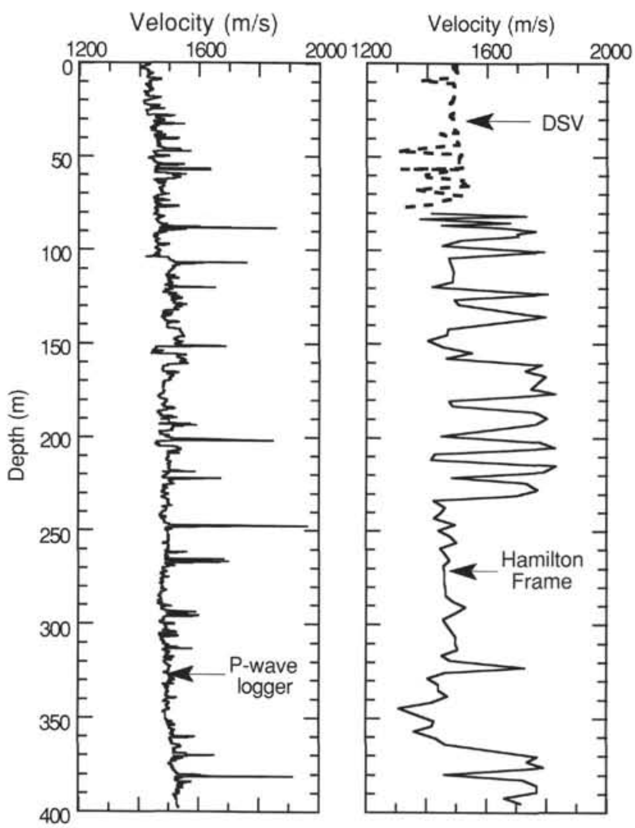

Figure 22. P-wave, DSV, and Hamilton Frame velocity data for Hole 882A.

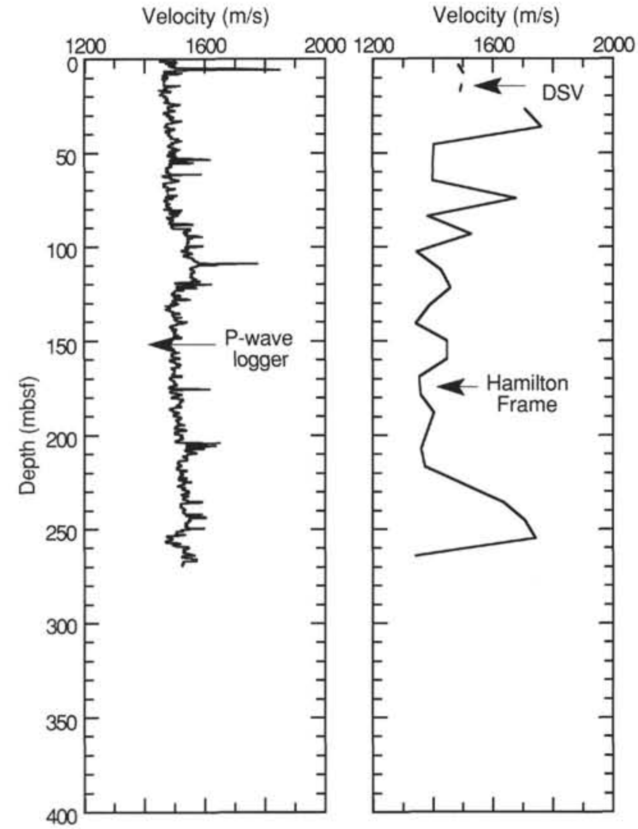

Figure 23. P-wave, DSV, and Hamilton Frame velocity data for Hole 882B.

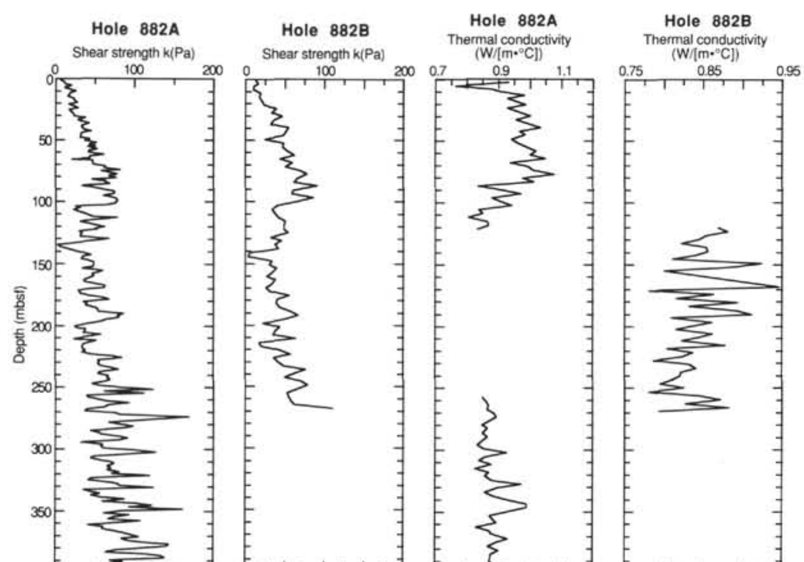

Figure 24. Shear strength and thermal conductivity data for Holes 882A and 882B.

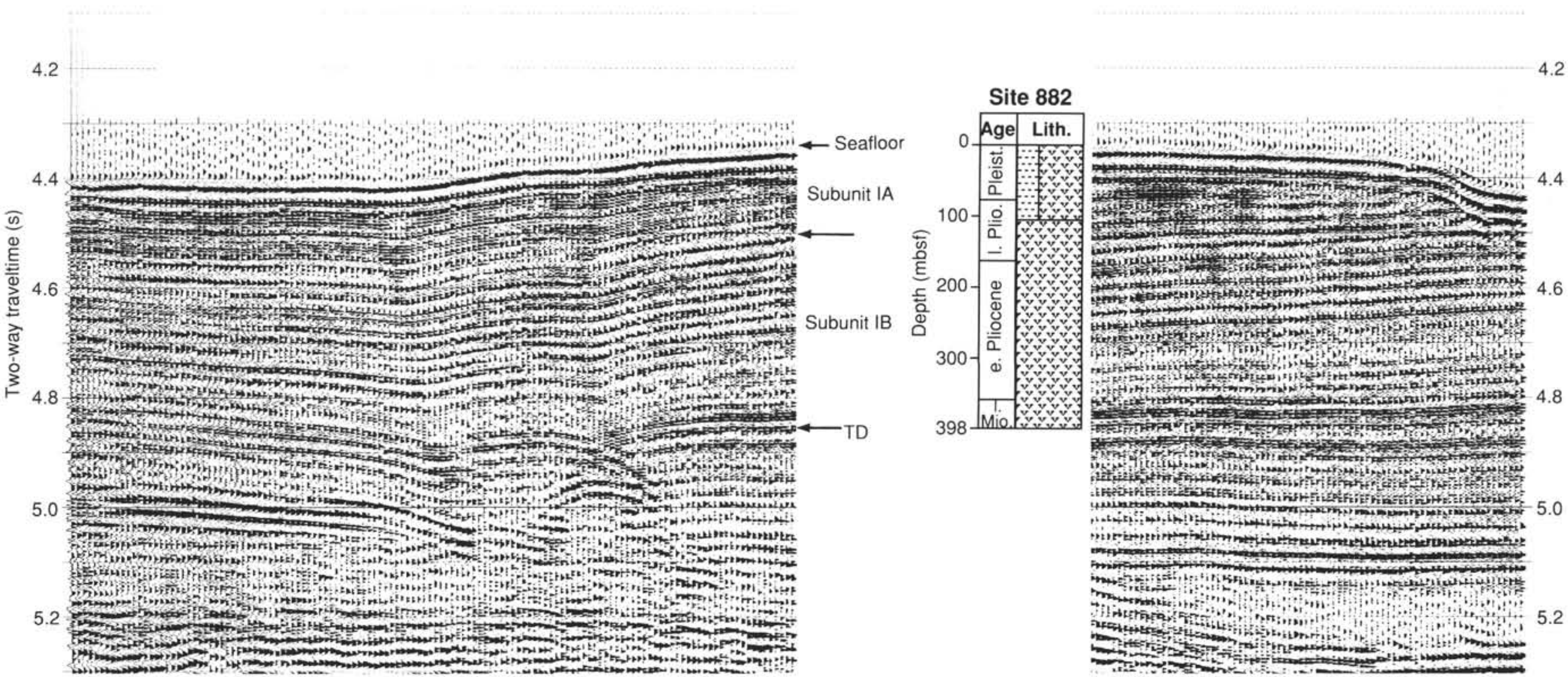

Figure 25. Processed seismic reflection profile crossing Site 882. Line trends north-northwesterly (north is to the right). The depth ranges of lithologic Subunits IA and IB are indicated on the profile inset.